Impact of wiggliness on the cosmic microwave background anisotropies generated by cosmic string networks

Rodrigo Pereira da Silva
Mestrado em Física
Departamento de Física e Astronomia
2022

Orientadora
Doutora Lara Rodrigues da Costa Gomes de Sousa, Instituto de Astrofísica e Ciências do Espaço

Coorientador
Doutor Ivan Rybak, Instituto de Astrofísica e Ciências do Espaço

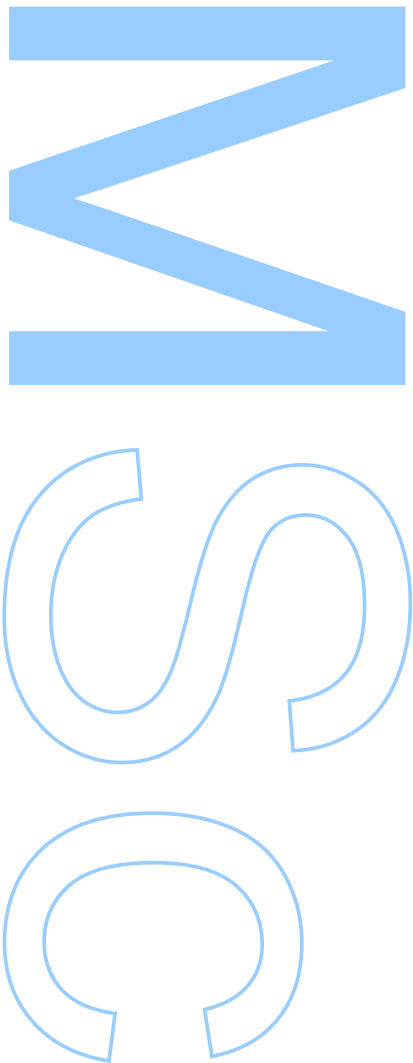

U.PORTO

FACULDADE DE CIÊNCIAS
UNIVERSIDADE DO PORTO

Todas as correções determinadas pelo júri, e só essas, foram efetuadas.

O Presidente do Júri,

Porto, _____/_____/_____

Universidade do Porto

Masters Thesis

Impact of wiggliness on the cosmic microwave background anisotropies generated by cosmic string networks

Author:
Rodrigo Pereira da Silva

Supervisor:
Dr. Lara Rodrigues da Costa Gomes de Sousa

Co-supervisor:
Dr. Ivan Rybak

A thesis submitted in fulfilment of the requirements for the degree of MSc. Physics

at the

Faculdade de Ciências da Universidade do Porto
Departamento de Física e Astronomia

November 14, 2022

“ You asked for my hustle and I gave you my heart ”

Kobe Bryant

Sworn Statement

I, Rodrigo Pereira da Silva, enrolled in the Master Degree of Theoretical Physics at the Faculty of Sciences of the University of Porto hereby declare, in accordance with the provisions of paragraph a) of Article 14 of the Code of Ethical Conduct of the University of Porto, that the content of this dissertation reflects perspectives, research work and my own interpretations at the time of its submission.

By submitting this dissertation, I also declare that it contains the results of my own research work and contributions that have not been previously submitted to this or any other institution.

I further declare that all references to other authors fully comply with the rules of attribution and are referenced in the text by citation and identified in the bibliographic references section. This dissertation does not include any content whose reproduction is protected by copyright laws.

I am aware that the practice of plagiarism and self-plagiarism constitute a form of academic offense.

Rodrigo Pereira da Silva

November 14, 2022

Acknowledgements

First and foremost, I want to express my gratitude to my supervisor, Lara Sousa, and my co-supervisor, Ivan Rybak, for their shared knowledge, support, and patience, as well as their faith in me throughout this dissertation. This work would not be possible without them.

I would also like to thank everyone who, directly or indirectly, helped me during this journey. In particular, to António Correia, Alexandra Oliveira, Beatriz Pinto, Bernardo Campilho, Filipe Costa, João Araújo, João Couto, João Silva, José Pereira and Ricardo Costa. Furthermore, I would like to give a special acknowledgment to Beatriz, Couto and Ricardo. I would like to thank Couto and Ricardo for always being there for me and pushing me to be a better academic version of myself since the first day of high school. I may not have enough words to express how grateful I am to you, Beatriz, but I would like to thank you for your belief in me, for never letting me give up on my dreams, and for your unwavering support.

Last but not least, I would like to thank my family, especially my grandparents and my parents for giving me the opportunity to pursue and for pushing me to do physics, even though they are unsure of what I study, and to my uncle Fernando for giving me that long lecture on if you love physics, you should do it.

UNIVERSIDADE DO PORTO

Abstract

Faculdade de Ciências da Universidade do Porto
Departamento de Física e Astronomia

MSc. Physics

Impact of wiggliness on the cosmic microwave background anisotropies generated by cosmic string networks

by Rodrigo Pereira da Silva

Cosmic strings are 1-dimensional topological defects that may be produced in phase transitions in the early universe. These defects are expected to persist throughout the evolution of the universe, leaving imprints in the Cosmic Microwave Background (CMB). Furthermore, as the universe evolves, cosmic strings interact with one another, resulting in the production of small-scale structures known as kinks, which may further enhance their CMB signatures.

In this dissertation, we aim to describe the impact of cosmic strings with kinks on the CMB anisotropies. For this purpose, we extended the Unconnected Segment Model (USM) to describe the stress-energy tensor of a network of strings with kinks throughout the evolution of the universe. We then implement this novel wiggly USM in the publicly available CMBACT code to obtain the Cold Dark Matter (CDM) linear power spectrum and the CMB anisotropies generated by a network of cosmic strings with kinks.

We find that when we consider wiggly string segments there is an increase in the amplitude of the CDM linear power spectrum and of the CMB anisotropies. This increase — that scales roughly as $1/\sin^2(\beta/2)$ — is larger when kinks are sharper, which may be explained by the fact that the energy density of the network increases when we increase the kink sharpness. Moreover, this increase is actually scale-dependent and some regions of the spectra are more enhanced than others. The region of the spectrum that is enhanced is approximately determined by the length of the subsegment (i.e. the distance between kinks), which depends on the number of kinks per string segment and their sharpness. As a matter of fact, in general, there is a shift of power from large to small scales. The larger

the number of kinks, the smaller the distance between kinks will be and, as a result, this power is shifted to increasingly smaller scales. However, if the kinks are extremely sharp, the subsegment may be quite large even if there is a large number of kinks per segment and there also may be visible effects on larger scales. Furthermore, our results also show that the enhancement of the relative amplitude of the spectrum is more prominent for vector modes, probably as a result of the discontinuity of the string at the kinks.

The original CMBACT uses an approach that consists of introducing a phenomenological wiggliness parameter to provide an effective description of wiggles on the string. We have also found that the standard effective approach leads, in general, to an underestimation of the amplitude of the CMB anisotropies and to a prediction of a different shape for the spectra. This may be seen in every component, but it is particularly prominent for the vector and tensor modes, highlighting the importance of our geometrical approach for an accurate prediction of the CMB power spectra.

Finally, we used our results to derive observational constraints on cosmic string tension for wiggly cosmic string. We found that, in general, the constraints on the tension of wiggly cosmic strings derived using CMB data are more stringent than those of Nambu Goto strings. For instance, for a wiggly string with kink sharpness equal to $\pi/9$, we obtain $G\mu_0 < 4.49 \times 10^{-9}$ which is different, and more stringent, than the regular constraint for Nambu-Goto strings by a factor of about 33.

UNIVERSIDADE DO PORTO

Resumo

Faculdade de Ciências da Universidade do Porto
Departamento de Física e Astronomia

Mestrado em Física

Impacto da estrutura de pequena escala nas anisotropias da radiação cósmica de fundo geradas por redes de cordas cósmicas

por Rodrigo Pereira da Silva

Cordas cósmicas são defeitos topológicos produzidos em transições de fase no universo primordial. Espera-se que estes defeitos sobrevivam à evolução do universo, deixando impressões na Radiação Cósmica de Fundo (RCF). Para além disso, com a evolução do universo, as cordas cósmicas interagem entre si resultando na produção de estruturas de pequena escala denominadas *kinks*, que poderão potenciar as assinaturas na RCF.

Nesta dissertação, procuramos descrever o impacto de cordas cósmicas com estruturas de pequena escala nas anisotropias da radiação cósmica de fundo. Para este propósito, desenvolvemos uma extensão do *Unconnected Segment Model* (USM) para descrever o tensor energia-momento de redes de cordas cósmicas com estrutura de pequena escala durante a evolução do universo. De seguida, implementamos este novo USM no código publicamente disponível CMBACT para obtermos o espetro linear da Matéria Escura Fria (MEF) e as anisotropias da RCF geradas por uma rede de cordas cósmicas com estrutura de pequena escala.

Quando consideramos segmentos de corda com estrutura de pequena escala verificamos que existe um aumento da amplitude do espetro linear da MEF e das anisotropias do RCF. Este aumento — que escala como $1/\sin^2(\beta/2)$ — é maior quando os kinks são mais agudos, o que pode ser explicado pelo aumento da densidade de energia da rede quando a agudeza destas estruturas aumenta. Além disso, este aumento depende da escala e algumas regiões dos espectros sofrem maiores aumentos que outras. A região do espetro que é potenciada é aproximadamente determinada pelo comprimento dos subsegmentos (i.e a distância entre os kinks), que depende do número de kinks por segmento de corda e a sua agudeza. De

facto, de um modo geral, há uma transferência de potência de grandes para pequenas escalas. Quanto maior for o número de kinks, menor será a distância entre eles e, como resultado, esta potência será deslocada para escalas cada vez menores. No entanto, se os kinks forem extremamente agudos, mesmo que haja um grande número de kinks por segmento, o subsegmento poderá tornar-se bastante longo e também poderá haver efeitos visíveis em escalas maiores. Além disso, os nossos resultados mostram que o aumento da amplitude relativa do espetro é mais proeminente para os modos vetoriais, provavelmente como resultado da descontinuidade da corda nos kinks.

O CMBACT original utiliza uma abordagem que consiste na introdução de um parâmetro fenomenológico para fornecer uma descrição efectiva da estrutura de pequena escala na corda. Também descobrimos que a abordagem efetiva padrão leva, em geral, a uma subestimação da amplitude das anisotropias e à previsão de uma forma diferente para os espectros. Isto pode ser visto em qualquer componente, mas é particularmente proeminente para o caso de modos vetoriais e tensoriais, demonstrando assim a importância da nossa abordagem geométrica para uma previsão precisa dos espectros de potência RCF.

Por último, usamos estes resultados para obter constrangimentos observacionais à tensão de cordas cósmicas com estrutura de pequena escala. Verificámos que, em geral, os constrangimentos sobre a tensão das cordas cósmicas com estrutura de pequena escala, derivadas utilizando dados RCF, são mais rigorosas do que as das cordas Nambu-Goto. Por exemplo, para uma corda com kinks com agudeza igual a $\pi/9$, obtemos $G\mu_0 < 4.49 \times 10^{-9}$ o que é diferente, e mais forte, do que os constrangimentos usuais para cordas Nambu-Goto por um fator de aproximadamente 33.

Notation and Units

In this dissertation, we use the following metric signature: $(+,-,-,-)$. We also use units in which $c = \hbar = k_B = 1$. Furthermore, the Greek indices run over 0,1,2,3 and Latin indices run over 0,1. Finally, we use $A_{\mu,\nu} \equiv \frac{\partial A_\mu}{\partial x^\nu}$ to express the partial derivative and the following notation for the covariant derivative $A^\rho_{;\sigma} \equiv \nabla_\sigma A^\rho$.

Contents

List of Figures

Glossary

CDM	Cold Dark Matter
CMB	Cosmic Microwave Background
COBE	COsmic Background Explorer
EFE	Einstein Field Equations
FLRW	Friedmann-Lemaître-Robertson-Walker
MEF	Matéria Escura Fria
RCF	Radiação Cósmica de Fundo
RMS	Root-Mean-Squared
VEV	Vacuum Expectation Value
VOS	Velocity-Dependent One Scale Model
USM	Unconnected Segment Model
WMAP	Wilkinson Microwave Anisotropy Probe

Chapter 1

Introduction

1.1 The Standard Cosmological Model

The standard cosmological model is the widely accepted explanation for the evolution of the universe from the Big Bang to the present. It is based on the assumption, known as the cosmological principle, that the universe is spatially homogeneous and isotropic at large scales.

In 1915, Albert Einstein published the field equations of gravitation [1], known as Einstein Field Equations (EFE), which relate the curvature of spacetime to the contents of the universe. In 1922, Alexander Friedmann found that the EFE has two types of solutions: one for an expanding universe and another for a contracting universe [2], completing the universe's description by discovering the missing piece, its dynamics. In 1927, Belgian priest Georges Lemaître proposed that the Doppler shift of nebula galaxies could be caused by the expansion of the universe [3]. Furthermore, in 1929 Edwin Hubble discovered that galaxies were receding from Earth, which can only be explained by an expanding universe. If the universe was static, galaxies would move at random velocities relative to the point of observation, with no direct relationship between distance and velocity. If the universe was contracting, galaxies would be approaching Earth [4].

In spherical coordinates, the line element for a homogeneous and isotropic expanding universe can be represented as follows:

$$ds^2 = a(\tau)^2 \left[d\tau^2 - \frac{dr^2}{1 - Kr^2} - r^2 \left(d\theta^2 + \sin^2 \theta d\phi^2 \right) \right] \quad , \tag{1.1}$$

where τ is the conformal time, which is related to physical time t via $d\tau = dt/a$, $a(t)$ is the scale factor, and K is a constant curvature that determines the geometry of the universe:

$$\begin{aligned} &K > 0\,, \text{ the universe is closed with an } S^3 \text{ topology }\,, \\ &K = 0\,, \text{ the universe is flat with an } R^3 \text{ topology }\,, \\ &K < 0\,, \text{ the universe is open with an } H^3 \text{ topology }\,. \end{aligned} \tag{1.2}$$

The metric that corresponds to the line element in Eq.(1.1) is known as Friedmann–Lemaître–Robertson–Walker (FLRW) metric.

The scale factor $a(\tau)$ describes the time evolution of the distance D between two points on a FLRW universe, which can be equated as:

$$D(\tau) = a(\tau) D_0 \,, \tag{1.3}$$

where D_0 is the distance at the initial time. Hubble's law provides the corresponding recessional velocity:

$$v = HD \,, \tag{1.4}$$

where the Hubble parameter was introduced:

$$H = \frac{1}{a}\frac{da}{dt} \,. \tag{1.5}$$

The dynamics of the universe is assumed to be governed by the EFE (1.6). The EFE may then be used to describe the expansion of the universe:

$$G_{\mu\nu} \equiv R_{\mu\nu} - \frac{1}{2}\mathcal{R} g_{\mu\nu} = 8\pi G T_{\mu\nu} \,, \tag{1.6}$$

where $G_{\mu\nu}$ is the Einstein tensor, $R_{\mu\nu}$ is the Ricci tensor, $\mathcal{R}$ is the Ricci scalar, $g_{\mu\nu}$ is the metric tensor, G is the gravitational constant and $T_{\mu\nu}$ is the stress-energy tensor. The Ricci scalar is obtained by contracting the Ricci tensor with the metric: $\mathcal{R} = R^{\mu\nu} g_{\mu\nu}$. The Ricci tensor is obtained by contracting the Riemann tensor's first and third indices:

$$R_{\mu\nu} = R^{\sigma}_{\mu\sigma\nu} = \Gamma^{\lambda}_{\mu\nu,\lambda} - \Gamma^{\lambda}_{\mu\lambda,\nu} + \Gamma^{\lambda}_{\rho\lambda}\Gamma^{\rho}_{\mu\nu} - \Gamma^{\lambda}_{\rho\nu}\Gamma^{\rho}_{\mu\lambda} \,, \tag{1.7}$$

where

$$\Gamma^{\mu}_{\lambda\sigma} = \frac{g^{\mu\nu}}{2}\left(g_{\mu\nu,\sigma} + g_{\sigma\nu,\lambda} - g_{\lambda\sigma,\nu}\right) \tag{1.8}$$

are the Christoffel symbols.

We assume that the content of the universe, in a FLRW spacetime, can be described by a perfect fluid, so the stress-energy tensor, $T_{\mu\nu}$, takes the form:

$$T_{\mu\nu} = \big(\rho(t) + p(t)\big)\, u_\mu u_\nu - p(t) g_{\mu\nu} \ , \tag{1.9}$$

where $\rho(t)$ is the time-dependent energy density, $p(t)$ is the time-dependent pressure, and u_μ is the perfect fluid's 4-velocity, which has the form:

$$u^\mu = \frac{dX^\mu}{dt} \ . \tag{1.10}$$

Local conservation of energy-momentum is imposed by $T^{\mu\nu}_{\ ;\nu} = 0$, which implies:

$$\frac{d\rho}{dt} + 3\frac{da}{dt}\frac{1}{a}(\rho + p) = 0 \ . \tag{1.11}$$

Using the "00"-component of Eq.(1.6) along with "00"-component of Eq.(1.9), we obtain the Friedmann equation for a homogeneous, isotropic, expanding universe which can be written as follows:

$$\left(\frac{da}{dt}\right)^2 + K = \frac{8\pi G\rho a^2}{3} \ . \tag{1.12}$$

WMAP and Planck missions have recently confirmed that the universe is flat with a 0.4% margin of error [5, 6], so, from now on, we set $K = 0$. In this case, Eq.(1.12) equals:

$$\left(\frac{da}{dt}\right)^2 = \frac{8\pi G\rho a^2}{3} \ . \tag{1.13}$$

The evolution of the scale factor, $a(t)$, is fully described by Eq.(1.12) and Eq.(1.11), along with the equation of state for a perfect fluid, which can be written as:

$$p = \omega\rho \ , \tag{1.14}$$

where ω is determined by the contents of the universe.

Assuming that ω is a constant then Eq.(1.11) with the equation of state (1.14) yields:

$$\rho = \rho_0 a^{-3(1+\omega)} \ , \tag{1.15}$$

where ρ_0 is the energy density in the present epoch.

We can calculate the evolution of the scale factor using Eq. (1.15) and Eq.(1.13):

$$a^{\frac{1}{2}(1+3\omega)} da = C_0 dt \ , \tag{1.16}$$

where $C_0 = \left(\frac{8\pi G\rho_0}{3}\right)^{1/2}$. This expression can be integrated to a closed-form expression, requiring $\omega \neq -1$. In this case, the scale factor can be written as:

$$a \propto t^{\frac{2}{3(1+\omega)}} . \tag{1.17}$$

Therefore, when relativistic matter dominates the universe, $\omega = 1/3$ and thus the scale factor will evolve as $a \propto t^{1/2}$. However, if non-relativistic matter dominates the energy density of the universe, pressure is negligible, so $\omega = 0$ and thus the scale factor will evolve as $a \propto t^{2/3}$.

The acceleration equation can be obtained by combining the non-zero components of Eq.(1.6) and the Friedmann Equation (1.13), and it is written as follows:

$$\frac{\ddot{a}}{a} = -\frac{4\pi G}{3}\left(\rho + 3p\right) . \tag{1.18}$$

During the radiation and matter-dominated eras, $\ddot{a} < 0$, implying that the universe's expansion is decelerating. Nonetheless, in the late 1990s, the High-z Supernova Search Team and the Supernova Cosmology Project published observational results of type-IA supernovas [7, 8] which implies that the universe's expansion is accelerating. This acceleration could only be explained by an additional component of unknown origin, which exerts negative pressure. As a result, it was hypothesized that the universe would be in an era dominated by an unknown component — dark energy. Furthermore, when $\omega \leq -1$, Eq.(1.18) always implies that the universe's expansion is accelerating, so dark energy is something with such equation of state. Finally, $\omega = -1$ is a special case corresponding to the cosmological constant, a component whose energy density remains constant. If we plug this equation of state in Eq.(1.16) we obtain:

$$a = a_i e^{C_0(t-t_i)} , \tag{1.19}$$

where a_i is the scale factor in the initial time, t_i, $\rho_0 = \rho_\Lambda$ and C_0 has the same definition as above. Moreover, Eq.(1.19) tell us that the universe, in a cosmological-constant-dominated era, will expand exponentially.

At last, we can express the energy density of each component as:

$$\begin{cases} \rho_r = \rho_{0r} a^{-4}, \\ \rho_m = \rho_{0m} a^{-3}, \\ \rho_\Lambda = const, \end{cases} \tag{1.20}$$

where the subscripts m and r represent matter and radiation, respectively.

We can see that the energy density of radiation decreases faster than that of matter and of dark energy with expansion. As a consequence, it must have been the dominant component in the early stages of the universe. Furthermore, matter's energy density decreases faster than dark energy, which appears to be constant throughout the universe's expansion and is the dominant component today. To summarize, the universe must have gone through a radiation, a matter, and a dark energy era, in that order, due to the dependence of each energy density on the scale factor.

1.2 Topological Defects

In condensed matter, phase transitions between different states of matter can cause structural defects such as vortex lines in liquid helium, flux tubes in type II superconductors, and disclination lines in liquid crystals [9, 10].

Similarly, many particle physics theories use the same concept, topological defects, to describe the hypothetical defects created by phase transitions in the early universe.

1.2.1 Phase Transition in Early Universe

1.2.1.1 Cosmological Phase Transitions

In the early universe, phase transitions are known to have occurred, therefore it is natural to speculate that topological defects may have formed during these processes. Despite the fact that topological defects in cosmology have never been observed, their existence is predicted by many high energy physics models [11–28].

A spontaneous symmetry breaking is intrinsically related to a phase transition. This concept arose from Condensed Matter Physics [29, 30] as well as the concept of topological defect, and later Kibble proposed using the same concept in Cosmology [31].

A symmetry group encodes the transformations that leave a physical system invariant. Consider the following figures:

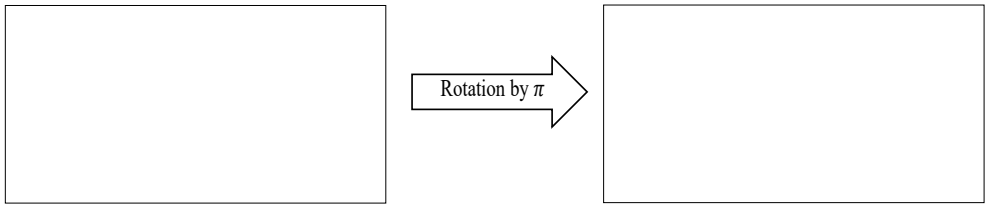

FIGURE 1.1: Representation of a transformation that leaves the rectangle invariant.

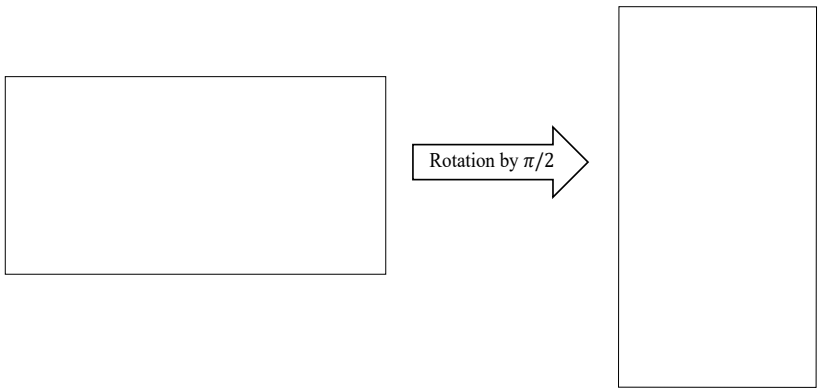

FIGURE 1.2: Representation of a transformation that does not leave the rectangle invariant.

In Fig.1.1, we can see that a rotation by an angle of π yields the initial rectangle. However, in Fig.1.2, we can see that after a rotation by $\pi/2$, we do not get the same rectangle. The transformation shown in Fig.1.1 is one of the transformations that leave the original rectangle invariant — in other words, it is a symmetry transformation — while that in Fig. 1.2 is not. The set of all the transformations that leave a rectangle invariant form a symmetry group known as the dihedral group D_2.

In physical systems, the idea is the same: if we have a symmetric system, the Lagrangian density must be invariant under the transformations of the corresponding symmetry group. When the symmetry breaks spontaneously, a stable state of the system is no longer invariant under these symmetry group transformations [32] and depending on its nature, different topological defects may appear.

As an example, consider the Goldstone model with a real scalar field, ϕ, in 3 + 1 dimensions. The potential of this model is as follows:

$$V(\phi) = \frac{\lambda}{4}\left(\phi^2 - \eta^2\right)^2 \quad , \tag{1.21}$$

which is invariant under reflection: $\phi \to -\phi$:

$$V(-\phi) = \frac{\lambda}{4}\left((-\phi)^2 - \eta^2\right)^2 = \frac{\lambda}{4}\left(\phi^2 - \eta^2\right)^2 = V(\phi) \quad . \tag{1.22}$$

Therefore, we can say that the potential possesses reflection or Z_2 symmetry [33]. When the temperature of the universe is above a critical temperature, ϕ will be established to a symmetric state: $\langle\phi\rangle = 0$. When the temperature of the universe reaches the critical temperature and then drops below it, a phase transition occurs, breaking the reflection symmetry. Below the critical temperature, the energy in the universe is insufficient to

allow ϕ to overcome the potential barrier, so $\langle\phi\rangle = 0$ is no longer a stable state, and ϕ will settle to one of the minima of the potential:

$$V(\phi) = 0 \iff \phi = \pm\eta \ . \tag{1.23}$$

Since all minima are equivalent, the field will settle to one of the minima at random at every point in space. The field then acquires different Vacuum Expectation Values (VEVs) in different regions of spacetime and, since the field must vary continuously in space, $\langle\phi\rangle$ will interpolate between $-\eta$ and η in the boundaries between regions with different VEVs. As a result, there exist regions in space where the field has energy – known as domain walls, which are 2+1-dimensional topological defects. Topological defects are regions where the ϕ has a non-trivial configuration or, in other words, is not in a vacuum state.

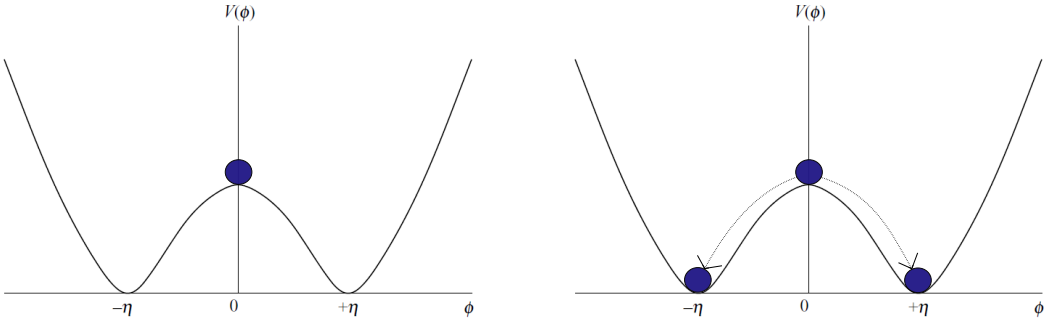

FIGURE 1.3: Representation of the behavior of ϕ (blue ball) before the phase transition (a) and after the phase transition (b). Figure adapted from [34].

1.2.1.2 Cosmic String Production

The simplest model in which cosmic strings appear is the Goldstone model with a complex field ϕ, with potential [34]:

$$V(\phi) = \frac{1}{2}\lambda\left(\phi^*\phi - \frac{1}{2}\eta^2\right)^2 \ . \tag{1.24}$$

Similarly to the case of domain walls, in the early stages of the universe, the temperature was higher than the critical temperature, below which the symmetry is broken. In this regime, ϕ develops a vacuum expectation value $\langle\phi\rangle = 0$. When the universe reaches a critical temperature and undergoes a phase transition that breaks the axial symmetry, characteristic of this model, ϕ rolls down to the valley of the potential, developing a non-vanishing vacuum expectation value: $\langle\phi\rangle \neq 0$. Since all points in the valley of the potential are equivalent, quantum and thermal fluctuations determine this choice at random at each

point in space. As a result of causality, regions separated by more than a correlation length will be independent, i.e. uncorrelated, and thus have, in general, different vacuum expectation values. By causality, this correlation length is constrained to be smaller than the particle horizon:

$$d_h = a(t) \int_0^t \frac{dt'}{a(t')} \quad . \tag{1.25}$$

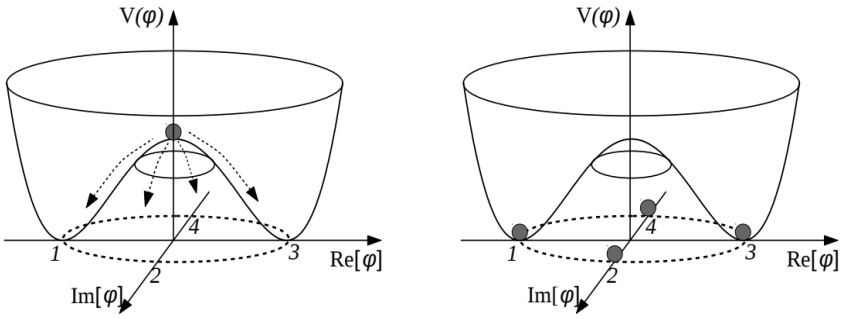

FIGURE 1.4: Representation of the behavior of the scalar field before and after the symmetry breaking. Figure adapted from [35].

Consider a closed curve, C, that connects the possible potential minima in Fig.1.5. If we begin, at a given point, to travel around the closed path, we can expect to return to the same point. The number of times around the circle of minima that it takes to reach the initial point is known as the *winding* number. Let's consider the closed path in Fig.1.5 with a non-zero winding number. If we shrink the closed curve to a point, the *winding* number becomes zero, which is a contradiction. The only way to avoid this is to consider that the path has, at least in one point, left the circle of minima of the potential, but this implies that there is a point inside curve C that is not a minimum of the potential [36]. In this case, the topological defect that arises is line-like and is denominated cosmic string.

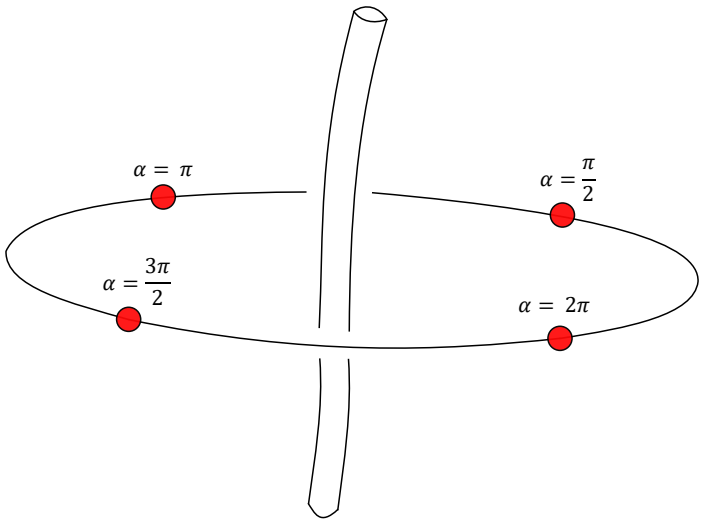

FIGURE 1.5: Schematic representation of the formation of cosmic strings. The red dots represent different vacuum expectation values, whose phases vary by 2π. Figure adapted from [34].

Finally, the type of strings presented here have a tension that is divergent and, as result, the energy is not confined to a small region around the core. However, strings originating from the breaking of a local axial symmetry — i.e a symmetry transformation that depends on the spacetime coordinates — do not have the same problem. In this case, the energy per unit length is finite — which is determined by the energy scale of the symmetry-breaking phase transition — and the energy is confined to the core of the strings.

In most situations of interest in cosmology, strings originate from the breaking of a local symmetry therefore, in this dissertation, we will only consider local strings, with energy localized within a thin core, that may then be treated as infinitely thin objects.

1.3 Cosmic Microwave Background

In 1948, George Gamow, Ralph Alpher, and Robert Herman predicted the existence of a cosmic background radiation [37–42]. In 1964, Arno Penzias and Robert Wilson detected a weak background radio signal uniformly distributed across the sky [43]. After investigating whether the weak signal was caused by the noise created by the horn antenna used to detect it or by any apparatus surrounding the antenna, they discovered that the signal did, in fact, come from a source in the universe. In 1965, Robert Dicke and his group deduced that the source of this faint signal was recombination in the early universe, and this weak background radio signal was labeled Cosmic Microwave Background (CMB) [44].

The COsmic Background Explorer (COBE) satellite demonstrated that the CMB has an almost perfect blackbody radiation spectrum characterized by a temperature of $2.728\ K$ [45]. In addition to the anisotropies caused by Earth's motion relative to the CMB rest-frame, the COBE satellite discovered faint anisotropies in the CMB. These anisotropies are very small:

$$\frac{\delta T}{T} \lesssim 10^{-5} \ . \tag{1.26}$$

Despite the fact that the CMB has anisotropies, the Wilkinson Microwave Anisotropy Probe (WMAP) and the Planck satellite have recently demonstrated that, if we ignore the anisotropy caused by Earth's motion, the universe is homogeneous and isotropic on sufficiently large scales, providing considerable confirmation of the Cosmological Principle [5, 6].

1.3.1 Cosmic Microwave Background Anisotropies

Perturbations in the energy density in the early universe were the origin of large-scale structures that we observe today. It was proposed that these perturbations were caused either by topological defects — *active* model — or that they arose in the very early universe (for example, during cosmological inflation) — *primordial perturbation* models.

CMB anisotropies can be decomposed into three modes: scalar, vector, and tensor, each corresponding to a perturbation of a quantity in the universe [46]. The scalar mode is associated with a change in the energy density of the fluid that makes up the universe. The vector mode is a perturbation corresponding to vortical motions of matter, where the velocity of the fluid $\mathbf{v}$ obeys $\nabla \cdot \mathbf{v} = 0$. Finally, the tensor mode is associated with transverse-traceless perturbations to the metric, which can be interpreted as gravitational waves [47].

In *primordial perturbation* models, perturbations are seeded in the early universe and grow throughout the universe's evolution to become the structures observed today. In contrast, in *active* models, perturbations are generated all the time [48, 49]. As a result, *active* models generate significant vector contributions, whereas *primordial perturbation* models do not. This becomes more clear when we consider the linearized EFE for the vector component [48]:

$$\dot{V} + 2\frac{\dot{a}}{a}V = \frac{64\pi G}{25\sqrt{3}k}C_\gamma - \frac{8\pi G}{k}\Theta^V \ , \tag{1.27}$$

where C_γ is a constant depending on the average photon density, the average neutrino density, the multipole moments, and the quadrupole component of the neutrino distribution. Moreover, Θ^V is the source of vector perturbations and V is the vector perturbation. In *primordial perturbation* models, there was an initial source of vector perturbations, but because these are only seeded at the start, there is no source after that ($\Theta^V = 0$) and C_γ is negligible. Therefore Eq.(1.27) reduces to:

$$\dot{V} + 2\frac{\dot{a}}{a}V = 0 \rightarrow V \propto a^{-2} \ . \tag{1.28}$$

Thus, the vector perturbations in this model will become negligible as the universe expands. However, in *active* models, this contribution is not negligible because anisotropies are continuously generated throughout cosmological evolution ($\Theta^V \neq 0$). Computations of the CMB anisotropies generated by cosmic string networks revealed that they generate vector and tensor perturbations of similar magnitude, both contributing significantly to the CMB anisotropies [50–53].

Recent observational missions have demonstrated that the measured CMB temperature anisotropy is consistent with primordial perturbations, such as those seeded by cosmological inflation [54]. Nonetheless, we cannot exclude from consideration a subdominant contribution of cosmic strings just yet. Although cosmic strings do not contribute significantly to the temperature anisotropies of the CMB, they may contribute or even dominate the B-mode polarization because they generate significant vector modes [55].

Finally, CMB observations constrain the cosmic string tension to $G\mu_0 < 1.49 \times 10^{-7}$ [56]. These constraints, however, were derived using models that assume cosmic strings do not have significant small-scale structure. Realistically, as a result of collisions and interactions, strings can become very wiggly. In this dissertation, we improve the modeling of the CMB anisotropies generated by cosmic strings by considering wiggly strings, in order to increase the precision of the constraints on the string tension.

Chapter 2

Cosmic Strings: Dynamics and Interactions

2.1 Cosmic Strings: An Overview

Several extensions of the Standard Model, such as the axion model [17, 18], brane inflation from string theory [19–22], and supersymmetric theory [23–28], to name a few, predict the existence of cosmic strings. All of these models can be validated if cosmic strings are detected. Cosmic strings are, in a sense, a probe of high-energy physics models.

2.1.1 The Nambu-Goto Action: From String Dynamics to String Energy

The dynamical equations of motion of a (local) cosmic string can be derived using the Nambu-Goto action. In spacetime, an infinitely thin string sweeps a 2-dimensional surface. The following 4-vector can represent this worldsheet:

$$X^\mu = X^\mu(\xi^a)\ ,\ a = 0, 1\ , \tag{2.1}$$

where ξ^0 denotes a timelike variable and ξ^1 denotes a spacelike variable that parameterizes the string worldsheet. An infinitely thin string obeys the Nambu-Goto action:

$$S = -\mu_0 \int d^2\xi \sqrt{-\gamma}, \tag{2.2}$$

where μ_0 is the cosmic string tension, which is the energy per unit length of the string, γ is the determinant of the worldsheet metric, $\gamma_{ab} = g^{\mu\nu} X_{\mu,a} X_{\nu,b}$ and $g^{\mu\nu}$ is the spacetime metric.

We consider a flat FLRW metric:

$$ds^2 = a(\tau)^2 \left(d\tau^2 - d\mathbf{x}^2\right) .$$

The Nambu-Goto action is invariant under worldsheet reparametrizations, therefore we can use any gauge that is convenient. It is common in a FLRW background to choose temporal-transverse gauge conditions:

$$\xi^0 = \tau \text{ and } \dot{\mathbf{X}} \cdot \mathbf{X}' = 0 , \tag{2.3}$$

where $X^\mu = (\tau, \mathbf{X})$, a dot and a prime denotes a derivative with respect to τ or σ, respectively, $\dot{\mathbf{X}}$ is the velocity of the string and $\mathbf{X}'$ is the string tangent vector.

The equations of motions are obtained by varying Eq. (2.2) with respect to X^μ:

$$X^\mu_{,a}{}^{;a} + \Gamma^\mu_{\rho\lambda} \gamma^{ab} X^\rho_{,a} X^\lambda_{,b} = 0 , \tag{2.4}$$

where

$$X^\mu_{,a}{}^{;a} = \frac{1}{\sqrt{-\gamma}} \partial_a \left(\sqrt{-\gamma}\gamma^{ab} X^\mu_{,b}\right) . \tag{2.5}$$

In the temporal-transverse gauge and for a FRLW metric, the equations of motion may be written as :

$$\ddot{\mathbf{X}} + 2\frac{\dot{a}}{a}\left(1 - \dot{\mathbf{X}}^2\right)\dot{\mathbf{X}} = \epsilon^{-1}\left(\epsilon^{-1}\mathbf{X}'\right)' , \tag{2.6}$$

$$\dot{\epsilon} = -2\frac{\dot{a}}{a}\epsilon\dot{\mathbf{X}}^2 . \tag{2.7}$$

with

$$\epsilon^2 = \left(\frac{\mathbf{X}'^2}{1 - \dot{\mathbf{X}}^2}\right) . \tag{2.8}$$

The dynamics of a cosmic string in an expanding, flat universe are completely described by Eqs.(2.6) and (2.7).

The stress-energy tensor is obtained by varying the Eq. (2.2) with respect to $g_{\mu\nu}$:

$$T^{\mu\nu} = -\frac{2}{\sqrt{-g}}\frac{\delta S}{\delta g_{\mu\nu}} = \mu_0 \int d^2\xi \sqrt{-\gamma}\gamma^{ab} X^\mu_{,a} X^\nu_{,b} \delta^{(4)}\left(X^\sigma - X^\sigma(\xi^a)\right) . \tag{2.9}$$

As a result, the energy of the string is given by:

$$E = \mu_0 a(\tau) \int \epsilon d\xi . \tag{2.10}$$

2.1.2 String Interactions

Strings moving through the universe can interact with one another. When two strings come into contact, they will reconnect.

Reconnection can result in three different outcomes: strings colliding in one point and exchanging partners, resulting in the formation of strings with kinks; strings colliding in two points, resulting in the formation of kinks and loops; and strings self-intersecting, also resulting in the formation of strings with kinks and loops. A schematic representation of these processes is shown in Fig.2.1 and 2.2.

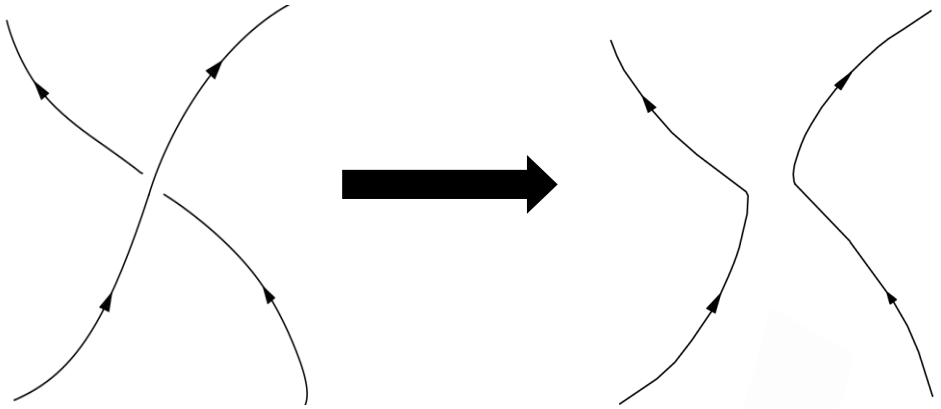

FIGURE 2.1: Formation of two cosmic strings with kinks as a result of reconnection. Image from [57].

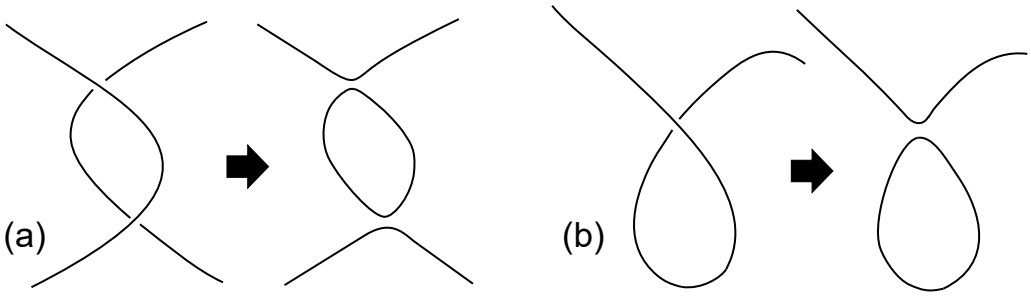

FIGURE 2.2: Loops are formed when two cosmic strings intersect (a) or when a string intersects itself (b). Image from Cambridge Cosmology Group.

Chapter 3

Modeling Cosmic Strings Networks

Cosmic Strings form a network, thus it is not sufficient to know the cosmological evolution of a single string. To describe the cosmological evolution of a cosmic string network, one must consider its dynamics and potential interactions between strings. This is especially important because cosmic strings are expected to survive throughout the universe's evolution, generating signatures in the CMB. Therefore, we must describe the evolution of cosmic strings throughout cosmological history and must know the network's stress-energy tensor in order to compute the CMB anisotropies.

The first attempt to describe the cosmological evolution of a network was made by Kibble when he proposed the *One-Scale* model [58], in which he assumed that the evolution of a network could be characterized by the correlation length, ζ. Numerical simulations [59, 60] revealed that Kibble's one-scale model ignored important small-scale physical processes because the simulations agreed with Kibble's model only on sufficiently large-scales [59].

In 1996, Martins and Shellard extended the one-scale model by adding another dynamical variable, the string Root-Mean-Squared (RMS) velocity and thus creating the *Velocity-dependent One-Scale* (VOS) model [61, 62]. Essentially, this model tells us how many strings exist on average per comoving volume and their mean velocity, then providing a quantitative description of the evolution of the string network [61]. The VOS model, like Kibble's model, describes a network on sufficiently large scales, but it does so with greater precision since it describes the radiation-matter transition.

In order to investigate the CMB anisotropies, we need a microscopic description of the stress-energy tensor, which cannot be achieved with the VOS or Kibble's model since they

only describe large-scale dynamics. With this objective in mind, the Unconnected Segment Model (USM) was introduced. The USM [48, 53] simplifies the network by considering a collection of randomly distributed and orientated straight string segments moving with random, uncorrelated velocities, in order to compute the stress-energy tensor of a cosmic string network. At last, after obtaining the stress-energy tensor and using the linearized Einstein-Boltzmann equations [63], it can be used to study the CMB anisotropies generated by a cosmic string network.

In this chapter, we are going to introduce the VOS model and the USM.

3.1 Cosmological Evolution of Cosmic String Networks

3.1.1 The Velocity-Dependent One-Scale Model

The VOS model considers a volume with long strings and assumes that their evolution can be described by a single length scale called correlation or physical length ζ, which is defined in terms of the bare string density:

$$\rho_0 = \frac{\mu_0}{\zeta^2} \,. \tag{3.1}$$

The bare string density corresponds to the energy density of the string excluding the energy density accommodated in kinks/wiggles or other additional degrees of freedom.

Furthermore, the VOS includes a dynamical variable called RMS velocity to describe the matter-radiation transition [62], which is defined as:

$$v^2 \equiv \langle \dot{\mathbf{x}}^2 \rangle = \frac{\int \dot{\mathbf{x}}^2 \epsilon d\sigma}{\int \epsilon d\sigma} \quad . \tag{3.2}$$

The energy of long strings can be defined in terms of the total energy density of the network:

$$E = \rho V \quad . \tag{3.3}$$

In this model, the characteristic length, ζ_c, is defined such that there is a string with size ζ_c per volume ζ_c^3. Thus, one can write:

$$\rho = \frac{\mu_0 \left(\zeta_c\right)}{\zeta_c^3} = \frac{\mu_0}{\zeta_c^2} \quad . \tag{3.4}$$

For strings without small-scale structure, the correlation and characteristic lengths coincide $\zeta = \zeta_c$, whereas if the strings are wiggly these lengths may differ significantly. For the

remainder of this section, we shall assume that strings are not wiggly and write all the equations in terms of the correlation length ζ.

To describe the evolution of the network, the VOS models also assume that strings can be described by the Nambu-Goto action. In this case, the equations of motion for the strings are Eqs.(2.6) and (2.7).

In order to obtain the evolution equation for ρ, we must consider the total energy in strings, including the contributions of all strings in the network, then differentiate it and apply the Nambu-Goto equations of motion (Eqs.(2.6) and (2.7)). We then obtain:

$$\frac{d\rho}{dt} + 2H\rho\left(1+v^2\right) = 0 \ . \tag{3.5}$$

When sub-horizon loops are formed, they completely detach from the network, altering its energy density. This process, which must be considered for an accurate description of the evolution of the network, is not accounted for in the above equation. As a result, we consider Kibble's proposed phenomenological term [58]:

$$\left(\frac{d\rho}{dt}\right) = \tilde{c}v\frac{\rho}{\zeta} \ , \tag{3.6}$$

where $\tilde{c}$ is a phenomenological parameter that characterizes loop chopping efficiency [62], which was calibrated using numerical simulations [59, 60] and has the following value [62]:

$$\tilde{c} = 0.23 \pm 0.04 \ . \tag{3.7}$$

For a probabilistic derivation of Eq.(3.6), see [61]. For a full description of the evolution equation for ρ, we need to subtract energy losses caused by loop formation Eq.(3.6) from Eq.(3.5), resulting in:

$$\frac{d\rho}{dt} + 2H\rho\left(1+v^2\right) - \tilde{c}v\frac{\rho}{\zeta} = 0 \ . \tag{3.8}$$

Using Eq.(3.4), we can write the evolution equation of the correlation length:

$$2\frac{d\zeta}{dt} = 2H\zeta\left(1+v^2\right) + \tilde{c}v \ . \tag{3.9}$$

Lastly, we must determine the evolution equation for v; to do so, we differentiate Eq.(3.2) and use the Nambu-Goto equations of motions Eqs.(2.6) and (2.7), yielding:

$$\frac{dv}{dt} = \left(1-v^2\right)\left[\frac{k(v)}{\zeta} - 2vH\right] \ , \tag{3.10}$$

where we assumed $\langle \dot{\mathbf{X}}^4 \rangle \approx \langle \dot{\mathbf{X}}^2 \rangle^2$. This expression is exact up to second-order terms [61]. $k(v)$ is the momentum parameter, which is defined as:

$$k(v) \equiv \frac{\langle \left(1 - \dot{\mathbf{X}}^2\right) \left(\dot{\mathbf{X}} \cdot \mathbf{u}\right) \rangle}{v(1-v^2)} \ , \tag{3.11}$$

where $\mathbf{u}$ is a unit vector parallel to the curvature radius. This parameter may be interpreted as describing, to a limited extent, the impact of small-scale structure [62]. In [62, 64, 65] the following form for $k(v)$ was proposed:

$$k(v) \equiv \frac{2\sqrt{2}}{\pi}(1-v^2)(1+2\sqrt{2}v^3)\frac{1-8v^6}{1+8v^6} \ . \tag{3.12}$$

3.1.2 Scaling Solutions

Numerical simulations [60, 66] revealed that cosmic strings networks evolve towards a linear scaling regime [67]; otherwise cosmic strings would dominate the energy density of the universe.

Linear scaling regimes appear when we assume that the scale factor behaves as a power law [62]:

$$a(t) \propto t^{\beta} \ , \ \beta = constant \ , \ 0 < \beta < 1 \ . \tag{3.13}$$

The characteristic length can be written as:

$$\zeta = \eta(t) t \ . \tag{3.14}$$

If we substitute Eq.(3.14) in expressions (3.9) and (3.10), we obtain:

$$2\frac{\dot{\eta}}{\eta} = \frac{1}{t}\left[2\beta\left(1+v^2\right) + \tilde{c}\frac{v}{\eta} - 2\right] \text{ and } \dot{v} = \frac{1}{t}\left[\left(1-v^2\right)\left(\frac{k}{\eta} - 2v\beta\right)\right] \ , \tag{3.15}$$

In a linear scaling regime, v and η are constant, implying that $\dot{v} = \dot{\eta} = 0$. In this regime, Eqs.(3.15) reduce to:

$$\eta^2 = \frac{k\left(k+\tilde{c}\right)}{4\beta\left(1-\beta\right)} \ , \ v^2 = \frac{k\left(1-\beta\right)}{\beta\left(k+\tilde{c}\right)} \ , \tag{3.16}$$

which is an attractor solution of the VOS equations. For these quantities to have physical significance we should have:

$$\eta > 0 \ , \ 0 < v < 1 \ , \ \zeta < d_H \ . \tag{3.17}$$

In linear scaling regimes, the fraction of energy density of strings and energy of the background remains constant in both the radiation and matter eras. The energy density

of strings can be written as:

$$\rho_{st} = \frac{\mu_0}{\zeta^2} = \frac{\mu_0}{\eta^2 t^2}\,. \tag{3.18}$$

In the matter era, we may write the fraction of the energies as:

$$\frac{\rho_{st}}{\rho_m} = \frac{\mu_0/\eta^2 t^2}{\rho_{0m} a^{-3}} \propto \frac{\mu_0/\eta^2 t^2}{\rho_{0m}(t^{2/3})^{-3}} = \frac{\mu_0}{\eta^2 \rho_{0m}}\,, \tag{3.19}$$

which is constant as we stated before. Similarly, in the radiation era, we can write the fraction of the energies as:

$$\frac{\rho_{st}}{\rho_r} = \frac{\mu_0/\eta^2 t^2}{\rho_{0r} a^{-4}} \propto \frac{\mu_0/\eta^2 t^2}{\rho_{0r}(t^{1/2})^{-4}} = \frac{\mu_0}{\eta^2 \rho_{0r}}\,, \tag{3.20}$$

which is also constant, as we expected. Consequently, strings do not have a tendency to dominate the universe's energy density.

3.2 The Stress Energy Tensor of a Cosmic String Network

3.2.1 The Unconnected Segment Model (USM)

As in the VOS model, we consider a volume containing a large number of strings. In order to study the CMB anisotropies generated by the cosmic string network, we would need to describe the stress-energy tensor for the entire volume, which is extremely difficult to do analytically. To achieve this, the Unconnected Segment Model (USM) was developed, which approximates the network in this volume by a collection of uncorrelated randomly distributed straight string segments moving with randomly orientated velocities. In this model, the stress-energy tensor is computed for this simplified network and then averaged over a large number of realizations in which the segments and velocities are assigned at random. Even though a realistic cosmic string network is not a collection of straight segments, we can describe its anisotropies accurately by averaging the CMB anisotropies generated over a large number of realizations of the USM. Moreover, the USM assumes that strings are created at an early epoch and decay in subsequent epochs to mimic the effect of energy loss caused by the creation of loops [48].

Each cosmic string within the volume generates perturbations that contribute to the anisotropies generated by the entire network. So, in order to fully describe the CMB anisotropies, we need to have a description of the stress-energy tensor of the whole network at any instant in time. We can write the network stress-energy tensor as the sum of the

stress-energy tensors of each string [53]:

$$\Theta_{\mu\nu}(\vec{k},\tau) = \sum_{m=1}^{N_s} \Theta^m_{\mu\nu}(\vec{k},\tau) T^{\text{off}}\left(\tau,\tau_f^m\right) \quad , \tag{3.21}$$

where N_s is the number of strings contained within the volume, τ_f^m is the conformal time of complete decay of the m-th segment, and T^{off} is a smooth function chosen to model segment decay. This function may be written as follows [48]:

$$T^{\text{off}}(\tau,\tau_f) = \begin{cases} 1 & \tau < \lambda_f \tau_f \\ \frac{1}{2} + \frac{1}{4}\left(x_{\text{off}}^3 - 3x_{\text{off}}\right) & \lambda_f\tau_f \leq \tau < \tau_f \\ 0 & \tau_f \leq \tau \end{cases} , \tag{3.22}$$

where

$$x_{\text{off}} = 2\frac{\ln(\lambda_f \tau_f/\tau)}{\ln(\lambda_f)} - 1 , \tag{3.23}$$

Based on the results of simulations [68–71] and the predictions of analytical models [61, 62], a large number of strings is expected to survive cosmological expansion. In fact, in order to have a single string surviving at the present time, we would have to start with $N_s \geq 10^{12}$ [53], which would require a lot of computational power. One way around this would be to avoid directly dealing with the individual segments and instead consolidate all string segments that decay at the same epoch into a single straight segment. The number of decaying segments N_d at a discrete conformal time is [48, 53]:

$$N_d(\tau) = V\left[n(\tau_{i-1}) - n(\tau_i)\right] \quad , \tag{3.24}$$

where V is the simulation volume and $n(\tau)$ is the string number density at time τ. Individual segments in real space are randomly oriented, which corresponds to random phases in Fourier space. The amplitude of the Fourier transformed stress-energy tensor describing the sum of the contributions of individual segments that decay at a given time is then essentially a random walk. As a result, in Fourier space, we can write the total stress-energy tensor as the stress-energy tensor of a single segment of string weighted by a factor of $\sqrt{N_d}$ [48, 53, 72]. Thus, one can write [53]:

$$\tilde{\Theta}_{\mu\nu}(\mathbf{k},\tau) = \sum_i \sqrt{N_d(\tau_i)}\,\Theta^1_{\mu\nu}(\mathbf{k},\tau) T^{\text{off}}(\tau,\tau_i) + \mathcal{T}_{\mu\nu} , \tag{3.25}$$

where the index i runs over the consolidated straight segments, $\Theta^1_{\mu\nu}(\mathbf{k},\tau)$ is the stress-energy tensor for a single straight segment, and $\mathcal{T}_{\mu\nu}$ is the contribution of any string

segments that did not decay until τ_{max}, which we consolidate into one straight segment with weight $\sqrt{N_d(\tau_{max})} = \sqrt{Vn(\tau_{max})}$. Therefore, we can write $\mathcal{T}_{\mu\nu}$ as [53]:

$$\mathcal{T}_{\mu\nu} = \sqrt{N_d(\tau_{max})}\Theta^1_{\mu\nu}(\mathbf{k},\tau)\,. \tag{3.26}$$

Finally, the number density of the decaying segments within the comoving volume is not directly proportional to L^{-3} due to the implementation of $T^{\text{off}}(\tau,\tau_i)$. Instead, we have:

$$n(\tau) = \frac{C(\tau)}{L^3}\,, \tag{3.27}$$

where L is the comoving correlation length and is defined as:

$$L = \frac{\zeta}{a(\tau)}\,. \tag{3.28}$$

Function $C(\tau)$ is determined by requiring that the total number of strings at any time is given by $V_0/L(\tau)^3$ [53], where V_0 is the comoving volume. For that reason:

$$\frac{1}{(L)^3} = \sum_i \left[n(\tau_{i-1}) - n(\tau)\right]\Theta^i_{\mu\nu}(\mathbf{k},\tau)T^{\text{off}}(\tau,\tau_i) + n(\tau_{max})\,, \tag{3.29}$$

where L is determined using the VOS model.

3.2.2 The VOS-USM connection and the computation of CMB anisotropies

To calculate the CMB anisotropies generated by cosmic string networks, we must first compute the network's stress-energy tensor using the USM. This model, however, tells us nothing about the average length of the segments, or, in other words, nothing about the energy density in the observed universe, nor does it tell us anything about the average velocity in the simulation volume, for which we use the VOS model. To compute the stress-energy tensor of a realistic cosmic string network, we must use both of these models in conjunction.

Finally, in order to compute the CMB anisotropies, we must solve the linearized Einstein-Boltzmann equations, with the stress-energy tensor calculated using both the USM and the VOS as a source. To accomplish this, we use the publicly available numerical tool CMBACT [53, 73] which is based on CMBFAST [63].

Chapter 4

A Wiggly Unconnected Segment Model

As we previously mentioned, cosmic strings collide throughout the course of cosmological evolution, and, as result, they will inevitably reconnect and kinks will form. A kink is a point in which the string tangent vectors are discontinuous. These are produced in substantial amounts during the intercommutation process, giving rise to a network of wiggly strings.

In [53], there is the first attempt to compute the CMB anisotropies generated by wiggly strings. Basically, this is done by giving strings an effective tension different from the actual physical tension — through a wiggliness parameter — and therefore there is no modification of the VOS model nor of the USM. In [74], the authors consider a modified Nambu-Goto action, where a wiggliness parameter dependent on a field that is a function of world-sheet time is introduced, which led to the development of a wiggly VOS model. In [75], this wiggly VOS model is introduced into CMBACT to compute the CMB anisotropies. In essence, they took into consideration straight segments with a modified dynamical effective tension. In [53, 75], the USM was never changed.

Our strategy is a little different. Since there is an abundance of kinks produced after intercommutation, resulting in a wiggly string, we consider, in the computation of the stress-energy tensor of the network, string segments with kinks instead of straight ones. In this chapter, we will therefore develop a novel USM for wiggly strings, with the objective of computing the CMB anisotropies.

4.1 Extending the VOS Model for Wiggly Strings

For clarity, the different lengths and lengthscales used in this chapter are recorded in Table 4.1.

Symbol	Definition
d	comoving subsegment length
L	comoving projective length of the string segments
L_{total}	total comoving length of the string segments
L_c	comoving characteristic length of the network
ζ	correlation length of the network
ζ_c	characteristic length of the network

TABLE 4.1: Different lengths and lengthscales used.

In this chapter, unless stated otherwise, all the mentioned lengths are comoving lengths. In our USM, we consider a network of string segments with kinks — or wiggly segments — in which each string has the same total length and number of kinks, N. Furthermore, each string is composed of $N+1$ straight segments with the same length, d, that meet at the kinks, which all have the same sharpness, β. Fundamentally, we also model the network as a collection of randomly oriented identical segments moving in random directions but now the segments have a "zig-zag" form.

To estimate the energy density of a network composed of wiggly strings, we must once again understand its evolution. The characteristic length of a network composed of straight strings coincides with the correlation length — which may be identified as the projective or physical length of the segments —– whereas it does not in strings with wiggles. In the case of straight strings, we can use the VOS model to describe the evolution of the network's energy density; however, for wiggly strings, the VOS model does not apply in general because the characteristic length differs from the correlation length.

In our approach, we will assume that the VOS model accurately describes the energy density of a network of strings without small-scale structure so that it is always a good description of the bare energy density of the network. In other words, we will always consider strings with the same physical length even if the number of kinks and/or kink sharpness changes, and assume that this length is well described by the VOS model. This is a first approximation to describe the dynamics of networks of wiggly cosmic strings,

other more complex models for describing networks of strings with small-scale structure were proposed in [74–79]. Finally, even though we use the simplest possible model as a first approximation, the wiggly USM we will develop can be used with these more complex models in a very straightforward way in the future.

For simplicity, we consider an odd number of kinks N — the number of subsegments is $N+1$. To determine the total length of a wiggly string segment, let us start by considering the case of a string with one kink.

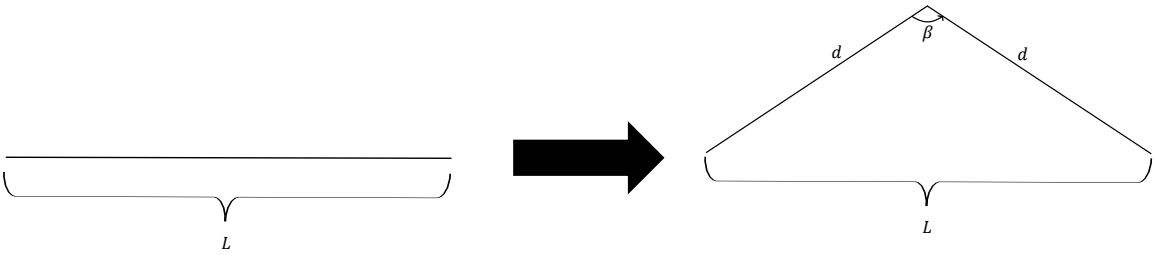

FIGURE 4.1: Transformation of a straight string segment into a segment with 1 kink. The projective length is denoted by L on both sides, while the subsegment length is d. Moreover, $L = 2d$ for a straight segment.

As Fig.4.1 shows, a segment with a kink splits into two straight subsegments with lengths d. These two subsegments meet at an angle that we will refer to as the kink sharpness or simply as β. We can express the relation between L, d and β in the following way:

$$d = \frac{L}{2\sin\left(\beta/2\right)}\,, \tag{4.1}$$

as Fig.4.2 illustrates.

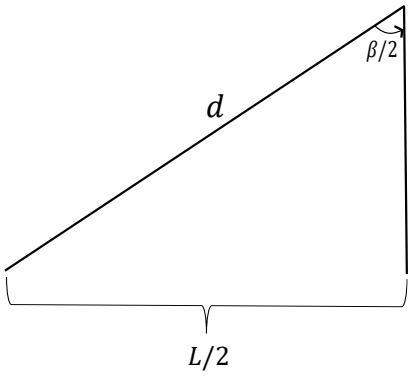

FIGURE 4.2: Relation between d, L and β for a segment with 1 kink.

Before generalizing, consider the case of a string with 3 kinks, illustrated in Fig.4.3.

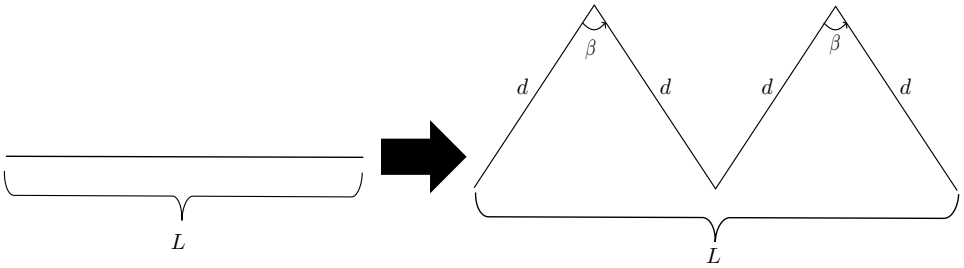

FIGURE 4.3: Transformation of a straight string segment into a segment with 3 kinks. The subsegment length is d, and the projective length is given by L on both sides.

Similarly to the 1-kink case, we consider the configuration illustrated in Fig.4.4.

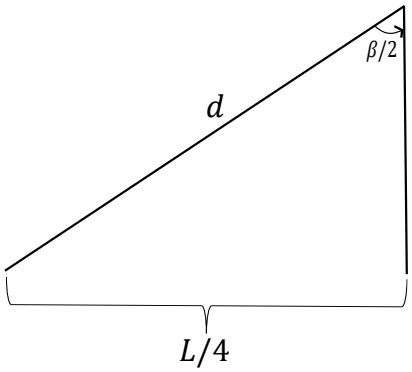

FIGURE 4.4: Relation between d, L and β for a segment with 3 kinks.

Therefore, we can write:

$$d = \frac{L}{4\sin\left(\beta/2\right)}\,. \tag{4.2}$$

At last, now the generalized expression is straightforward and can be written as follows:

$$d = \frac{L}{(N+1)\sin\left(\beta/2\right)}\,. \tag{4.3}$$

Furthermore, a segment with N kinks has $N+1$ straight segments and therefore we can write:

$$L_{Total} = (N+1)d\,. \tag{4.4}$$

Substituting, Eq.(4.3) in Eq.(4.4) we obtain:

$$L_{Total} = \frac{L}{\sin\left(\beta/2\right)}\,, \tag{4.5}$$

which is the total length of the wiggly segments considered here.

Moreover, using Eq.(2.10) we notice that for a wiggly segment:

$$E_s = a\left(\tau\right)\mu_0\gamma\left(N+1\right)d \longrightarrow E_s = a\left(\tau\right)\mu_0\gamma\frac{L}{\sin(\beta/2)}, \tag{4.6}$$

where γ is the Lorentz factor:

$$\gamma = \frac{1}{\sqrt{1-v^2}}\,, \tag{4.7}$$

and where we have used Eq.(4.3) in order to simplify it. We also notice that the energy for this string with wiggles does not depend on the number of kinks, but rather on the sharpness of the kinks. On the other hand, the bare string's energy — which is the energy of the strings excluding kinks/wiggles or other additional degrees of freedom — can be written as follows:

$$E_0 = a\left(\tau\right)\mu_0\gamma L. \tag{4.8}$$

By comparing, Eq.(4.6) and Eq.(4.8) we notice that wiggly segments have larger energy than straight segments, so the energy density of a network composed of wiggly segments will differ from the bare energy density predicted by the VOS model.

Nonetheless, in spite of these differences in energy, changing the wiggliness of the segments does not change the number of strings in the volume considered by the VOS model. Therefore, we will assume that the number of segments is that predicted for a network of bare strings, which can be written as follows:

$$E_0 = V\rho_0 \iff N_s(\tau)\mu_0\zeta = \frac{\mu_0 V}{\zeta^2} \longrightarrow N_s(\tau) = \frac{V}{\zeta^3} \iff n_s(\tau) = \frac{1}{\zeta^3} = \frac{1}{\left(a(\tau)L\right)^3}\,, \tag{4.9}$$

where $N_s(\tau)$ is the total number of strings, V is the simulation volume, and ζ is the correlation length — which, in our assumption, coincides with the projective length.

The total energy density can be written as follows*:

$$\rho = n_s E_s \longrightarrow \rho = \frac{\mu_0}{\left(a\left(\tau\right)L\right)^2\sin(\beta/2)}\,, \tag{4.10}$$

where n_s is the string number density, E_s is the string energy and $0 \leq \beta \leq 2\pi$. Furthermore, comparing Eq.(4.10) and Eq.(3.1) we may notice that the energy density of the network of wiggly strings is larger than the energy density of the network composed of bare strings. Finally, the energy density can be used to define a characteristic length for the wiggly cosmic string network:

$$\rho \equiv \frac{\mu_0}{\left(a\left(\tau\right)L_c\right)^2}\,. \tag{4.11}$$

*The Lorentz factor in Eq.(4.6) was absorbed into the definition of L.

Comparing Eq.(4.10) and Eq.(4.11) we may see that the characteristic length can be written in terms of the kink sharpness and the projective length:

$$L_c^2 = L^2 \sin(\beta/2)\,, \tag{4.12}$$

and is, in general, smaller than the correlation length of the network.

In order to quantify how wiggly the string segments are, we introduce an *effective* string tension, μ_{eff}. The effective string tension is defined in such a way that we have:

$$\rho = \frac{\mu_{eff}}{\big(a(\tau)L\big)^2}\,. \tag{4.13}$$

Substituting Eq.(4.10) in Eq.(4.13) we obtain:

$$\frac{\mu_0}{L^2\sin(\beta/2)} = \frac{\mu_{eff}}{L^2} \longrightarrow \mu_{eff} = \frac{\mu_0}{\sin(\beta/2)}\,. \tag{4.14}$$

From Eq.(4.14), we can see that the effective tension for wiggly segments is larger than μ_0. When $\beta = \pi$, Eq.(4.14) is equal to μ_0 implying that the segment under consideration has no wiggles and is therefore a straight segment, as expected.

4.2 The Stress-Energy Tensor of a String with Kinks

We are missing one component to complete the development of a wiggly USM: the stress-energy tensor of a wiggly cosmic string segment. To compute the stress-energy tensor of a string with kinks, we assume that the string is in the xy-plane, that it behaves as a rigid body — the velocity is the same in each point of the string — with a velocity, $\dot{\mathbf{X}}$, orthogonal to the xy-plane and that kinks do not propagate*. Moreover, the basis of our coordinate system is defined by the following orthogonal unit vectors:

$$\hat{\mathbf{e}}_x = \begin{pmatrix} \sin(\theta)\sin(\phi) \\ -\sin(\theta)\cos(\phi) \\ \cos(\theta) \end{pmatrix}, \tag{4.15}$$

$$\hat{\mathbf{e}}_y = \begin{pmatrix} -\cos(\phi)\sin(\psi) - \cos(\psi)\sin(\phi)\cos(\theta) \\ -\sin(\phi)\sin(\psi) + \cos(\psi)\cos(\phi)\cos(\theta) \\ \sin(\theta)\cos(\psi) \end{pmatrix}, \tag{4.16}$$

*In general, kinks are expected to propagate along the cosmic string.

$$\hat{\mathbf{e}}_z = \begin{pmatrix} \cos(\phi)\cos(\psi) - \sin(\psi)\sin(\phi)\cos(\theta) \\ \sin(\phi)\cos(\psi) + \sin(\psi)\cos(\phi)\cos(\theta) \\ \sin(\theta)\sin(\psi) \end{pmatrix}, \tag{4.17}$$

where θ, ϕ, ψ are attributed randomly in each realization to define the orientation and the velocity of each segment. Additionally, $0 \leq \theta < \pi$ and $0 \leq \phi, \psi < 2\pi$.

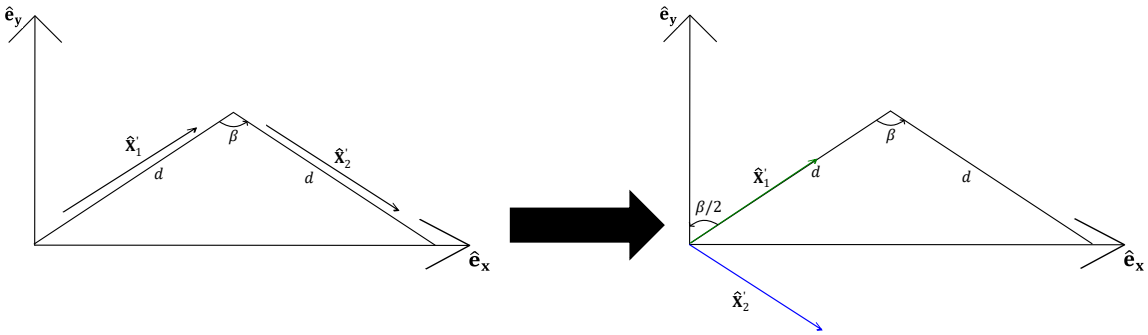

FIGURE 4.5: Illustration of the decomposition of the tangent vectors in terms of the basis vectors.

From Fig.4.5, we see that vectors $\hat{\dot{\mathbf{X}}}$, — which is the unit vector along the direction of the string's velocity — $\hat{\mathbf{X}}'_1$ and $\hat{\mathbf{X}}'_2$ — which are unit vectors with directions tangent to the first and second subsegments, respectively — can be decomposed into the basis defined by the previous vectors as follows:

$$\begin{aligned} \hat{\mathbf{X}}'_1 &= \sin(\beta/2)\hat{\mathbf{e}}_x + \cos(\beta/2)\hat{\mathbf{e}}_y\,, \\ \hat{\mathbf{X}}'_2 &= \sin(\beta/2)\hat{\mathbf{e}}_x - \cos(\beta/2)\hat{\mathbf{e}}_y\,, \\ \hat{\dot{\mathbf{X}}} &= \hat{\mathbf{e}}_z\ . \end{aligned} \tag{4.18}$$

When the vectors are written on a given basis, the transversal gauge should also be verified. As a matter of fact, we have that:

$$\begin{aligned} \hat{\mathbf{X}}'_1 \cdot \hat{\dot{\mathbf{X}}} &= \sin(\beta/2)\hat{\mathbf{e}}_x \cdot \hat{\mathbf{e}}_z + \cos(\beta/2)\hat{\mathbf{e}}_y \cdot \hat{\mathbf{e}}_z = 0\,, \\ \hat{\mathbf{X}}'_2 \cdot \hat{\dot{\mathbf{X}}} &= \sin(\beta/2)\hat{\mathbf{e}}_x \cdot \hat{\mathbf{e}}_z - \cos(\beta/2)\hat{\mathbf{e}}_y \cdot \hat{\mathbf{e}}_z = 0\ . \end{aligned} \tag{4.19}$$

Finally, we are ready to compute the stress-energy tensor for strings with a different number of kinks.

4.2.1 String with 1 Kink

Let us consider a string segment with a kink as illustrated in Fig.4.6. The stress-energy tensor for this configuration may be written as:

$$T^{\mu\nu} = \frac{\mu_0}{\sqrt{-g}}\Bigg[\int\left(\epsilon_1\dot{X}_1^\mu\dot{X}_1^\nu - \epsilon_1^{-1}X_1'^\mu X_1'^\nu\right)\delta_1^{(4)}d\tau d\sigma + \int\left(\epsilon_2\dot{X}_2^\mu\dot{X}_2^\nu - \epsilon_2^{-1}X_2'^\mu X_2'^\nu\right)\delta_2^{(4)}d\tau d\sigma\Bigg], \tag{4.20}$$

where $\delta_j^{(4)} \equiv \delta_j^{(4)}(x_j^\eta - X_j^\eta(\tau,\sigma))$ is a Dirac-delta function and 1 and 2 label each of the strings subsegments.

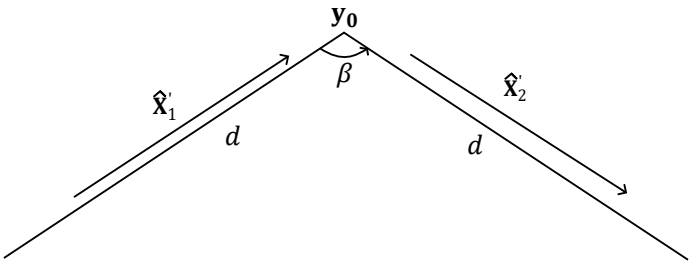

FIGURE 4.6: Illustration of a segment with 1 kink.

Since integrating Eq.(4.20) in real space is difficult, we write the stress-energy tensor in momentum space, which we do by Fourier transforming Eq.(4.20):

$$\Theta^{\mu\nu} = \mu_0\Bigg[\int_{-d}^{0}d\sigma e^{i\mathbf{k}\cdot\mathbf{X}_1}\left(\epsilon_1\dot{X}_1^\mu\dot{X}_1^\nu - \epsilon_1^{-1}X_1'^\mu X_1'^\nu\right) + \int_0^d d\sigma e^{i\mathbf{k}\cdot\mathbf{X}_2}\left(\epsilon_2\dot{X}_2^\mu\dot{X}_2^\nu - \epsilon_2^{-1}X_2'^\mu X_2'^\nu\right)\Bigg], \tag{4.21}$$

where $\mathbf{X}_1$ and $\mathbf{X}_2$ can be parameterized as follows:

$$\mathbf{X}_1 = \mathbf{y}_0 + v\tau\hat{\dot{\mathbf{X}}} + \sigma\hat{\mathbf{X}}_1' \ , \ \mathbf{X}_2 = \mathbf{y}_0 + v\tau\hat{\dot{\mathbf{X}}} + \sigma\hat{\mathbf{X}}_2', \tag{4.22}$$

$\mathbf{y}_0$ is the position of the kink, $v = |\dot{\mathbf{X}}|$ and $\hat{\dot{\mathbf{X}}}_1 = \hat{\dot{\mathbf{X}}}_2 \equiv \hat{\dot{\mathbf{X}}}$ because we assumed that the segment behaves as a rigid body. Moreover, we shall assume, without loss of generality, that $\mathbf{k} = k\hat{\mathbf{e}}_3$, thus Eq.(4.21) reduces to:

$$\Theta^{\mu\nu} = \mu_0 e^{i\left(\mathbf{k}\cdot\mathbf{y}_0 + kv\tau\hat{\dot{\mathbf{X}}}_3\right)}\Bigg[\int_{-d}^{0}d\sigma e^{ik\sigma\hat{\mathbf{X}}_{13}'}\left(\epsilon_1\dot{X}_1^\mu\dot{X}_1^\nu - \epsilon_1^{-1}X_1'^\mu X_1'^\nu\right) + \int_0^d d\sigma e^{ik\sigma\hat{\mathbf{X}}_{23}'}\left(\epsilon_2\dot{X}_2^\mu\dot{X}_2^\nu - \epsilon_2^{-1}X_2'^\mu X_2'^\nu\right)\Bigg]. \tag{4.23}$$

The real-part of the "00"-component of Eq.(4.23) — for a detailed computation check appendix A — can be written as follows:

$$\Re\left(\Theta^{00}\right) = \mu_0\gamma\left[\cos(A)\left(\frac{\sin(B_1)}{k\hat{\mathbf{X}}'_{13}} + \frac{\sin(B_2)}{k\hat{\mathbf{X}}'_{23}}\right) + \sin(A)\left(\frac{\hat{\mathbf{X}}'_{23} - \hat{\mathbf{X}}'_{13}}{k\hat{\mathbf{X}}'_{23}\hat{\mathbf{X}}'_{13}} + \frac{\cos(B_2)}{k\hat{\mathbf{X}}'_{23}} - \frac{\cos(B_1)}{k\hat{\mathbf{X}}'_{13}}\right)\right], \tag{4.24}$$

where

$$A = \mathbf{k}\cdot\mathbf{y}_0 + kv\tau\hat{\hat{\mathbf{X}}}_{\mathbf{3}}\ ,\ B_1 = kd\hat{\mathbf{X}}'_{13}\ ,\ B_2 = kd\hat{\mathbf{X}}'_{23}\,. \tag{4.25}$$

4.2.2 String with 3 Kinks

For a string with three kinks, we basically translate the structure in Fig. 4.6 once, creating the configuration shown in Fig.4.7.

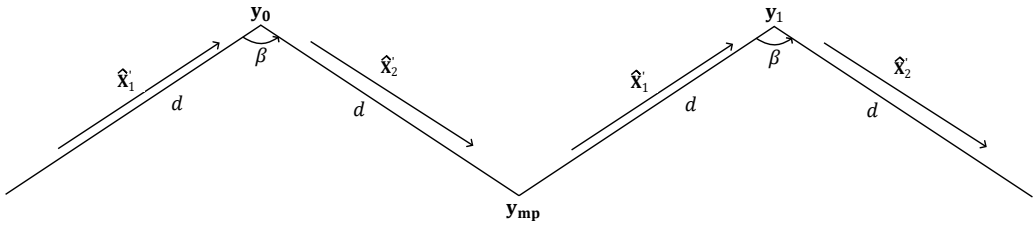

FIGURE 4.7: Illustration of a segment with 3 kinks.

Basically, we can regard this case as two strings with one kink located at different points. In this case, the stress-energy tensor can be written as:

$$T^{\mu\nu} = \frac{\mu_0}{\sqrt{-g}}\sum_{j=1}^{4}\left[\int\left(\epsilon_j\dot{X}_j^{\mu}\dot{X}_j^{\nu} - \epsilon_j^{-1}X_j'^{\mu}X_j'^{\nu}\right)\delta_j^{(4)}d\tau d\sigma\right]. \tag{4.26}$$

The Fourier transformed stress-energy tensor can be written as follows:

$$\Theta^{\mu\nu} = \mu_0\sum_{m=0}^{1}\left[\int_{-d}^{0}d\sigma e^{i\mathbf{k}\cdot\mathbf{X}_{2m+1}}\left(\epsilon_{2m+1}\dot{X}^{\mu}_{2m+1}\dot{X}^{\nu}_{2m+1} - \epsilon^{-1}_{2m+1}X'^{\mu}_{2m+1}X'^{\nu}_{2m+1}\right) + \int_{0}^{d}d\sigma e^{i\mathbf{k}\cdot\mathbf{X}_{2m+2}}\left(\epsilon_{2m+2}\dot{X}^{\mu}_{2m+2}\dot{X}^{\nu}_{2m+2} - \epsilon^{-1}_{2m+2}X'^{\mu}_{2m+2}X'^{\nu}_{2m+2}\right)\right], \tag{4.27}$$

where $\mathbf{X}_j$, with $j = 1,2,3,4$, can be parameterized as follows:

$$\begin{aligned}\mathbf{X}_1 &= \mathbf{y}_0 + v\tau\hat{\hat{\mathbf{X}}} + \sigma\hat{\mathbf{X}}'_1\,,\ \mathbf{X}_2 = \mathbf{y}_0 + v\tau\hat{\hat{\mathbf{X}}} + \sigma\hat{\mathbf{X}}'_2\,,\\ \mathbf{X}_3 &= \mathbf{y}_1 + v\tau\hat{\hat{\mathbf{X}}} + \sigma\hat{\mathbf{X}}'_1\,,\ \mathbf{X}_4 = \mathbf{y}_1 + v\tau\hat{\hat{\mathbf{X}}} + \sigma\hat{\mathbf{X}}'_2\,,\end{aligned} \tag{4.28}$$

and $\mathbf{y}_0$ and $\mathbf{y}_1$ are the positions of the kinks. Furthermore, the tangent vectors of the first and third segments are equal, as well as the tangent vectors of the second and fourth

segments. As in the previous case, we set $\mathbf{k} = k\hat{\mathbf{e}}_3$ then Eq.(4.27) simplifies to:

$$\Theta^{\mu\nu} = \mu_0 \sum_{m=0}^{1} e^{i\left(\mathbf{k}\cdot\mathbf{y}_m + kv\tau\hat{\mathbf{X}}_3\right)} \left[\int_{-d}^{0} d\sigma e^{ik\sigma\hat{\mathbf{X}}'_{13}} \left(\epsilon_{2m+1}\dot{X}^{\mu}_{2m+1}\dot{X}^{\nu}_{2m+1} - \epsilon^{-1}_{2m+1}X'^{\,\mu}_{2m+1}X'^{\,\nu}_{2m+1} \right) \right.$$
$$\left. + \int_{0}^{d} d\sigma e^{ik\sigma\hat{\mathbf{X}}'_{23}} \left(\epsilon_{2m+2}\dot{X}^{\mu}_{2m+2}\dot{X}^{\nu}_{m+2} - \epsilon^{-1}_{2m+2}X'^{\,\mu}_{2m+2}X'^{\,\nu}_{2m+2} \right) \right]. \tag{4.29}$$

As we have stated before, essentially we are dealing with two segments with one kink at different positions, therefore the "00"-component of Eq.(4.29) will be the sum of the contributions of two strings with one kink Eq.(4.24) located at $\mathbf{y}_0$ and at $\mathbf{y}_1$ — for more details see appendix A. We then have that:

$$\begin{aligned} \Re\left(\Theta^{00}\right) =& \mu_0\gamma \left[\cos(A_0) + \cos(A_1) \right] \left(\frac{\sin(B_1)}{k\hat{\mathbf{X}}'_{13}} + \frac{\sin(B_2)}{k\hat{\mathbf{X}}'_{23}} \right) \\ &+ \left[\sin(A_0) + \sin(A_1) \right] \left(\frac{\hat{\mathbf{X}}'_{23} - \hat{\mathbf{X}}'_{13}}{k\hat{\mathbf{X}}'_{23}\hat{\mathbf{X}}'_{13}} + \frac{\cos(B_2)}{k\hat{\mathbf{X}}'_{23}} - \frac{\cos(B_1)}{k\hat{\mathbf{X}}'_{13}} \right), \end{aligned} \tag{4.30}$$

where

$$A_{j-1} = \mathbf{k}\cdot\mathbf{y}_{j-1} + kv\tau\hat{\mathbf{X}}_3\,,\ B_j = kd\hat{\mathbf{X}}'_{j3} \text{ with } j = 1,2\,. \tag{4.31}$$

In order to simplify Eq.(4.30), let us rewrite it in terms of the position of the kink located at the middle point $\mathbf{y}_{mp}$. From Fig.4.7, we see that $\mathbf{y}_0$ and $\mathbf{y}_1$ may be written as:

$$\mathbf{y}_j = \mathbf{y_{mp}} - (-1)^j d\hat{\mathbf{X}}'_{2-j}\,,\ \text{with } j = 0,1. \tag{4.32}$$

Substituting in the definition of A_0 and A_1, we obtain:

$$A_{2-j} = A_{mp} - (-1)^j dk\hat{\mathbf{X}}'_{j3}\,,\ \text{with } j = 1,2, \tag{4.33}$$

where

$$A_{mp} = \mathbf{k}\cdot\mathbf{y_{mp}} + v\tau\hat{\mathbf{X}}_3\,. \tag{4.34}$$

Consequently, Eq.(4.30) can be written as follows:

$$\begin{aligned} \Re\left(\Theta^{00}\right) =& \mu_0\gamma \left[\cos(A_{mp} - dk\hat{\mathbf{X}}'_{23}) + \cos(A_{mp} + dk\hat{\mathbf{X}}'_{13}) \right] \left(\frac{\sin(B_1)}{k\hat{\mathbf{X}}'_{13}} + \frac{\sin(B_2)}{k\hat{\mathbf{X}}'_{23}} \right) \\ &+ \mu_0\gamma \left[\sin(A_{mp} - dk\hat{\mathbf{X}}'_{23}) + \sin(A_{mp} + dk\hat{\mathbf{X}}'_{13}) \right] \left(\frac{\hat{\mathbf{X}}'_{23} - \hat{\mathbf{X}}'_{13}}{k\hat{\mathbf{X}}'_{23}\hat{\mathbf{X}}'_{13}} + \frac{\cos(B_2)}{k\hat{\mathbf{X}}'_{23}} - \frac{\cos(B_1)}{k\hat{\mathbf{X}}'_{13}} \right). \end{aligned} \tag{4.35}$$

Furthermore, we can decompose $\hat{\mathbf{X}}'_{13}$ and $\hat{\mathbf{X}}'_{23}$ in terms of the basis vectors Eq.(4.18) and thus Eq.(4.35) can be expressed as:

$$\begin{aligned}\Re\left(\Theta^{00}\right) = 2\mu_0\gamma\cos\left(\frac{L}{4}\mathbf{k}\cdot\hat{\mathbf{e}}_x\right)\Bigg[&\cos\left(A'_{mp}\right)\left(\frac{\sin(B_1)}{k\hat{\mathbf{X}}'_{13}}+\frac{\sin(B_2)}{k\hat{\mathbf{X}}'_{23}}\right)\\&+\sin\left(A'_{mp}\right)\left(\frac{\hat{\mathbf{X}}'_{23}-\hat{\mathbf{X}}'_{13}}{k\hat{\mathbf{X}}'_{23}\hat{\mathbf{X}}'_{13}}+\frac{\cos(B_2)}{k\hat{\mathbf{X}}'_{23}}-\frac{\cos(B_1)}{k\hat{\mathbf{X}}'_{13}}\right)\Bigg],\end{aligned} \tag{4.36}$$

where we defined $A'_{mp} = A_{mp} + d\mathbf{k}\cdot\left(\cos(\beta/2)\hat{\mathbf{e}}_y\right)$. For more details see appendix A.

4.2.3 String with 5 Kinks

A string with 5 kinks can be regarded as 3 strings with one kink located in different positions. An illustration of a string with 5 kinks can be found in Fig.4.8.

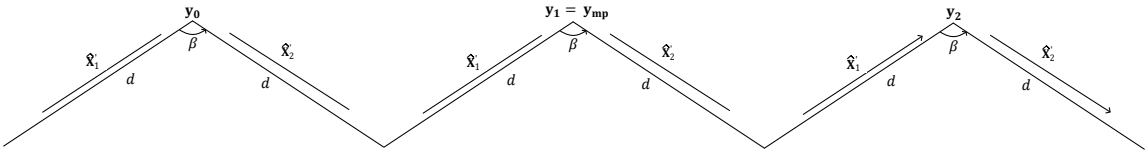

FIGURE 4.8: Illustration of a segment with 5 kinks.

Proceeding as in the previous sections, we can write the Fourier transform for the string with 5 kinks:

$$\begin{aligned}\Theta^{\mu\nu} = \mu_0\sum_{m=0}^{2}\Bigg[&\int_{-d}^{0}d\sigma e^{i\mathbf{k}\cdot\mathbf{X}_{2m+1}}\left(\epsilon_{2m+1}\dot{X}^{\mu}_{2m+1}\dot{X}^{\nu}_{2m+1}-\epsilon^{-1}_{2m+1}X'^{\,\mu}_{2m+1}X'^{\,\nu}_{2m+1}\right)\\&+\int_{0}^{d}d\sigma e^{i\mathbf{k}\cdot\mathbf{X}_{2m+2}}\left(\epsilon_{2m+2}\dot{X}^{\mu}_{2m+2}\dot{X}^{\nu}_{2m+2}-\epsilon^{-1}_{2m+2}X'^{\,\mu}_{2m+2}X'^{\,\nu}_{2m+2}\right)\Bigg],\end{aligned} \tag{4.37}$$

where $\mathbf{X}_j$, with $j = 1,2,3,4,5,6$, can be written as follows:

$$\begin{aligned}&\mathbf{X}_1 = \mathbf{y}_0 + v\tau\hat{\dot{\mathbf{X}}} + \sigma\hat{\mathbf{X}}'_1\,,\ \mathbf{X}_2 = \mathbf{y}_0 + v\tau\hat{\dot{\mathbf{X}}} + \sigma\hat{\mathbf{X}}'_2\,,\ \mathbf{X}_3 = \mathbf{y}_1 + v\tau\hat{\dot{\mathbf{X}}} + \sigma\hat{\mathbf{X}}'_1\,,\\&\mathbf{X}_4 = \mathbf{y}_1 + v\tau\hat{\dot{\mathbf{X}}} + \sigma\hat{\mathbf{X}}'_2\,,\ \mathbf{X}_5 = \mathbf{y}_2 + v\tau\hat{\dot{\mathbf{X}}} + \sigma\hat{\mathbf{X}}'_1\,,\ \mathbf{X}_6 = \mathbf{y}_2 + v\tau\hat{\dot{\mathbf{X}}} + \sigma\hat{\mathbf{X}}'_2\,.\end{aligned} \tag{4.38}$$

As in the previous sections, we set $\mathbf{k} = k\hat{\mathbf{e}}_3$ therefore Eq.(4.37) simplifies to:

$$\begin{aligned}\Theta^{\mu\nu} = \mu_0\sum_{m=0}^{2}e^{i\left(\mathbf{k}\cdot\mathbf{y}_m + kv\tau\hat{\dot{\mathbf{X}}}_3\right)}\Bigg[&\int_{-d}^{0}d\sigma e^{ik\sigma\hat{\mathbf{X}}'_{13}}\left(\epsilon_{2m+1}\dot{X}^{\mu}_{2m+1}\dot{X}^{\nu}_{2m+1}-\epsilon^{-1}_{2m+1}X'^{\,\mu}_{2m+1}X'^{\,\nu}_{2m+1}\right)\\&+\int_{0}^{d}d\sigma e^{ik\sigma\hat{\mathbf{X}}'_{23}}\left(\epsilon_{2m+2}\dot{X}^{\mu}_{2m+2}\dot{X}^{\nu}_{m+2}-\epsilon^{-1}_{2m+2}X'^{\,\mu}_{2m+2}X'^{\,\nu}_{2m+2}\right)\Bigg].\end{aligned} \tag{4.39}$$

which is the sum of the contributions of the stress-energy tensor of 3 different strings with one kink, located at $\mathbf{y}_0$, $\mathbf{y}_1$ and $\mathbf{y}_2$, and thus Eq.(4.39) has the solution:

$$\begin{aligned}\Re\left(\Theta^{00}\right) =&\mu_0\gamma\left[\cos(A_0)+\cos(A_1)+\cos(A_2)\right]\left(\frac{\sin(B_1)}{k\hat{\mathbf{X}}'_{13}}+\frac{\sin(B_2)}{k\hat{\mathbf{X}}'_{23}}\right)\\ &+\mu_0\gamma\left[\sin(A_0)+\sin(A_1)+\sin(A_2)\right]\left(\frac{\hat{\mathbf{X}}'_{23}-\hat{\mathbf{X}}'_{13}}{k\hat{\mathbf{X}}'_{23}\hat{\mathbf{X}}'_{13}}+\frac{\cos(B_2)}{k\hat{\mathbf{X}}'_{23}}-\frac{\cos(B_1)}{k\hat{\mathbf{X}}'_{13}}\right),\end{aligned} \tag{4.40}$$

where

$$A_{i-1}=\mathbf{k}\cdot\mathbf{y}_{i-1}+kv\tau\hat{\hat{\mathbf{X}}}_{\mathbf{3}}\,,\ B_j=kd\hat{\mathbf{X}}'_{j3}\ \text{with}\ i=1,2,3\,;\ j=1,2\,. \tag{4.41}$$

In order to simplify Eq.(4.40), we need write $\mathbf{y}_0$, $\mathbf{y}_1$, $\mathbf{y}_2$ and $\mathbf{y}_3$ in terms of $\mathbf{y}_{mp}$. From Fig.4.8, we can see that:

$$\mathbf{y}_0=\mathbf{y}_{mp}-\frac{L}{3}\hat{\mathbf{e}}_{\mathbf{x}}\,,\ \mathbf{y}_1=\mathbf{y}_{mp}\,,\ \mathbf{y}_2=\mathbf{y}_{mp}+\frac{L}{3}\hat{\mathbf{e}}_{\mathbf{x}}\,, \tag{4.42}$$

thus A_0, A_1 and A_2 can be rewritten as:

$$A_j=A_{mp}+(j-1)\frac{L}{3}\mathbf{k}\cdot\hat{\mathbf{e}}_{\mathbf{x}}\,,\ j=0,1,2\,, \tag{4.43}$$

where A_{mp} has the same definition as before (Eq.(4.34)).

Using the quantities defined above Eq.(4.40) may be written as:

$$\begin{aligned}\Re\left(\Theta^{00}\right)=\mu_0\gamma\left(1+2\cos\left(\frac{L}{3}\mathbf{k}\cdot\hat{\mathbf{e}}_{\mathbf{x}}\right)\right)&\left[\cos\left(A_{mp}\right)\left(\frac{\sin(B_1)}{k\hat{\mathbf{X}}'_{13}}+\frac{\sin(B_2)}{k\hat{\mathbf{X}}'_{23}}\right)\right.\\ &\left.+\sin\left(A_{mp}\right)\left(\frac{\hat{\mathbf{X}}'_{23}-\hat{\mathbf{X}}'_{13}}{k\hat{\mathbf{X}}'_{23}\hat{\mathbf{X}}'_{13}}+\frac{\cos(B_2)}{k\hat{\mathbf{X}}'_{23}}-\frac{\cos(B_1)}{k\hat{\mathbf{X}}'_{13}}\right)\right].\end{aligned} \tag{4.44}$$

4.2.4 String with 7 Kinks

As in the previous cases, a string with 7 kinks can be thought of as four strings with one kink at different locations (see Fig.4.9).

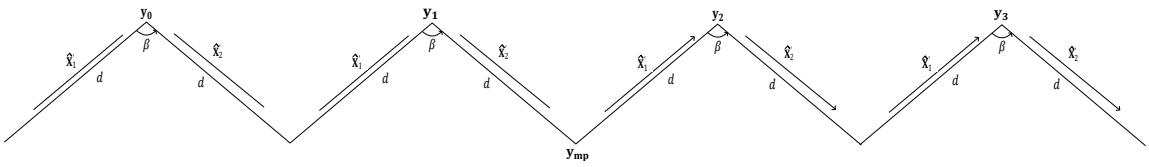

FIGURE 4.9: Illustration of a segment with 7 kinks.

Proceeding as before, we can write the Fourier transformed stress-energy tensor for this case as:

$$\begin{aligned}\Theta^{\mu\nu} = \mu_0 \sum_{m=0}^{3} \Bigg[\int_{-d}^{0} d\sigma e^{i\mathbf{k}\cdot\mathbf{X}_{2m+1}} \left(\epsilon_{2m+1} \dot{X}^{\mu}_{2m+1} \dot{X}^{\nu}_{2m+1} - \epsilon^{-1}_{2m+1} X'^{\mu}_{2m+1} X'^{\nu}_{2m+1} \right) \\ + \int_{0}^{d} d\sigma e^{i\mathbf{k}\cdot\mathbf{X}_{2m+2}} \left(\epsilon_{2m+2} \dot{X}^{\mu}_{2m+2} \dot{X}^{\nu}_{2m+2} - \epsilon^{-1}_{2m+2} X'^{\mu}_{2m+2} X'^{\nu}_{2m+2} \right) \Bigg] ,\end{aligned} \tag{4.45}$$

where $\mathbf{X}_j$, with $j = 1,2,3,4,5,6,7,8$, can be expressed as:

$$\begin{aligned}&\mathbf{X}_1 = \mathbf{y}_0 + v\tau\hat{\dot{\mathbf{X}}} + \sigma\hat{\mathbf{X}}'_1 \,,\ \mathbf{X}_2 = \mathbf{y}_0 + v\tau\hat{\dot{\mathbf{X}}} + \sigma\hat{\mathbf{X}}'_2 \,,\ \mathbf{X}_3 = \mathbf{y}_1 + v\tau\hat{\dot{\mathbf{X}}} + \sigma\hat{\mathbf{X}}'_1 \,, \\ &\mathbf{X}_4 = \mathbf{y}_1 + v\tau\hat{\dot{\mathbf{X}}} + \sigma\hat{\mathbf{X}}'_2 \,,\ \mathbf{X}_5 = \mathbf{y}_2 + v\tau\hat{\dot{\mathbf{X}}} + \sigma\hat{\mathbf{X}}'_1 \,,\ \mathbf{X}_6 = \mathbf{y}_2 + v\tau\hat{\dot{\mathbf{X}}} + \sigma\hat{\mathbf{X}}'_2 \,, \\ &\mathbf{X}_7 = \mathbf{y}_3 + v\tau\hat{\dot{\mathbf{X}}} + \sigma\hat{\mathbf{X}}'_1 \,,\ \mathbf{X}_8 = \mathbf{y}_3 + v\tau\hat{\dot{\mathbf{X}}} + \sigma\hat{\mathbf{X}}'_2 \,.\end{aligned} \tag{4.46}$$

As in the previous sections, we set $\mathbf{k} = k\hat{\mathbf{e}}_3$ then Eq.(4.45) simplifies to:

$$\begin{aligned}\Theta^{\mu\nu} = \mu_0 \sum_{m=0}^{3} e^{i\left(\mathbf{k}\cdot\mathbf{y}_m + kv\tau\hat{\dot{\mathbf{X}}}_3\right)} \Bigg[\int_{-d}^{0} d\sigma e^{ik\sigma\hat{\mathbf{X}}'_{13}} \left(\epsilon_{2m+1} \dot{X}^{\mu}_{2m+1} \dot{X}^{\nu}_{2m+1} - \epsilon^{-1}_{2m+1} X'^{\mu}_{2m+1} X'^{\nu}_{2m+1} \right) \\ + \int_{0}^{d} d\sigma e^{ik\sigma\hat{\mathbf{X}}'_{23}} \left(\epsilon_{2m+2} \dot{X}^{\mu}_{2m+2} \dot{X}^{\nu}_{m+2} - \epsilon^{-1}_{2m+2} X'^{\mu}_{2m+2} X'^{\nu}_{2m+2} \right) \Bigg] .\end{aligned} \tag{4.47}$$

which is the stress-energy tensor of a string with one kink, located at $\mathbf{y}_0$, $\mathbf{y}_1$, $\mathbf{y}_2$ and $\mathbf{y}_3$. Furthermore, Eq.(4.47) has the following solution:

$$\begin{aligned}\Re\left(\Theta^{00}\right) =& \mu_0\gamma \Big[\cos(A_0) + \cos(A_1) + \cos(A_2) + \cos(A_3) \Big] \left(\frac{\sin(B_1)}{k\hat{\mathbf{X}}'_{13}} + \frac{\sin(B_2)}{k\hat{\mathbf{X}}'_{23}} \right) \\ &+ \mu_0\gamma \Big[\sin(A_0) + \sin(A_1) + \sin(A_2) + \sin(A_3) \Big] \left(\frac{\hat{\mathbf{X}}'_{23} - \hat{\mathbf{X}}'_{13}}{k\hat{\mathbf{X}}'_{23}\hat{\mathbf{X}}'_{13}} + \frac{\cos(B_2)}{k\hat{\mathbf{X}}'_{23}} - \frac{\cos(B_1)}{k\hat{\mathbf{X}}'_{13}} \right) ,\end{aligned} \tag{4.48}$$

where

$$A_{i-1} = \mathbf{k}\cdot\mathbf{y}_{i-1} + kv\tau\hat{\dot{\mathbf{X}}}_{\mathbf{3}} \,,\ B_j = kd\hat{\mathbf{X}}'_{j3} \text{ with } i = 1,2,3,4 \,;\ j = 1,2 \,. \tag{4.49}$$

As in the previous cases, let us write $\mathbf{y}_0$, $\mathbf{y}_1$, $\mathbf{y}_2$ and $\mathbf{y}_3$ in terms of $\mathbf{y}_{mp}$. Using Fig.4.9 it is straightforward to see that:

$$\begin{aligned}&\mathbf{y}_0 = \mathbf{y}_{mp} - d\hat{\mathbf{X}}'_2 - \frac{L}{4}\hat{\mathbf{e}}_{\mathbf{x}} \,,\ \mathbf{y}_1 = \mathbf{y}_{mp} - d\hat{\mathbf{X}}'_2 \\ &\mathbf{y}_2 = \mathbf{y}_{mp} + d\hat{\mathbf{X}}'_1 \,,\ \mathbf{y}_3 = \mathbf{y}_{mp} + d\hat{\mathbf{X}}'_1 + \frac{L}{4}\hat{\mathbf{e}}_{\mathbf{x}} \,,\end{aligned} \tag{4.50}$$

Therefore, we can write A_0, A_1, A_2 and A_3 as:

$$\begin{aligned} A_j &= A_{mp} - d\hat{\mathbf{X}}'_{m3} - (j-1)\,\frac{L}{4}\mathbf{k}\cdot\hat{\mathbf{e}}_{\mathbf{x}}\,,\ j=0,1;\ m=2\,,\\ A_j &= A_{mp} + d\hat{\mathbf{X}}'_{m3} + (j-2)\,\frac{L}{4}\mathbf{k}\cdot\hat{\mathbf{e}}_{\mathbf{x}}\,,\ j=2,3;\ m=1\,, \end{aligned} \tag{4.51}$$

where A_{mp} is defined in Eq.(4.34). We then have that (for more details, see appendix A):

$$\begin{aligned} \Re\left(\Theta^{00}\right) =& 2\mu_0\gamma\left(\cos\left(\frac{L}{8}\mathbf{k}\cdot\hat{\mathbf{e}}_{\mathbf{x}}\right)+\cos\left(\frac{3L}{8}\mathbf{k}\cdot\hat{\mathbf{e}}_{\mathbf{x}}\right)\right)\left[\cos\left(A_{mp}\right)\left(\frac{\sin(B_1)}{k\hat{\mathbf{X}}'_{13}}+\frac{\sin(B_2)}{k\hat{\mathbf{X}}'_{23}}\right)\right.\\ &\left.+\sin\left(A_{mp}\right)\left(\frac{\hat{\mathbf{X}}'_{23}-\hat{\mathbf{X}}'_{13}}{k\hat{\mathbf{X}}'_{23}\hat{\mathbf{X}}'_{13}}+\frac{\cos(B_2)}{k\hat{\mathbf{X}}'_{23}}-\frac{\cos(B_1)}{k\hat{\mathbf{X}}'_{13}}\right)\right]. \end{aligned} \tag{4.52}$$

4.2.5 Generalization to a String with N kinks

We have computed the temporal component of the stress-energy tensor for a string with 1, 3, 5, and 7 kinks in previous sections; now it is straightforward to write the "00"-component of the stress-energy tensor for a string with an arbitrary odd number N of kinks:

$$\begin{aligned} \Re\left(\Theta^{00}\right) = \mu_0\gamma F(N)&\left[\cos\left(A_{mp}\right)\left(\frac{\sin(B_1)}{k\hat{\mathbf{X}}'_{13}}+\frac{\sin(B_2)}{k\hat{\mathbf{X}}'_{23}}\right)\right.\\ &\left.+\sin\left(A_{mp}\right)\left(\frac{\hat{\mathbf{X}}'_{23}-\hat{\mathbf{X}}'_{13}}{k\hat{\mathbf{X}}'_{23}\hat{\mathbf{X}}'_{13}}+\frac{\cos(B_2)}{k\hat{\mathbf{X}}'_{23}}-\frac{\cos(B_1)}{k\hat{\mathbf{X}}'_{13}}\right)\right], \end{aligned} \tag{4.53}$$

where

$$F(N) = \begin{cases} 2\sum_{q=0}^{(N-3)/4}\cos\left((2q+1)\frac{L}{N+1}\mathbf{k}\cdot\hat{\mathbf{e}}_x\right), \text{if } (N-1)/2 \text{ is odd}\,,\\ 1+2\sum_{q=1}^{(N-1)/4}\cos\left((2q)\frac{L}{N+1}\mathbf{k}\cdot\hat{\mathbf{e}}_x\right), \text{if } (N-1)/2 \text{ is even}\,. \end{cases} \tag{4.54}$$

Note that the summations in Eq.(4.54), can be computed analytically (see appendix B for a detailed demonstration):

$$2\left(\sum_{q=0}^{(N-3)/4}\cos\left((2q+1)\frac{L}{N+1}\mathbf{k}\cdot\hat{\mathbf{e}}_x\right)\right) = \frac{\sin\left(\frac{L}{2}\mathbf{k}\cdot\hat{\mathbf{e}}_x\right)}{\sin\left(\frac{L}{N+1}\mathbf{k}\cdot\hat{\mathbf{e}}_x\right)}\ \text{(Odd term)}, \tag{4.55}$$

$$\left(1+2\left(\sum_{q=1}^{(N-1)/4}\cos\left((2q)\frac{L}{N+1}\mathbf{k}\cdot\hat{\mathbf{e}}_x\right)\right)\right) = \frac{\sin\left(\frac{L}{2}\mathbf{k}\cdot\hat{\mathbf{e}}_x\right)}{\sin\left(\frac{L}{N+1}\mathbf{k}\cdot\hat{\mathbf{e}}_x\right)}\ \text{(Even term)}. \tag{4.56}$$

This means that we can compute the total stress-energy tensor without explicitly summing over each subsegment or resorting to a consolidation analogous to Eq.(3.25). As a result,

we can consider an arbitrarily large number of kinks without losing accuracy or increasing computational cost.

As we can see, the summations for the even term and the odd term yield exactly the same result. Therefore, we may write the temporal component of the stress-energy tensor in the following closed form:

$$\begin{aligned}\Theta^{00} =&\mu_0\gamma\frac{\sin\left(\frac{L}{2}\mathbf{k}\cdot\hat{\mathbf{e}}_x\right)}{\sin\left(\frac{L}{N+1}\mathbf{k}\cdot\hat{\mathbf{e}}_x\right)}\Bigg\{\cos\left(A_{mp}\right)\left[\frac{\sin\left(dk\hat{\mathbf{X}}'_{13}\right)}{k\hat{\mathbf{X}}'_{13}}+\frac{\sin\left(dk\hat{\mathbf{X}}'_{23}\right)}{k\hat{\mathbf{X}}'_{23}}\right]\\&+\sin\left(A_{mp}\right)\left[\frac{\hat{\mathbf{X}}'_{23}-\hat{\mathbf{X}}'_{13}}{k\hat{\mathbf{X}}'_{13}\hat{\mathbf{X}}'_{23}}+\frac{\cos\left(dk\hat{\mathbf{X}}'_{23}\right)}{k\hat{\mathbf{X}}'_{23}}-\frac{\cos\left(dk\hat{\mathbf{X}}'_{13}\right)}{k\hat{\mathbf{X}}'_{13}}\right]\Bigg\},\end{aligned} \tag{4.57}$$

where

$$A_{mp}=\begin{cases}\mathbf{k}\cdot\mathbf{y_{mp}}+kv\tau\hat{\mathbf{X}}_{\mathbf{3}}\,, & \text{if } (N-1)/2 \text{ even}\\ \mathbf{k}\cdot\mathbf{y_{mp}}+kv\tau\hat{\mathbf{X}}_{\mathbf{3}}+d\cos(\beta/2)\mathbf{k}\cdot\hat{\mathbf{e}}_y\,, & \text{if } (N-1)/2 \text{ odd}\,.\end{cases} \tag{4.58}$$

Finally, for a string with N kinks, the spatial components of the stress-energy tensor can be written as follows:

$$\Theta^{ij}=\sum_{T=1}^{2}\left[v^2\hat{\mathbf{X}}_{Ti}\hat{\mathbf{X}}_{Tj}-\left(1-v^2\right)\hat{\mathbf{X}}'_{Ti}\hat{\mathbf{X}}'_{Tj}\right]\Theta^{00}_{(T)}\,, \tag{4.59}$$

where, for numerical implementation purposes, we have separated the contributions of the segments with tangent $\mathbf{X}'_1$ and $\mathbf{X}'_2$. Moreover, $\Theta^{00}_{(T)}$ may be written as:

$$\begin{aligned}\Theta^{00}_{(T)} =\mu_0\gamma&\frac{\sin\left(\frac{L}{2}\mathbf{k}\cdot\hat{\mathbf{e}}_x\right)}{\sin\left(\frac{L}{N+1}\mathbf{k}\cdot\hat{\mathbf{e}}_x\right)}\Bigg\{\cos\left(A_{mp}\right)\left[\frac{\sin\left(dk\hat{\mathbf{X}}'_{T3}\right)}{k\hat{\mathbf{X}}'_{T3}}\right]\\&+(-1)^{T+1}\sin\left(A_{mp}\right)\left[\frac{1}{k\hat{\mathbf{X}}'_{T3}}-\frac{\cos\left(dk\hat{\mathbf{X}}'_{T3}\right)}{k\hat{\mathbf{X}}'_{T3}}\right]\Bigg\},\ T=1,2\,.\end{aligned} \tag{4.60}$$

Finally, the scalar, vector, and tensor components of the stress-energy tensor (4.60) are given, respectively, by:

$$\begin{aligned}\Theta_S&=\left(2\Theta^{33}-\Theta^{11}-\Theta^{22}\right)/2\,,\\ \Theta_V&=\Theta^{13}_V\,,\\ \Theta_T&=\Theta^{12}_T\,.\end{aligned} \tag{4.61}$$

By imposing local energy-momentum conservation [48], the traces $\Theta=\Theta_{ii}$ and the velocity field $\Theta^D=\Theta_{03}$ are fixed.

Chapter 5

CMB Anisotropies Generated by Wiggly Cosmic Strings

In order to compute the CMB anisotropies generated by wiggly cosmic strings, we modified the publicly available numerical tool CMBACT [53, 73], — which is a code based on CMBFAST [63] that computes the CMB anisotropies generated by active sources — by changing the stress-energy tensor to describe segments with kinks (Eq.(4.59)).

In this section, we will present the CMB anisotropies and the linear Cold Dark Matter (CDM) power spectrum generated by the modified CMBACT. The CMB anisotropies are characterized by the angular power spectrum:

$$C_\ell \equiv \frac{1}{2\ell+1} \sum_{m=-\ell}^{\ell} \langle a_{\ell m}^* a_{\ell m} \rangle \,, \tag{5.1}$$

where $\langle\rangle$ represents the ensemble average. The a_{lm} are the coefficients of the decomposition of the temperatures anisotropies in terms of spherical harmonics functions $Y_{\ell m}(\hat{\mathbf{r}})$:

$$\frac{\Delta T}{T}(\hat{\mathbf{r}}) = \sum_{\ell=0}^{\infty} \sum_{m=-\ell}^{\ell} a_{\ell m} Y_{\ell m}(\hat{\mathbf{r}}) \,, \tag{5.2}$$

where $\hat{\mathbf{r}}$ is the direction along the line of sight.

The linear CDM power spectrum is defined as:

$$P(k) = \Delta(\mathbf{k}) \,, \tag{5.3}$$

where $\Delta(\mathbf{k})$ is the Fourier transform of the density contrast

$$\Delta(\mathbf{x}) = \frac{\rho_m(\mathbf{x}) - \langle \rho_m \rangle}{\langle \rho_m \rangle} \,, \tag{5.4}$$

where ρ_m is the matter density at the position $\mathbf{x}$ and $\langle\rho_m\rangle$ is its average value.

Finally, our results are averaged over 500 realizations of a wiggly cosmic string network with the updated cosmological parameters given by the Planck mission [6] and string tension is fixed to $G\mu_0 = 10^{-7}$.

5.1 Wiggly string network in the straight string limit

When the kink sharpness is $\beta = \pi$, the segment becomes straight, and thus the expression for the straight string should be recovered in this limit. Moreover, in this limit $\hat{\mathbf{e}}_x = \hat{\mathbf{X}}_1' = \hat{\mathbf{X}}_2' \equiv \hat{\mathbf{X}}'$, $A_{mp} = \mathbf{k}\cdot\mathbf{y_{mp}} + kv\tau\hat{\mathbf{X}}_3$, regardless of whether $(N-1)/2$ is odd or even, the position of the middle point, $\mathbf{y}_{mp}$, coincides with the position of the center of mass, $\mathbf{x}_0$, and $d = L/(N+1)$. When $\beta = \pi$, Eq.(4.60) then reduces to:

$$\begin{aligned}
\Theta^{00} =& \mu_0\gamma\frac{\sin\left(\frac{L}{2}\mathbf{k}\cdot\hat{\mathbf{X}}'\right)}{\sin\left(\frac{L}{N+1}\mathbf{k}\cdot\hat{\mathbf{X}}'\right)}\left\{\cos\left(A_{mp}\right)\left[\frac{\sin\left(dk\hat{\mathbf{X}}_3'\right)}{k\hat{\mathbf{X}}_3'}+\frac{\sin\left(dk\hat{\mathbf{X}}_3'\right)}{k\hat{\mathbf{X}}_3'}\right]\right.\\
&\left.+\sin\left(A_{mp}\right)\left[\frac{\hat{\mathbf{X}}_3'-\hat{\mathbf{X}}_3'}{k\hat{\mathbf{X}}_3'\hat{\mathbf{X}}_3'}+\frac{\cos\left(dk\hat{\mathbf{X}}_3'\right)}{k\hat{\mathbf{X}}_3'}-\frac{\cos\left(dk\hat{\mathbf{X}}_3'\right)}{k\hat{\mathbf{X}}_3'}\right]\right\}\\
=&\mu_0\gamma\frac{\sin\left(\frac{L}{2}\hat{\mathbf{X}}_3'\right)}{\sin\left(\frac{L}{N+1}k\hat{\mathbf{X}}_3'\right)}\cos\left(A_{mp}\right)\left[\frac{\sin\left(\frac{L}{N+1}k\hat{\mathbf{X}}_3'\right)}{k\hat{\mathbf{X}}_3'/2}\right]\\
=&\mu_0\gamma\cos\left(\mathbf{k}\cdot\mathbf{x_0}+kv\tau\hat{\mathbf{X}}_3'\right)\frac{\sin\left(\frac{L}{2}k\hat{\mathbf{X}}_3'\right)}{k\hat{\mathbf{X}}_3'/2}\,,
\end{aligned}\tag{5.5}$$

which is the stress-energy tensor of a straight cosmic string segment [48, 53].

In order to compute the CMB anisotropies and the linear CDM power spectrum generated by a network of strings with N kinks, we first modify the CMBACT code to include the contribution of the stress-energy tensor presented in Eq. (4.59). We anticipate, for $\beta = \pi$, the linear CDM power spectrum and the CMB anisotropies generated by both models to be identical. So, this instance serves as a test for our numerical implementation of the wiggly USM.

For the sake of simplicity, from now on, we will refer to the modified CMBACT as WCMBACT and to the original CMBACT as CMBACT.

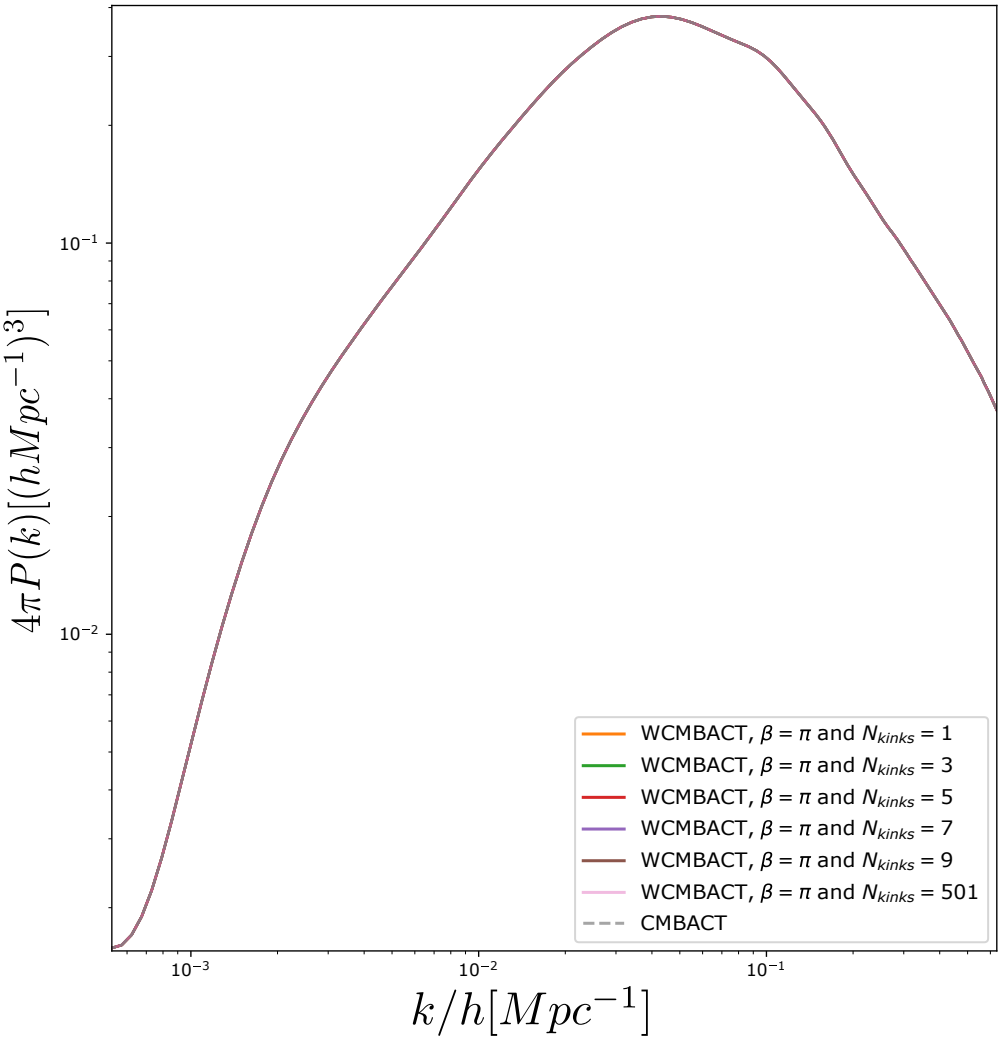

FIGURE 5.1: Linear CDM power spectrum generated by a cosmic string network with a different number of kinks and sharpness equal to π, compared with the original CMBACT code. In both cases, we averaged over 500 realizations of cosmic string networks.

The linear CDM power spectrum generated by the original and modified codes are, indeed, identical as shown in Fig.5.1. Furthermore, we see that the number of kinks has no effect on the linear CDM power spectrum when the kink sharpness is π.

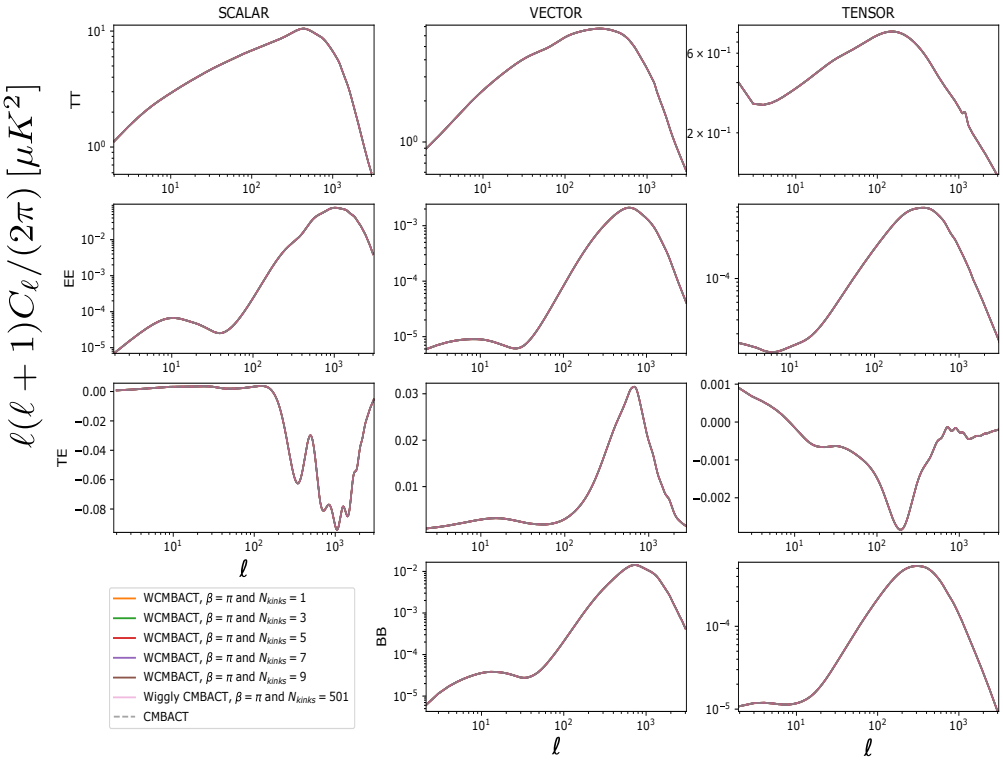

FIGURE 5.2: CMB anisotropies generated by a cosmic string network with a different number of kinks and sharpness equal to π, compared with the original CMBACT code. For both cases, we averaged over 500 realizations of cosmic string networks.

As we can see in Fig.5.2, the anisotropies generated by different models — with a different number of kinks — are completely overlapped, because we set the kink sharpness to π. This behavior was expected because the anisotropies are generated by solving the Einstein-Boltzmann equations, in which we select the source to be the stress-energy tensor of the configuration of a cosmic string — a string with kinks (wiggly string) and a straight string — and the stress-energy tensor is the same when $\beta = \pi$.

5.2 Impact of kink sharpness on the CMB anisotropies

In Eq.(4.3), we see that the subsegment length is dependent on the number of kinks, N, and the kink sharpness, β. To investigate the effect of kink sharpness on the CMB anisotropies, we first fix the number of kinks and vary the kink sharpness. By inspecting Eq.(4.3), we can see that the subsegment length will increase as $\beta \to 0$.

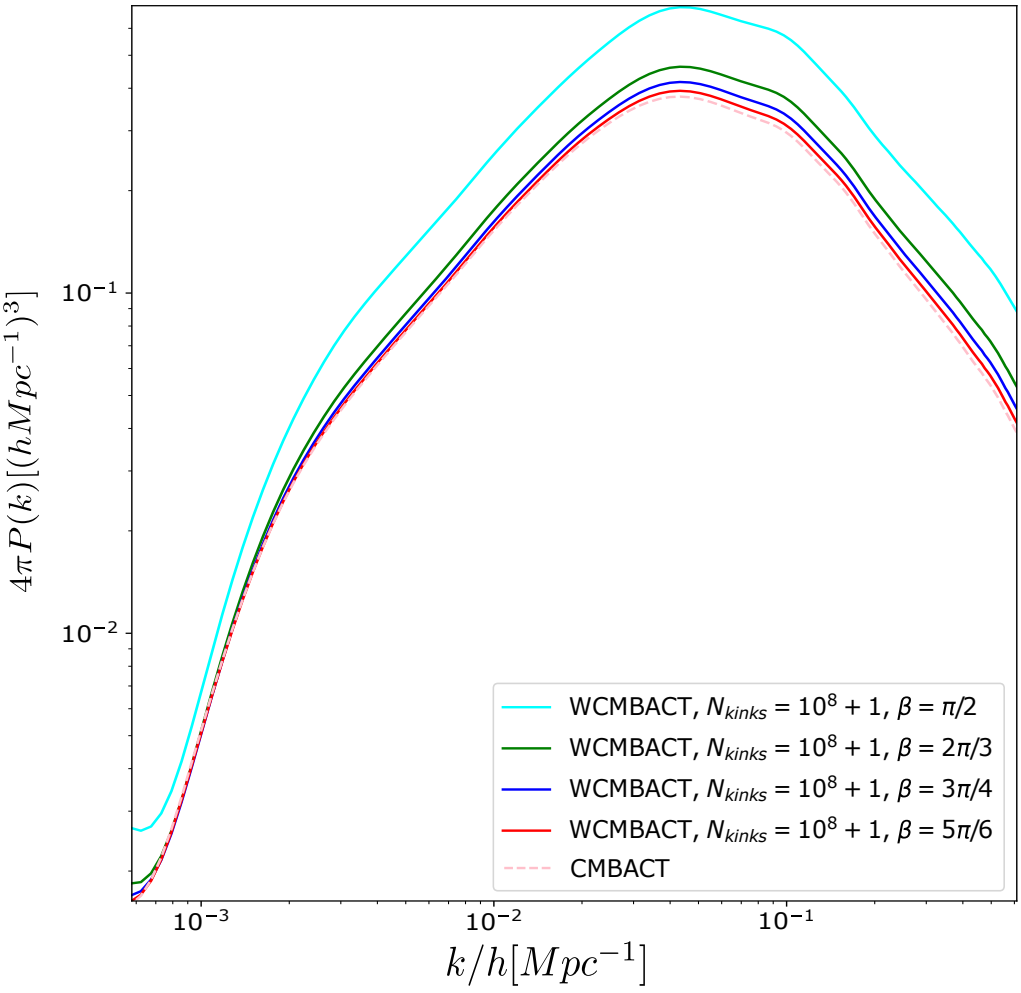

FIGURE 5.3: Linear CDM Power Spectrum generated by the CMBACT code and by the WCMBACT code, for different values of the kink sharpness equal to or greater than $\pi/2$. We chose $G\mu_0 = 10^{-7}$ and averaged over 500 realizations of cosmic strings network realizations.

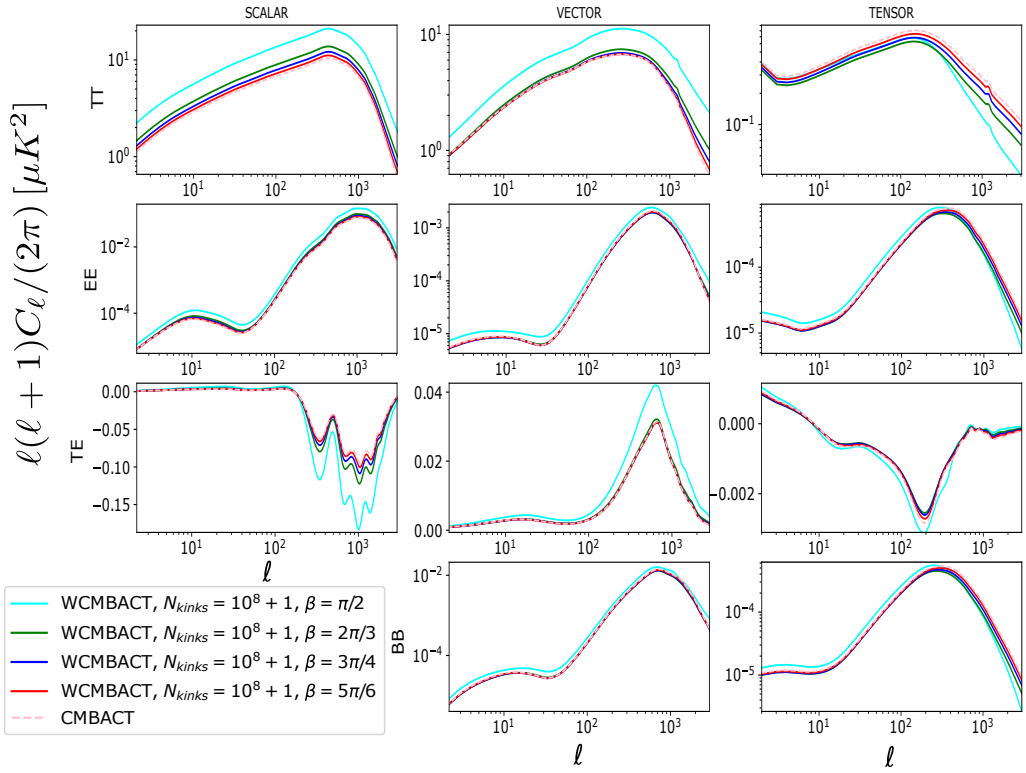

FIGURE 5.4: CMB anisotropies produced by the CMBACT code as well as the WCMBACT code, for different values of the kink sharpness equal to or greater than $\pi/2$. We chose $G\mu_0 = 10^{-7}$ and averaged over 500 realizations of cosmic strings network realizations.

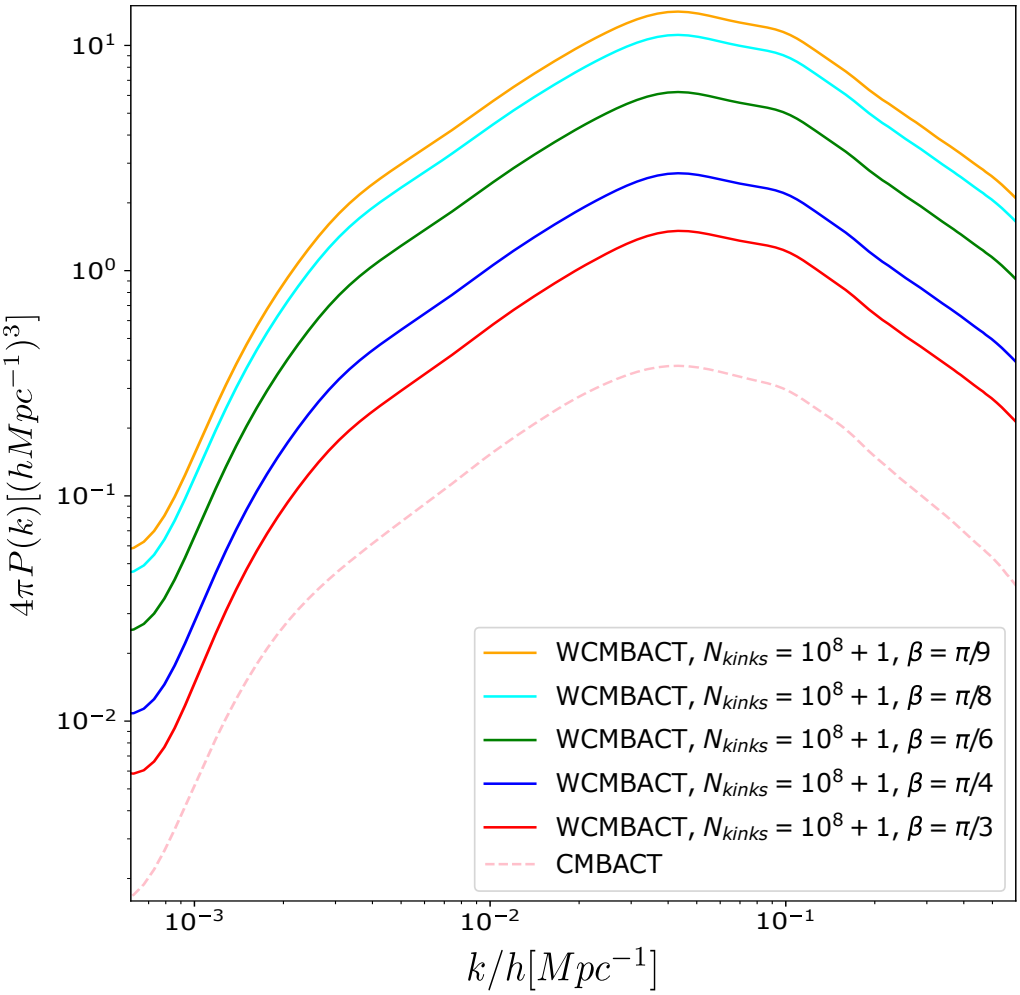

FIGURE 5.5: Linear CDM Power Spectrum generated by the CMBACT code and by the WCMBACT code, for different values of the kink sharpness smaller than $\pi/2$. Finally, we chose $G\mu_0 = 10^{-7}$ and averaged over 500 realizations of cosmic strings network realizations.

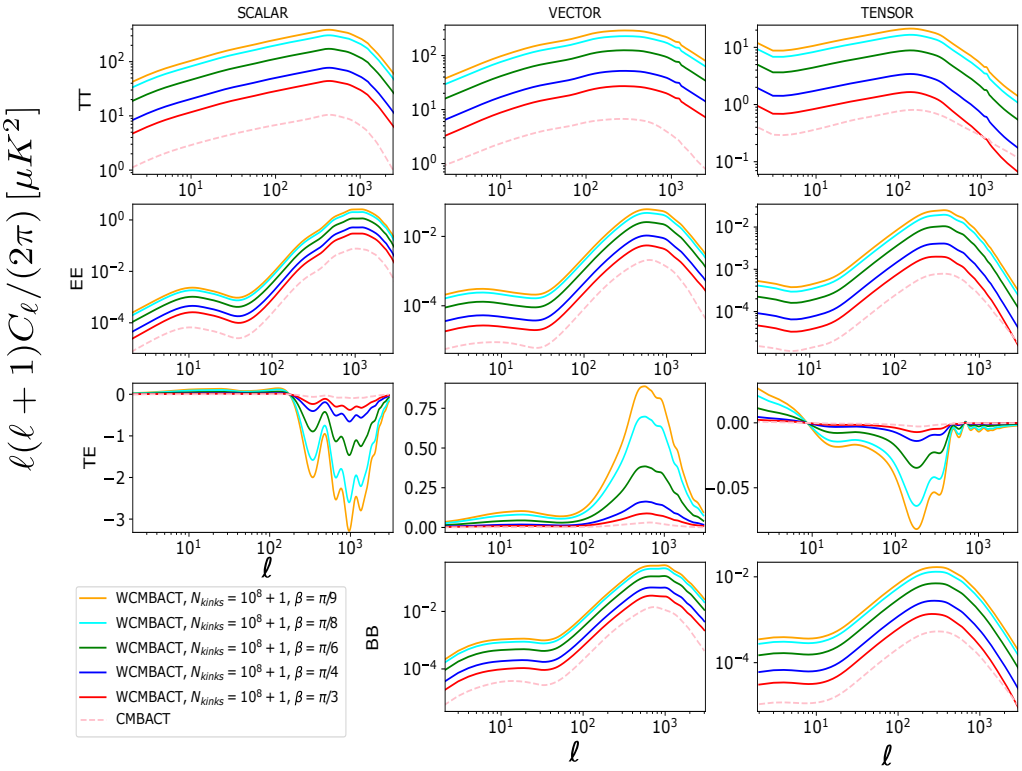

FIGURE 5.6: CMB anisotropies produced by the CMBACT code as well as the WCMBACT code, for different values of the kink sharpness smaller than $\pi/2$. We chose $G\mu_0 = 10^{-7}$ and averaged over 500 realizations of cosmic strings network realizations.

As could be expected, and as we can see in Figs.5.3 and 5.5, a higher energy density of the network, when we decrease β, enhances the amplitude of the power spectrum. Moreover, the amplitude of the CMB anisotropies also increases with the increase of the kink sharpness (or a decrease of β), as is shown in Figs.5.4 and 5.6.

In order to better understand how the shape of the power spectrum and CMB anisotropies are affected when we change the sharpness of the kinks, we normalize the plots to unity at large-scales (i.e. in the first point of each graph).

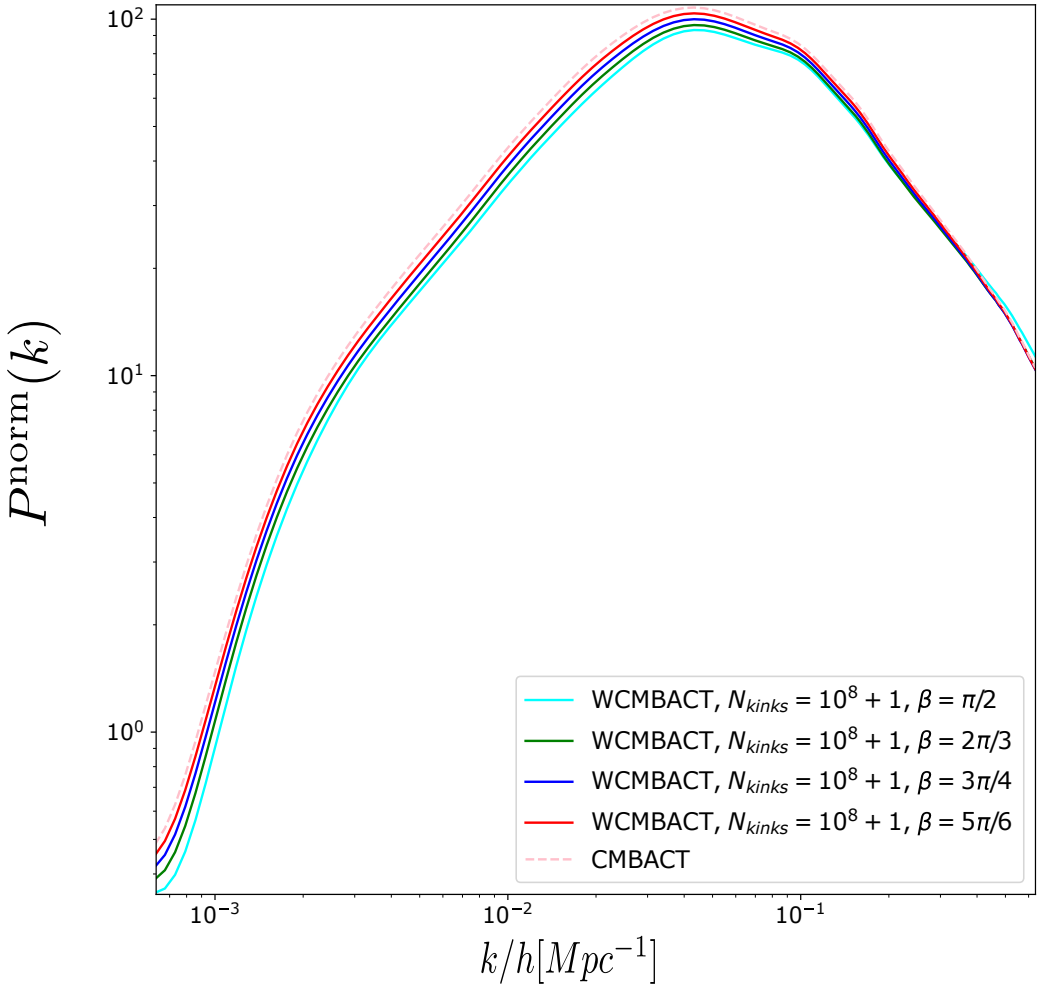

FIGURE 5.7: CMB anisotropies produced by the CMBACT code as well as the WCMBACT code, normalized to unity, with kink sharpeness equal to or greater than $\pi/2$. We chose $G\mu_0 = 10^{-7}$ and averaged over 500 realizations of cosmic strings network realizations.

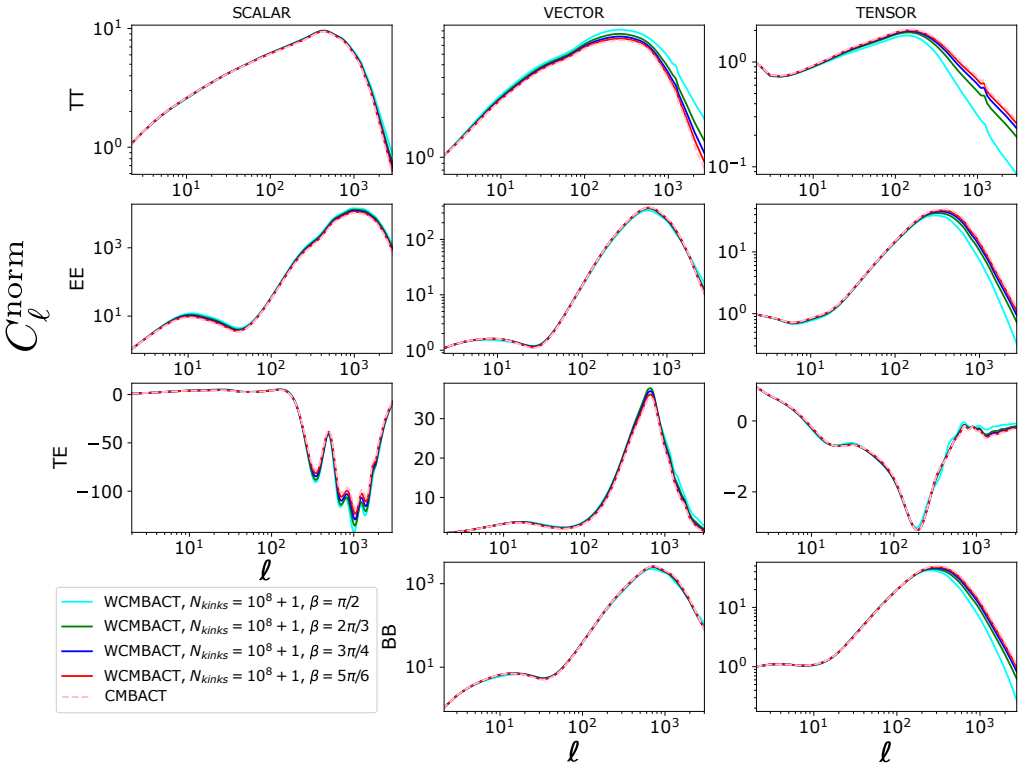

FIGURE 5.8: CMB anisotropies produced by the CMBACT code as well as the WCMBACT code, normalized to unity, with kink sharpeness equal to or greater than $\pi/2$. We chose $G\mu_0 = 10^{-7}$ and averaged over 500 realizations of cosmic strings network realizations.

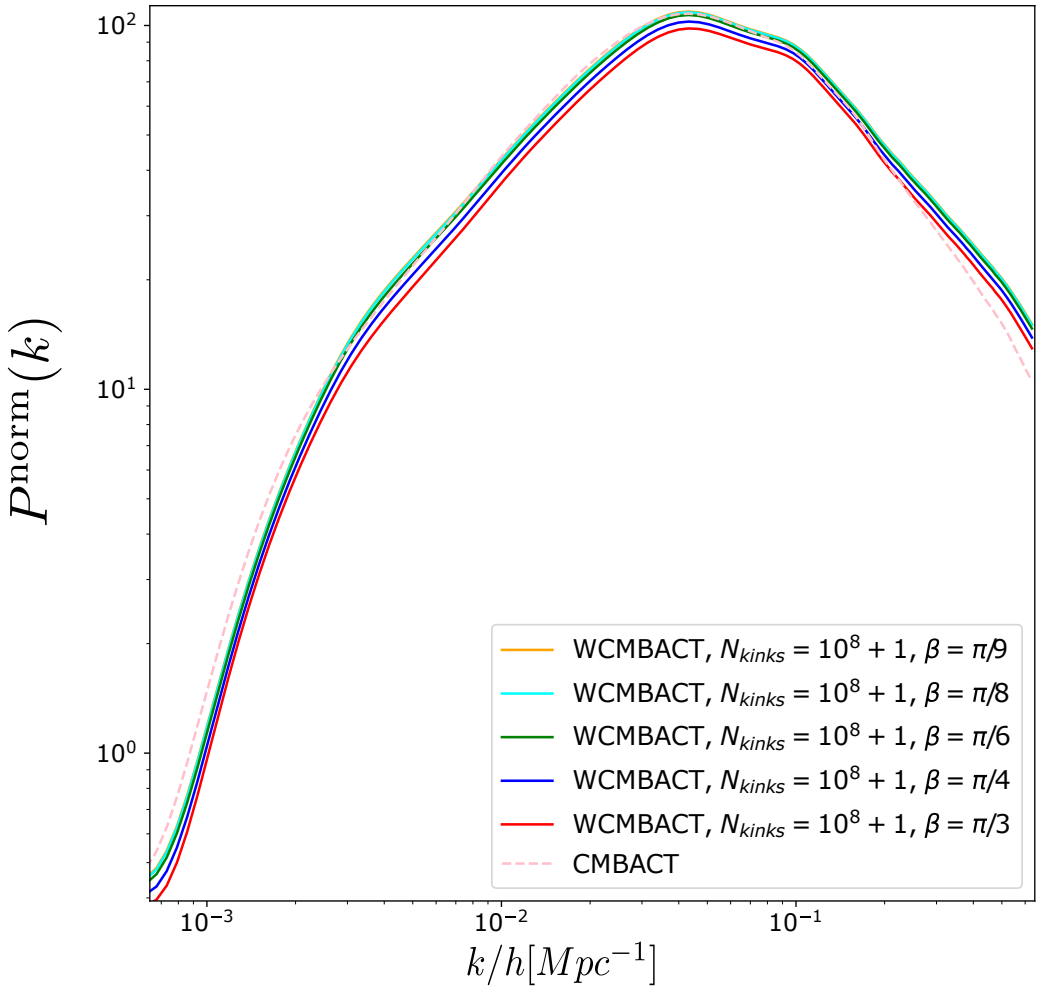

FIGURE 5.9: CMB anisotropies produced by the CMBACT code as well as the WCMBACT code, normalized to unity, with kink sharpeness smaller than $\pi/2$. We chose $G\mu_0 = 10^{-7}$ and averaged over 500 realizations of cosmic strings network realizations and normalized the plots to unity.

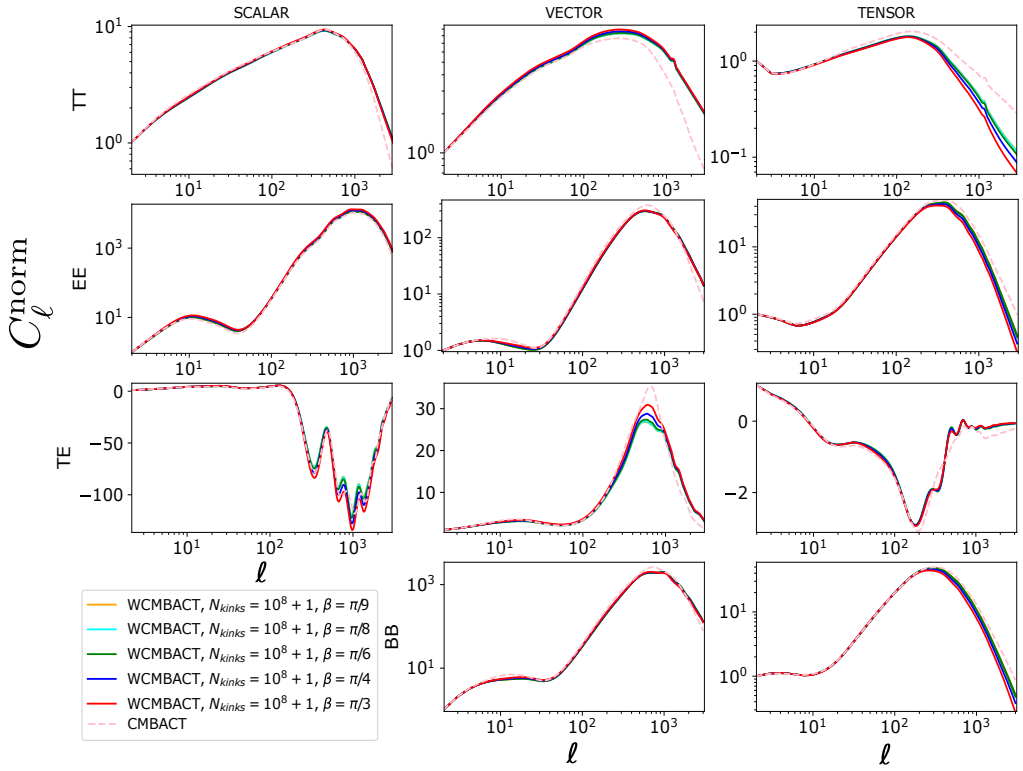

FIGURE 5.10: CMB anisotropies produced by the CMBACT code as well as the WCMBACT code, normalized to unity, with kink sharpeness smaller than $\pi/2$. We chose $G\mu_0 = 10^{-7}$ and averaged over 500 realizations of cosmic strings network realizations and normalized the plots to unity.

When the β is equal to or greater than $\pi/2$, Fig.5.7, the maximum relative amplitude of the linear CDM power spectrum seems to decrease. In fact, this happens for most of the power spectrum, except on small scales — or large k. Therefore, we may say that there is a shift in power from large scales to small scales as the string becomes wiggly, which can be explained by our approach. When we make strings wiggly we introduce a new scale to the cosmic string network — the subsegment length — that is smaller than its correlation length in this limit. This then results in a relative increase of the contribution on small scales.

On the other hand, when β is smaller than $\pi/2$, Fig.5.9, the maximum relative amplitude seems to increase over all scales. Nonetheless, on large scales — small k — the relative amplitude is still smaller than that generated by straight strings. Generally speaking, we may say the peak of the power spectrum, in this case, becomes more prominent and a bit

broader. This may be explained by the fact that, as we decrease sharpness, we are making subsegments longer, thus increasing slightly the power on larger scales.

Regarding the CMB anisotropies: when β is equal to or greater than $\pi/2$, Fig.5.8, we may see that the shapes of the TT and EE scalar power spectra do not seem to differ significantly from that generated by straight strings, — even though there is a slight relative increase on small-scales — whereas the shape of the vector and tensor contributions change. The relative amplitude of the vector component increases over all scales, but very prominently on small scales. This may be explained by the string configuration — illustrated in, for example, Fig.4.6. That configuration assumes a pointy kink, which may result in vortical motions of matter and thus increase the relative amplitude of the vector component.

On the other hand, the relative amplitude of the tensor component decreases as kink sharpness increases. This decrease seems to be more prominent for small scales, but, as we will see in the next section, this may not be the full picture. The shape of the cross-correlation power spectrum TE is also not significantly affected and it is also most affected on small scales.

Finally, for the B-mode polarization, the shape of the vector component stays roughly the same, whilst the relative amplitude of the tensor component decreases on small scales in a similar way as the rest of the other tensor components.

The picture changes somewhat when we consider β smaller than $\pi/2$, as illustrated in Fig.5.10. In the TT anisotropies, we see that the shape of the scalar modes seems to stabilize and that changing the kink sharpness does not cause further changes to the shape of the spectrum. This behavior is also present on small scales for the vector modes, although there seems to be a slight increase of the relative amplitude on intermediate scales that leads to higher relative peak amplitude. At last, the tensor modes seem to increase the relative amplitude contribution on small scales, when we decrease β below $\pi/2$. However, this relative amplitude is still smaller than that predicted for straight strings. On top of that, the plots show that this increase "decelerates" and the shape of the spectrum seems to maintain its shape once the kinks are sharp enough.

The TE and EE anisotropies behave similarly, excluding the scalar mode. The relative amplitude of the scalar component of the EE anisotropy decreases, while that of TE anisotropy increases as we decrease the kink sharpness. The vector modes decrease on all scales, except on very small scales, where the spectra seem to also stabilize, which leads to

a smaller relative amplitude of the peaks. The tensor modes behave similarly to what we see for the TT spectrum.

In BB anisotropies, the shape of the vector modes is not significantly affected by the kink sharpness increasing. The tensor component, on large scales, increases until it saturates.

Finally, for a different number of kinks, we have verified that these components behave roughly the same.

5.3 Impact of the number of kinks on the CMB anisotropies

To investigate the impact of the number of kinks on the CMB anisotropies, let us start by setting kink sharpness to $\pi/9$, $\pi/2$, and $4\pi/5$ and varying the number of kinks in the string segments.

Regarding the linear CDM power spectrum, Figs.5.11, 5.12 and 5.13, we notice that beyond a given point, it does not seem to matter much if we increase the number of kinks or not, since its shape and amplitude is not significantly affected. However, the number of kinks for which this stabilization happens is different in each figure.

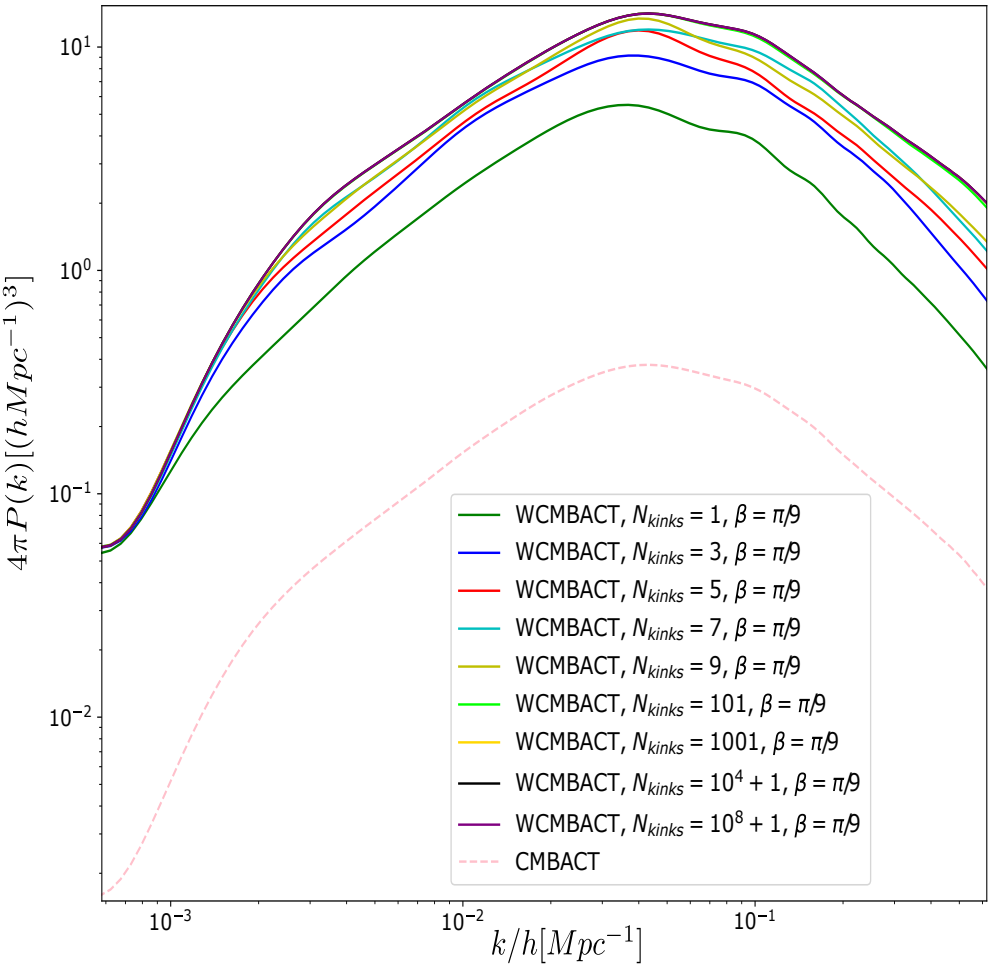

FIGURE 5.11: Linear CDM Power Spectrum generated by the CMBACT code and by the WCMBACT code, where the kink sharpness is fixed ($\beta = \pi/9$) and we vary the number of kinks. We chose $G\mu_0 = 10^{-7}$ and averaged over 500 realizations of cosmic strings network realizations.

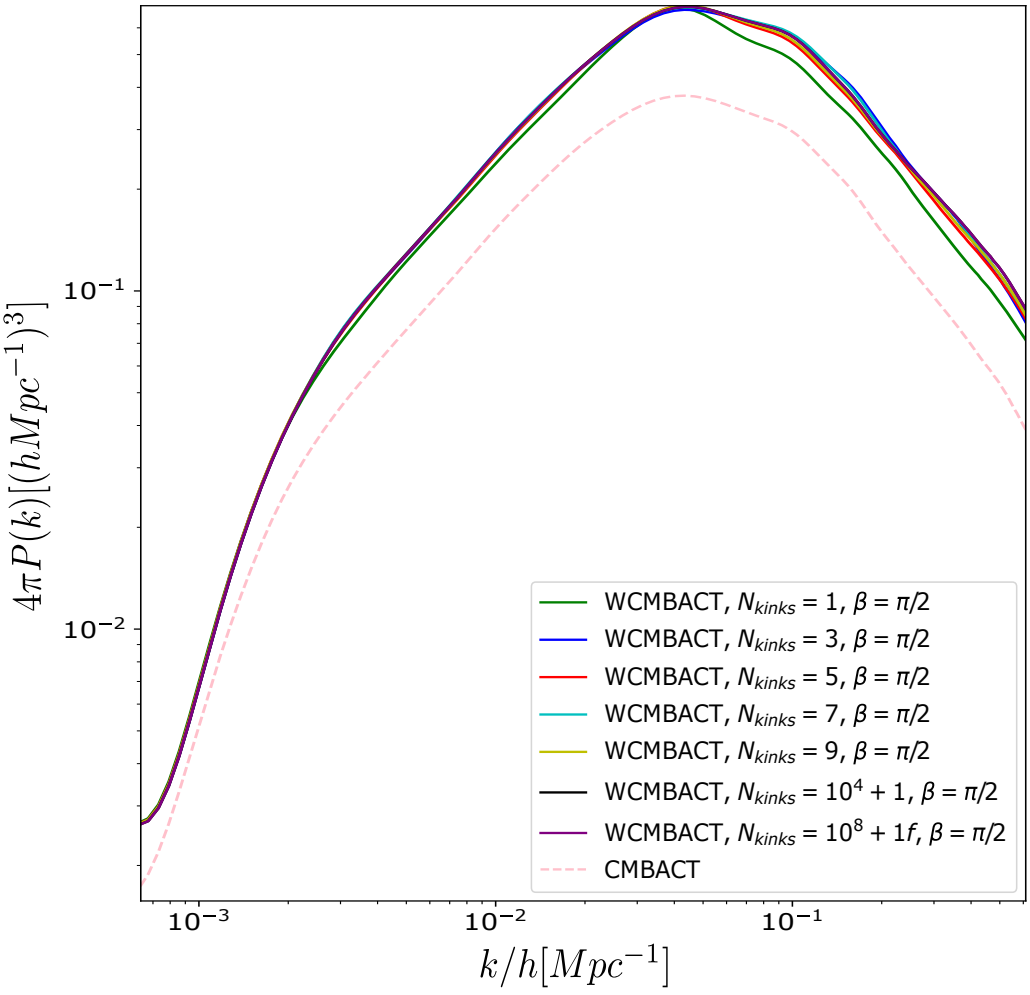

FIGURE 5.12: Linear CDM Power Spectrum generated by the CMBACT code and by the WCMBACT code, where the kink sharpness is fixed ($\beta = \pi/2$) and we vary the number of kinks. We chose $G\mu_0 = 10^{-7}$ and averaged over 500 realizations of cosmic strings network realizations.

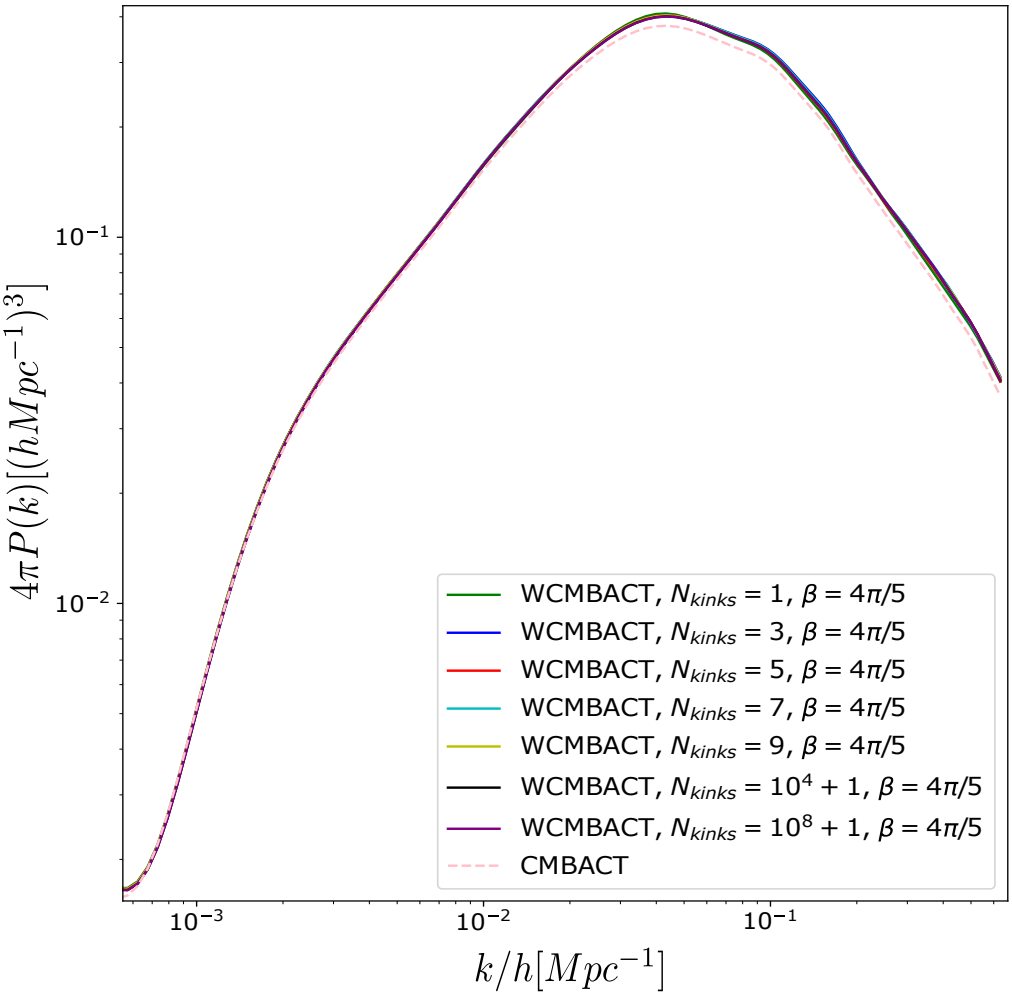

FIGURE 5.13: Linear CDM Power Spectrum generated by the CMBACT code and by the WCMBACT code, where the kink sharpness is fixed ($\beta = 4\pi/5$) and we vary the number of kinks. We chose $G\mu_0 = 10^{-7}$ and averaged over 500 realizations of cosmic strings network realizations.

This may be explained by the fact that, when we make strings wiggly, we introduce a new scale — corresponding to the length of the subsegment — such that:

$$\frac{L}{(N+1)\sin(\beta/2)} = d < L_c < L\,. \tag{5.6}$$

When we increase the number of kinks, we are increasing the number of subsegments — for reference, see Figs. 4.1 and 4.3 — and, therefore, we are adding power to the corresponding lengthscale. Moreover, as we increase the number of kinks, the segments become smaller and this contribution shifts towards smaller scales. Depending on kink sharpness, this

added power may be noticeable in different scales of the spectra. For instance, if $\beta = \pi/9$ and $N = 9$ we obtain:

$$d \approx 0.58L\,, \tag{5.7}$$

which implies that we are adding power around the scale of the peak — the peak of the spectrum corresponds to scales around the average distance between strings (or correlation length) [80]. Furthermore, if we maintain the angle and increase N to 1001, we get:

$$d \approx 0.0058L << L_c < L\,, \tag{5.8}$$

which corresponds to an increase on small scales, beyond the range of the spectrum. Therefore, we can conclude that with the increase in the number of kinks there is an enhancement of power on increasingly smaller scales.

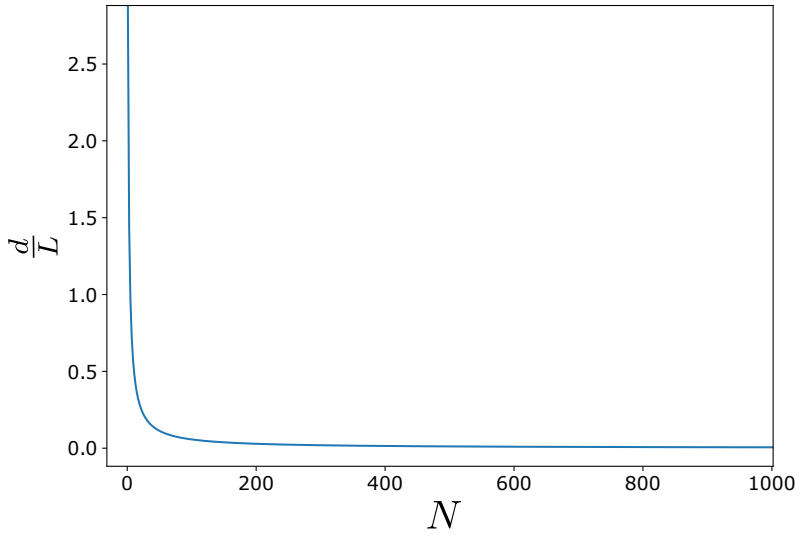

FIGURE 5.14: Impact of the number of kinks, with $\beta = \pi/9$, on the subsegment length.

As shown in Figs.5.11, 5.12, and 5.13, the overall magnitude of the power spectrum increases when wiggles are included. The increase in the energy density of the string network, due to wiggles, is responsible for this increment, as we discussed in the previous section.

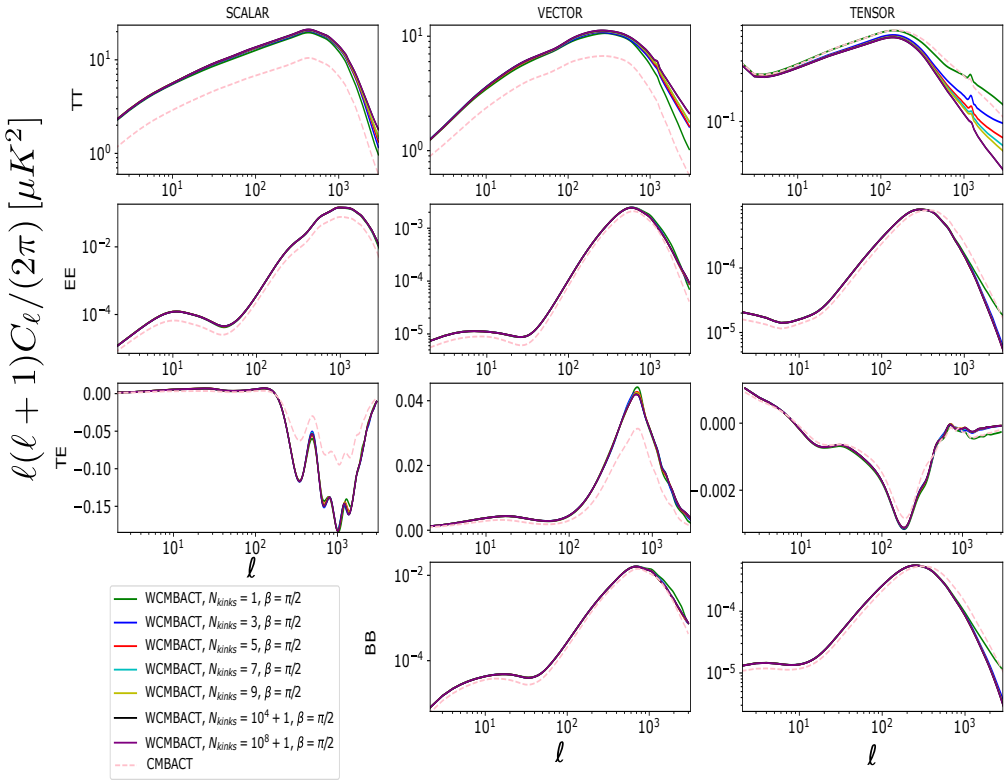

FIGURE 5.15: CMB anisotropies produced by the CMBACT code as well as the WCMBACT code, where the kink sharpness is fixed ($\beta = \pi/2$) and we vary the number of kinks. We chose $G\mu_0 = 10^{-7}$ and averaged over 500 realizations of cosmic strings network realizations.

Furthermore, in Fig. 5.15, it is shown that the CMB anisotropies are changed with the variation of the number of kinks. For the temperature anisotropies, the magnitude of the scalar and vector components increases with the number of kinks on sufficiently small scales (large ℓ). This may be explained by the fact that, when we increase the number of kinks, the length of the subsegments decreases, then contributing to the anisotropies dominantly on smaller scales. Additionally, for a smaller β this increase spans a wider range of ℓ, leading to an overall increase in the amplitude of the scalar and vector components as may be seen in Fig.5.16. The amplitude of the tensor component decreases over all scales and this is particularly accentuated on small scales.

A thorough examination on small scales hints at an enhancement of the spectrum on these scales, — when compared to straight strings — which appears to always be present, but at smaller and smaller scales — beyond the range of the plot — as the number of kinks increases. This suggests that the impact of increasing the number of kinks may result in

a significant shift on power towards very small scales in the cases of the tensor modes. This behavior is more evident in Fig.5.16, when we consider a larger kink sharpness (and consequently larger subsegments, thus shifting this effect towards slightly larger scales)*.

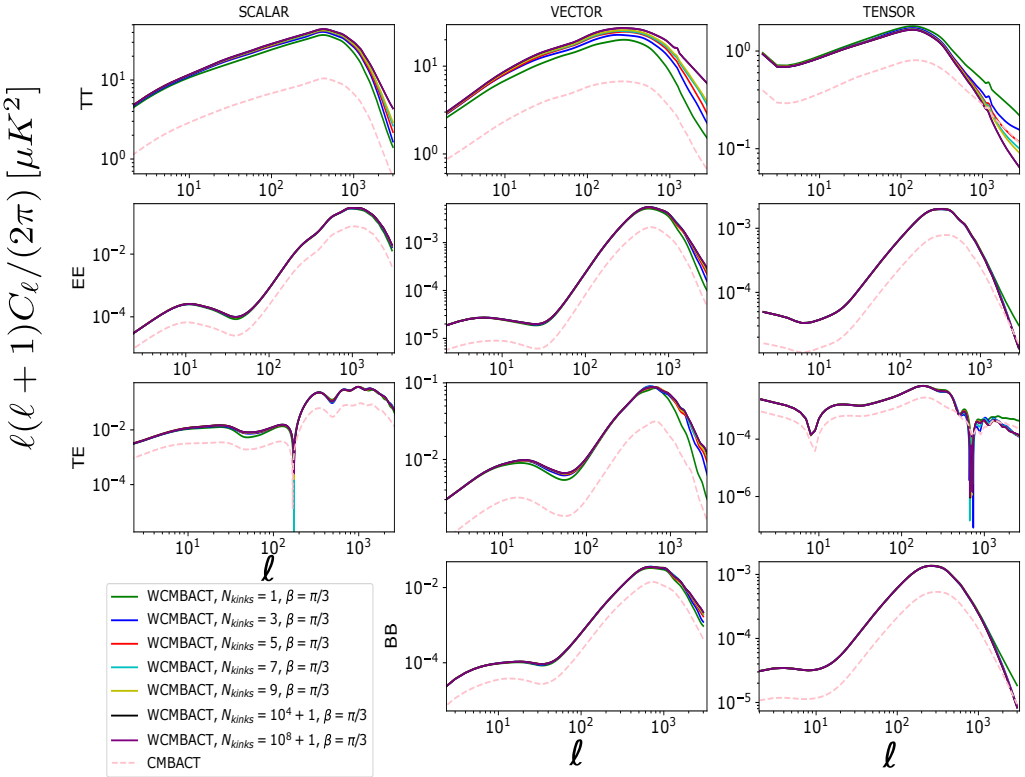

FIGURE 5.16: CMB anisotropies produced by the CMBACT code as well as the WCMBACT code, where the kink sharpness is fixed ($\beta = \pi/3$) and we vary the number of kinks. We chose $G\mu_0 = 10^{-7}$ and averaged over 500 realizations of cosmic strings network realizations.

In EE polarization spectrum, we may see there are no significant changes in the amplitude of the scalar mode, except for a slight decrease of the amplitude between $\ell = 10^1$ and $\ell = 10^3$. The vector component seems to have a slight decrease, as in the previous case, but this increase is moved towards higher scales and the amplitude of the tensor component decreases on small scales with the increase in the number of kinks, but remains, as the power spectrum, almost unchanged if we include a large enough number of kinks.

Finally, both TE and BB anisotropies modes seem to behave similarly to EE.

*For $\beta = \pi/3$ this behavior is clearer. For smaller β, the behavior is the same, but, since the anisotropies generated by wiggly strings are much larger than those of straight strings, it is harder to see this behavior in the figures.

5.4 Impact of Wiggliness on Constraints on Cosmic String Tension

As we have seen in Sec.5.3, the impact of changing the number of kinks on the amplitude of the anisotropies, on large scales, is not significant, therefore we may only look at the impact of the kink sharpness. Moreover, the increase in kink sharpness corresponds to an increase in effective string tension, which implies an increase in the CMB anisotropies. Since the signal from cosmic string is not detected there are two possibilities: either cosmic strings do not exist or they have smaller tension and are thus undetected with the current observational data.

The constraints on the cosmic string contribution to the CMB temperature anisotropies are often derived using the multipole moment $\ell = 10$. Now, we will estimate how much the constraints on cosmic string tension should change if we consider wiggly string segments. To do so, we must first examine the dependence of the CMB anisotropies on kink sharpness.

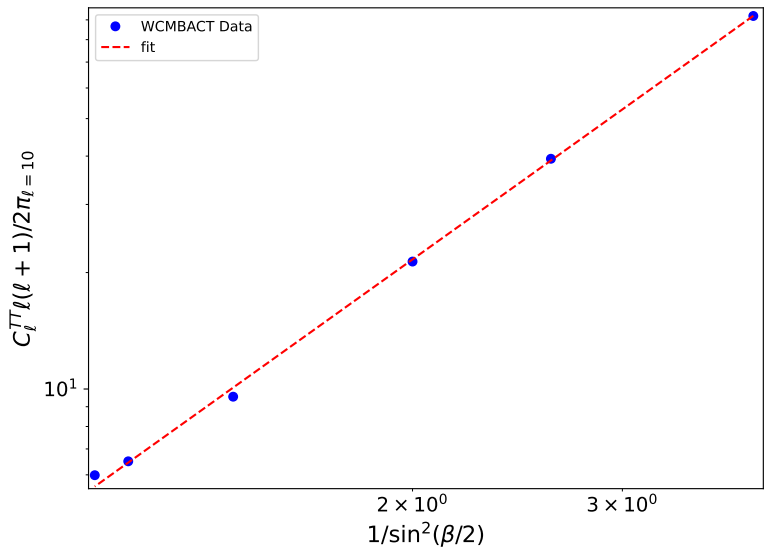

FIGURE 5.17: Variation of the amplitude of the TT anisotropies as a function of $1/\sin^2(\beta/2)$ for $\ell = 10$.

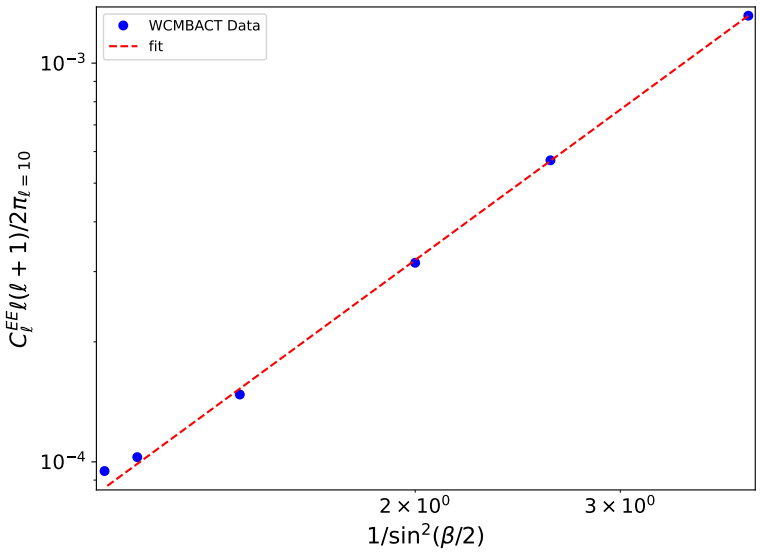

FIGURE 5.18: Variation of the amplitude of the EE anisotropies as a function of $1/\sin^2(\beta/2)$ for $\ell = 10$.

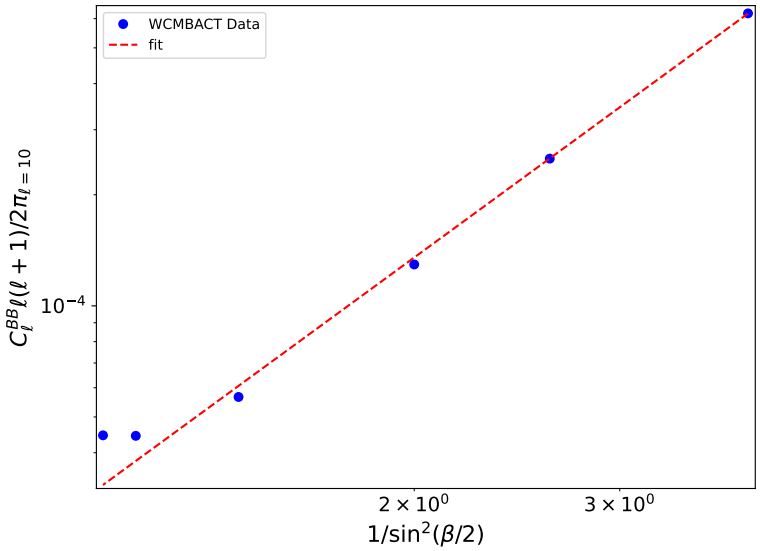

FIGURE 5.19: Variation of the amplitude of the BB anisotropies as a function of $1/\sin^2(\beta/2)$ for $\ell = 10$.

From Figs.5.17, 5.18 and 5.19, we may see that the amplitude of the CMB anisotropies varies proportionally to $\left(1/\sin^2(\beta/2)\right)$. In [55], it is stated that:

$$C_\ell^{strings} \propto N_s \left(G\mu_0\right)^2 . \tag{5.9}$$

In our case, we should have the same expression, but with effective tension:

$$C_\ell^{strings} \propto N_s \left(G\mu_{eff}\right)^2 \propto \frac{1}{\sin(\beta/2)^2}\,, \tag{5.10}$$

which is the result we obtained computationally.

We also noticed that configurations with the sharpest kinks contribute more to the CMB anisotropies, which corresponds to the behavior illustrated in Figs.5.4 and 5.6. Now that we have "parameterized" the behavior of the CMB anisotropies, we can predict it and estimate the constraints on the tension for different values of kink sharpness. In order to achieve it, we start by considering the constraints derived for Nambu-Goto strings [56]:

$$G\mu_0 < 1.49 \times 10^{-7}\,, \tag{5.11}$$

and translate them into constraints on the tension of wiggly strings. Essentially, we discover the value of the wiggly strings' effective tension that would generate a temperature power spectrum with the same amplitude of $\ell = 10$.

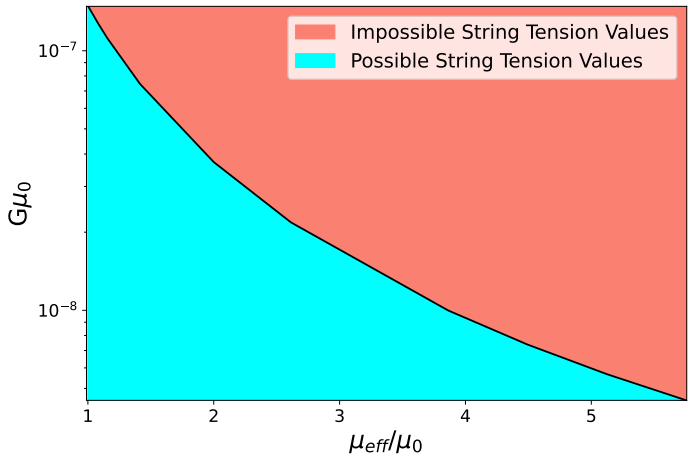

FIGURE 5.20: Variation of the constraints on string tension with the effective tension.

We can see from Fig.5.20 that the allowed tension decreases with the increase of the effective string tension. Therefore, we can conclude that a larger effective string tension will increase the constraints on string tension, as one would naturally expect.

Chapter 6

Comparison Between Different Models

The USM describes the stress-energy tensor of a network composed of straight string segments. The model in [53] introduces a phenomenological parameter called wiggliness parameter, α, to provide an effective description of wiggles on the string. Essentially, Ref. [53] parameterizes a wiggly string by assuming that to describe segments with small scale structure it is sufficient to make strings heavier, ignoring any geometrical impact. Our novel model does not rely on this assumption; instead, we consider string segments with kinks, thus including this effect by a geometrical modification of string segments in the CMBACT code.

In this section, we will look more closely at the case where the kink sharpness is different from π and highlight the main differences between the two models.

6.1 Geometrical Approach vs. Increasing String Effective Tension

In [53], the impact of small-scale structure is included by making the string segments heavier, through the introduction of a wiggliness parameter defined as:

$$\alpha = \frac{E}{E_0} \,, \tag{6.1}$$

where E_0 is the energy of the bare string — without wiggles — and E is the energy of the wiggly string.

In [53], α is chosen arbitrarily, with $\alpha = 1$ representing a string with no small-scale structure and $\alpha > 1$ representing a string with wiggles. In our geometrical approach, wiggliness is actually determined by the sharpness of the kinks:

$$\alpha_w = \frac{L/\sin(\beta/2)}{L} = \frac{1}{\sin(\beta/2)} = \frac{\mu_{eff}}{\mu_0}, \tag{6.2}$$

where β is the kink sharpness.

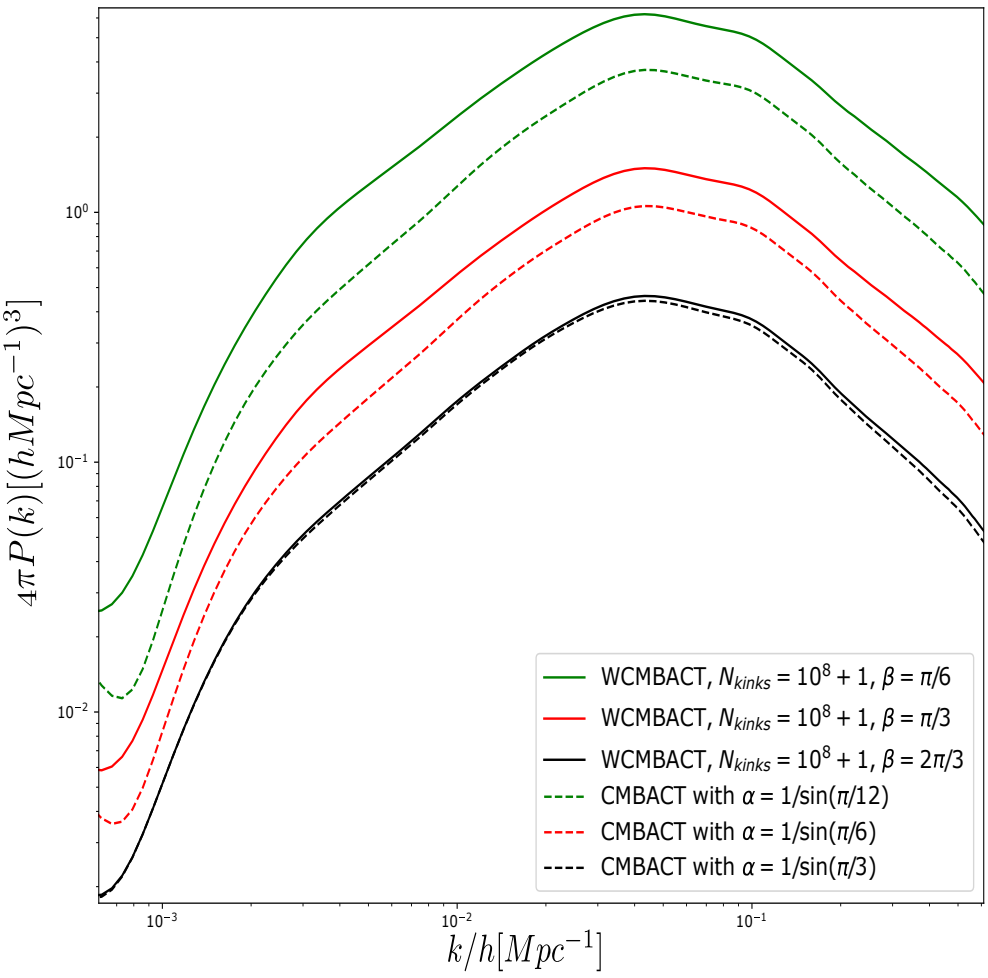

FIGURE 6.1: Linear Power Spectrum generated by the CMBACT code and by the WCMBACT code. The dashed lines are generated by the CMBACT code, with different values of the wiggliness parameter associated with kink sharpness $\pi/6$, $\pi/3$ and $2\pi/3$, respectively. The solid lines are generated by modified CMBACT code with kink sharpness $\pi/6$, $\pi/3$ and $2\pi/3$, respectively. We chose $G_{\mu_0} = 10^{-7}$ and averaged over 500 realizations of cosmic strings network realizations.

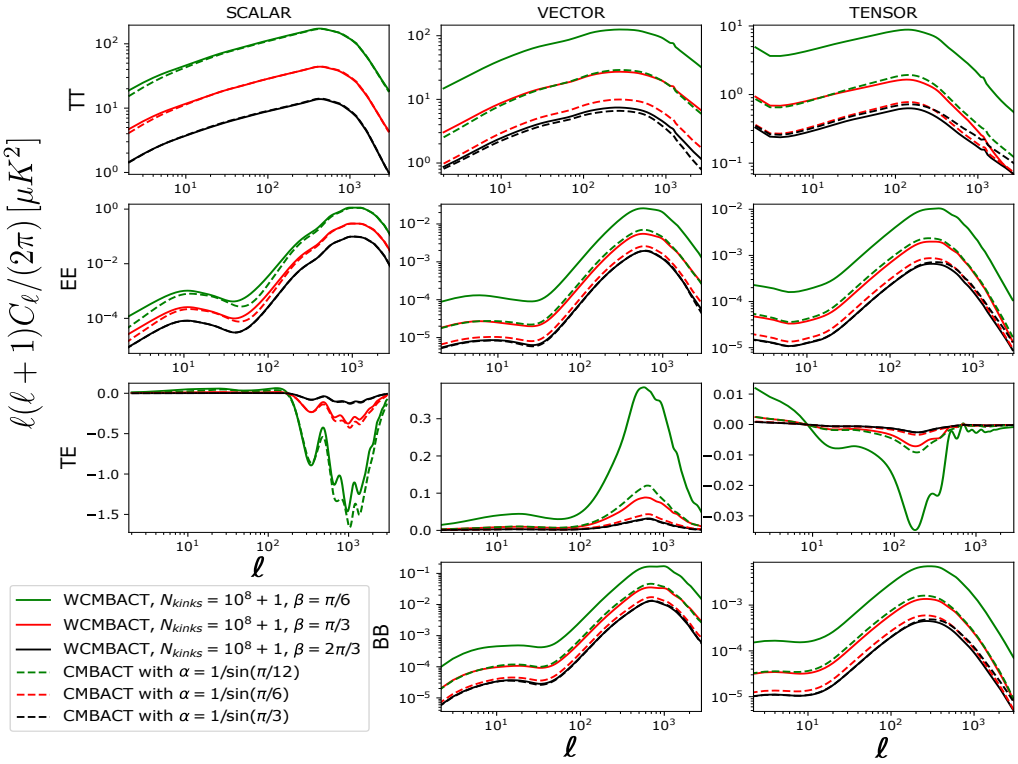

FIGURE 6.2: CMB anisotropies produced by the CMBACT code as well as the WCMBACT code. The dashed lines are produced by the CMBACT code, with the wiggly parameter associated with kink sharpness $\pi/6$, $\pi/3$, $2\pi/3$, respectively. The solid lines are created using a modified CMBACT code with kink sharpnesses of $\pi/6$, $\pi/3$ and $2\pi/3$, respectively. We chose $G_{\mu_0} = 10^{-7}$ and averaged over 500 realizations of cosmic strings network realizations.

The effective treatment of wiggliness introduced in [53] does not describe the same behavior as that introduced by our geometrical approach. Their approach underestimates the amplitude of the power spectrum, and the magnitude of the CMB anisotropies and does not predict the same shape, as we may see in Figs.6.1 and 6.2. This is clear for the cases in which kink sharpnesses are farthest from π; in fact, when the kink sharpness is π, the linear power spectrum and CMB anisotropies are the same, for $\alpha = 1$, as shown in Figs.5.1 and 5.2.

These differences are clearer in Figs 6.3 and 6.4, where we plot the ratio between the amplitude predicted for WCMBACT and that predicted by the standard CMBACT. In Fig.6.3, we notice that this ratio is different from the unity — the blue line on the figure — on all scales and this difference increases with the increase of the kink sharpness. Basically, if the ratio is larger than one, then the original CMBACT code is underestimating the

amplitude of the spectrum (i.e. predicting a lower amplitude). On the other hand, if it is smaller than 1, it is in fact predicting a larger amplitude than our model and, therefore, overestimating the anisotropies. In the case of the power spectrum, the underestimation of the amplitude in the effective approach used in CMBACT is, in general, particularly significant on large scales (small k).

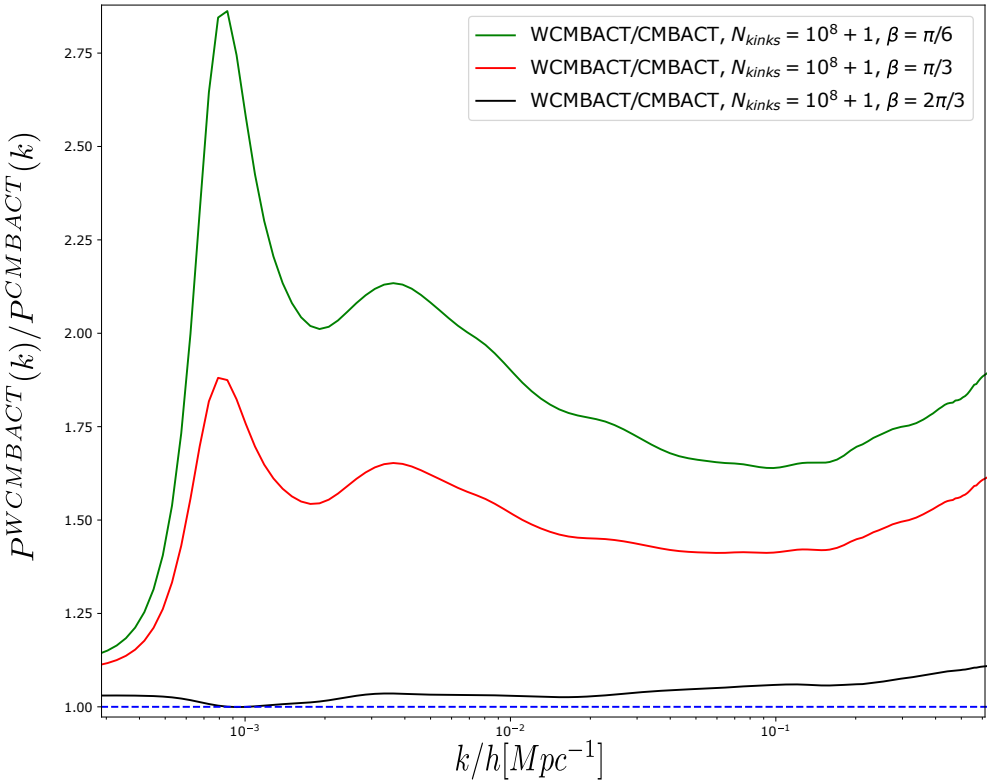

FIGURE 6.3: Ratio between the amplitude of the Linear Power Spectrum generated by the WCMBACT and that predicted by the CMBACT code, for kink sharpness $\pi/6$, $\pi/3$, $2\pi/3$. We chose $G_{\mu_0} = 10^{-7}$ and averaged over 500 realizations of cosmic strings network realizations.

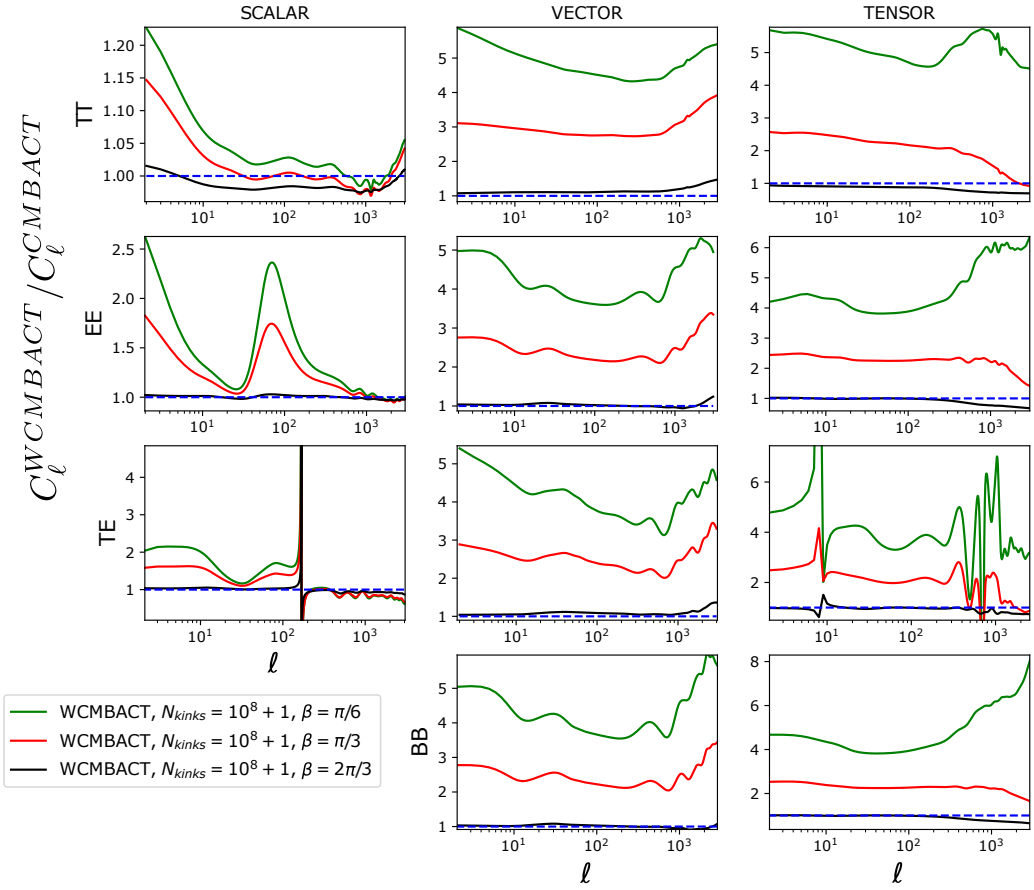

FIGURE 6.4: Ratio between the CMB anisotropies produced by the WCMBACT code and those predicted by the CMBACT code, for kink sharpness $\pi/6$, $\pi/3$, $2\pi/3$ and π. We chose $G_{\mu_0} = 10^{-7}$ and averaged over 500 realizations of cosmic strings network realizations and normalized the plots to unity.

Regarding the CMB anisotropies, something similar happens. For the scalar component of the temperature anisotropies, we notice that the CMBACT underestimates the amplitude of the spectrum both on large and small scales and that this difference increases when we decrease β. Additionally, for intermediate scales around $10 < \ell < 10^3$, this underestimation of the spectrum becomes less significant and there is actually an overestimation of the amplitude of the spectrum above a certain scale (which depends on the sharpness of the kinks). CMBACT, then, predicts a more prominent peak. In the case of the vector component, there is an underestimation of the amplitude — that is more significant than that on scalar modes — of the spectrum on all scales — that increases with sharpness. This demonstrates that our geometrical approach is essential to describe this component

accurately since it captures the impact that the discontinuities on strings may have. A similar thing may be said about the tensor modes, but in this case, for large enough β, there may also be an overestimation of the amplitude of the spectrum on small enough scales. The impact on tensor modes may, as we have seen in Sec.5.3, depend on the number of kinks. In principle, if we consider a smaller number of kinks, this overestimation should appear on significantly larger scales.

In the scalar component of the E-mode polarization spectrum and in the cross-correlation TE power spectrum, what we may see is that the CMBACT code underestimates the amplitude of the first peak of the spectrum (located at $\ell = 10$) and also predicts a narrower peak on small scales ($\ell = 10^3$). This may be seen better in Fig.6.2. Besides this, we may see that the vector and tensor components in all cases show the same trend as the temperature anisotropies.

In conclusion, and as a result of the differences depicted above, our approach is essential in order to account for the full effect of the cosmic string network with wiggles.

Chapter 7

Conclusions and Further Work

In this dissertation, we developed a formalism to describe the CMB anisotropies generated by cosmic strings with kinks. To do so, we started by developing a wiggly USM to describe the stress-energy tensor of a network of cosmic strings with kinks throughout the universe's evolution. Subsequently, we implemented this novel wiggly USM to the publicly available CMBACT [53] in order to obtain the linear CDM power spectrum and the CMB anisotropies generated by cosmic string networks with kinks.

With this approach, we noticed that the amplitude of the power spectrum increases when we increase the kink sharpness, which happens as a consequence of the energy density increasing with the decrease of β. We also found that the amplitude of the power spectrum increases with the number of kinks with non-zero kink sharpness. The region of the spectrum where this enhancement happens, however, is determined by the length of the subsegments, which in turn depends on the number of kinks per segment and their sharpness. Consequently, beyond a certain number of kinks, the shape of the spectrum is not significantly affected because the length of the subsegments is much smaller than the correlation length and, therefore, this enhancement happens at scales much smaller than the peak of the spectrum. Our results, in fact, show that when the kink sharpness is equal to or greater than $\pi/2$, there is a shift in relative power from large scales to small scales as the string becomes less straight. By contrast, when the kink sharpness is smaller than $\pi/2$, subsegments are longer, and thus the maximum relative amplitude increases over most scales.

Regarding the CMB anisotropies, we found that all the components of the angular power spectra grow as $1/\sin^2(\beta/2)$ at angular scales of $\ell = 10$. In addition, the whole spectra scales roughly as $1/\sin^2(\beta/2)$, but this enhancement is also scale dependent: in

particular, as in the case of the linear power spectrum, we have a stronger enhancement on angular scales corresponding to the length of the subsegment. As before, this usually translates into a shift in power from large to small scales, when compared to straight strings, for the scalar and vector temperature anisotropies. The other angular power spectra components decrease quicker for small scales than those of networks composed of straight strings. Yet there is some evidence that particularly in the case of tensor modes, there may be a shift to even smaller scales beyond the range of the plot *.

Additionally, we used our results to study the impact of wiggliness on constraints on cosmic string tension. We considered constraints on cosmic string tension derived for strings without small-scale structure and used our results to derive, using CMB data, constraints of the tension of wiggly strings. For instance, for a straight segment we obtain $G\mu_0 < 1.49 \times 10^{-7}$, which is the constraint derived for Nambu-Goto strings in [56], but if we consider a wiggly segment with $\beta = \pi/9$ we obtain $G\mu_0 < 4.49 \times 10^{-9}$. The increase in the effective string tension leads to more stringent constraints on string tension.

At last, we compared the results of the original CMBACT — with different wiggliness parameters — to the results obtained using our novel WCMBACT — with the corresponding kink sharpness. This demonstrated that CMBACT underestimates the amplitude of the power spectrum and the magnitude of the CMB anisotropies and that it does not predict the same shape. This underestimation can be significant, — especially for vector and tensor components — and thus, the extension presented in this dissertation is crucial to provide a more accurate description of the full effect of the cosmic string network with wiggles.

In our approach, we derived a model which only includes the impact of wiggly strings at a geometrical level, but we did not consider the impact of small-scale structure on the cosmic string network dynamics. In other words, we are assuming a fixed number of kinks and sharpness. However, in general, kinks are created dynamically, and we do not expect the number of kinks and their sharpness to be fixed. For instance, string intercommutations result in new kinks, but they are also subject to being stretched by expansion and decay due to the emission of gravitational radiation. Moreover, some kinks may also be removed when loops are created. These phenomena change the average distance between kinks and their sharpness as the network evolves. In the future, this model may be used straightforwardly with a time-varying kink sharpness and a number of kinks per segment to also account

*The CMBACT is affected by large uncertainties at very small scales and, thus, this computation is currently not possible.

for the dynamical effects of small-scale structure, for example, by using the more complex models to describe wiggly networks that exist in the literature [74–79].

The dynamical impact of kinks was considered in [74, 75]. Therein, they found that the velocity and the characteristic length of the networks should decrease as they become more wiggly and that this may result in a decrease in the amplitude of the CMB anisotropies. However, these studies do not take the geometrical impact of kinks into consideration in the computation of the CMB power spectra and, consequently, they necessarily underestimate the impact of wiggliness. These results, however, indicate that what we achieve, in this dissertation, may be viewed as the maximum impact of kinks on the amplitude of the CMB anisotropies generated by cosmic string networks. Once we include the dynamical effects of wiggliness on the cosmic string network, the anisotropies may decrease. Finally, combining our approach with a model to describe the number of kinks per string and their average sharpness may allow us to get a more accurate characterization of this signature and to derive more precise constraints on cosmic string tension in the future.

Bibliography

[1] A. Einstein, "The Field Equations of Gravitation," *Sitzungsber. Preuss. Akad. Wiss. Berlin (Math. Phys.)*, vol. 1915, pp. 844–847, 1915. [Cited on page 1.]

[2] A. Friedman, "On the Curvature of space," *Z. Phys.*, vol. 10, pp. 377–386, 1922. [Cited on page 1.]

[3] G. Lemaitre, "A Homogeneous Universe of Constant Mass and Growing Radius Accounting for the Radial Velocity of Extragalactic Nebulae," *Annales Soc. Sci. Bruxelles A*, vol. 47, pp. 49–59, 1927. [Cited on page 1.]

[4] E. Hubble, "A relation between distance and radial velocity among extra-galactic nebulae," *Proc. Nat. Acad. Sci.*, vol. 15, pp. 168–173, 1929. [Cited on page 1.]

[5] E. Komatsu and C. L. Bennett, "Results from the Wilkinson Microwave Anisotropy Probe," *PTEP*, vol. 2014, p. 06B102, 2014. [Cited on pages 3 and 10.]

[6] N. Aghanim *et al.*, "Planck 2018 results. VI. Cosmological parameters," *Astron. Astrophys.*, vol. 641, p. A6, 2020, [Erratum: Astron.Astrophys. 652, C4 (2021)]. [Cited on pages 3, 10, and 42.]

[7] A. G. Riess *et al.*, "Observational evidence from supernovae for an accelerating universe and a cosmological constant," *Astron. J.*, vol. 116, pp. 1009–1038, 1998. [Cited on page 4.]

[8] S. Perlmutter *et al.*, "Measurements of Ω and Λ from 42 high redshift supernovae," *Astrophys. J.*, vol. 517, pp. 565–586, 1999. [Cited on page 4.]

[9] M. B. Hindmarsh and T. W. B. Kibble, "Cosmic strings," *Rept. Prog. Phys.*, vol. 58, pp. 477–562, 1995. [Cited on page 5.]

[10] A. Gangui, "Topological defects in cosmology," 10 2001. [Cited on page 5.]

[11] A. C. Davis and T. W. B. Kibble, "Fundamental cosmic strings," *Contemp. Phys.*, vol. 46, pp. 313–322, 2005. [Cited on page 5.]

[12] Y. Gouttenoire, G. Servant, and P. Simakachorn, "Beyond the Standard Models with Cosmic Strings," *JCAP*, vol. 07, p. 032, 2020.

[13] J. Chakrabortty, R. Maji, and S. F. King, "Unification, Proton Decay and Topological Defects in non-SUSY GUTs with Thresholds," *Phys. Rev. D*, vol. 99, no. 9, p. 095008, 2019.

[14] G. 't Hooft, "Magnetic Monopoles in Unified Theories," in *17th International Conference on High-Energy Physics*, 1974, pp. III.84–85.

[15] W. Buchmüller, V. Domcke, K. Kamada, and K. Schmitz, "The Gravitational Wave Spectrum from Cosmological $B - L$ Breaking," *JCAP*, vol. 10, p. 003, 2013.

[16] J. A. Dror, T. Hiramatsu, K. Kohri, H. Murayama, and G. White, "Testing the Seesaw Mechanism and Leptogenesis with Gravitational Waves," *Phys. Rev. Lett.*, vol. 124, no. 4, p. 041804, 2020.

[17] R. A. Battye and E. P. S. Shellard, "Axion string cosmology and its controversies," in *2nd International Conference Physics Beyond the Standard Model: Beyond the Desert 99: Accelerator, Nonaccelerator and Space Approaches*, 9 1999, pp. 565–572. [Cited on page 13.]

[18] G. Ballesteros, J. Redondo, A. Ringwald, and C. Tamarit, "Standard Model—axion—seesaw—Higgs portal inflation. Five problems of particle physics and cosmology solved in one stroke," *JCAP*, vol. 08, p. 001, 2017. [Cited on page 13.]

[19] E. J. Copeland, R. C. Myers, and J. Polchinski, "Cosmic F and D strings," *JHEP*, vol. 06, p. 013, 2004. [Cited on page 13.]

[20] S. Sarangi and S. H. H. Tye, "Cosmic string production towards the end of brane inflation," *Phys. Lett. B*, vol. 536, pp. 185–192, 2002.

[21] H. Firouzjahi and S. H. H. Tye, "Brane inflation and cosmic string tension in superstring theory," *JCAP*, vol. 03, p. 009, 2005.

[22] N. T. Jones, H. Stoica, and S. H. H. Tye, "The Production, spectrum and evolution of cosmic strings in brane inflation," *Phys. Lett. B*, vol. 563, pp. 6–14, 2003. [Cited on page 13.]

[23] R. Jeannerot, J. Rocher, and M. Sakellariadou, "How generic is cosmic string formation in SUSY GUTs," *Phys. Rev. D*, vol. 68, p. 103514, 2003. [Cited on page 13.]

[24] Y. Cui, S. P. Martin, D. E. Morrissey, and J. D. Wells, "Cosmic Strings from Supersymmetric Flat Directions," *Phys. Rev. D*, vol. 77, p. 043528, 2008.

[25] R. Jeannerot and M. Postma, "Chiral cosmic strings in supergravity," *JHEP*, vol. 12, p. 043, 2004.

[26] A. Achucarro, A. Celi, M. Esole, J. Van den Bergh, and A. Van Proeyen, "D-term cosmic strings from N=2 supergravity," *JHEP*, vol. 01, p. 102, 2006.

[27] A.-C. Davis and M. Majumdar, "Inflation in supersymmetric cosmic string theories," *Phys. Lett. B*, vol. 460, pp. 257–262, 1999.

[28] E. Allys, "Bosonic condensates in realistic supersymmetric GUT cosmic strings," *JCAP*, vol. 04, p. 009, 2016. [Cited on pages 5 and 13.]

[29] J. Bardeen, L. N. Cooper, and J. R. Schrieffer, "Microscopic theory of superconductivity," *Phys. Rev.*, vol. 106, p. 162, 1957. [Cited on page 5.]

[30] N. N. Bogolyubov, V. V. Tolmachev, and D. V. Shirkov, "A New method in the theory of superconductivity," *Fortsch. Phys.*, vol. 6, pp. 605–682, 1958. [Cited on page 5.]

[31] T. W. B. Kibble, "Topology of Cosmic Domains and Strings," *J. Phys. A*, vol. 9, pp. 1387–1398, 1976. [Cited on page 5.]

[32] A. J. Beekman, L. Rademaker, and J. van Wezel, "An Introduction to Spontaneous Symmetry Breaking," *SciPost Phys. Lect. Notes*, vol. 11, p. 1, 2019. [Cited on page 6.]

[33] T. Vachaspati, *Kinks and domain walls: An introduction to classical and quantum solitons*. Cambridge University Press, 4 2010. [Cited on page 6.]

[34] Y. Bunkov and H. Godfrin, "Book review: Topological defects and the non-equilibrium dynamics of symmetry-breaking phase transitions / kluwer, 2000," *The Observatory*, vol. 121, p. 116, 03 2001. [Cited on pages 7 and 9.]

[35] I. Rybak, "Cosmic Paleontology: Searching for Superstrings," Ph.D. dissertation, Porto U., 2018. [Cited on page 8.]

[36] A. Rajantie, "Defect formation in the early universe," *Contemp. Phys.*, vol. 44, pp. 485–502, 2003. [Cited on page 8.]

[37] B. Ryden, *Introduction to cosmology*. Cambridge University Press, 1970. [Cited on page 9.]

[38] R. A. Alpher and R. C. Herman, "On the Relative Abundance of the Elements," *Phys. Rev.*, vol. 74, no. 12, pp. 1737–1742, 1948.

[39] R. A. Alpher, H. Bethe, and G. Gamow, "The origin of chemical elements," *Phys. Rev.*, vol. 73, pp. 803–804, Apr 1948. [Online]. Available: https://link.aps.org/doi/10.1103/PhysRev.73.803

[40] G. Gamow, "The origin of elements and the separation of galaxies," *Phys. Rev.*, vol. 74, pp. 505–506, Aug 1948. [Online]. Available: https://link.aps.org/doi/10.1103/PhysRev.74.505.2

[41] G. Gamow, "The Evolution of the Universe," *Nature*, vol. 162, no. 4122, pp. 680–682, 1948.

[42] R. A. Alpher and R. C. Herman, "Evolution of the Universe," *Nature*, vol. 162, no. 4124, pp. 774–775, 1948. [Cited on page 9.]

[43] A. A. Penzias and R. W. Wilson, "A Measurement of excess antenna temperature at 4080-Mc/s," *Astrophys. J.*, vol. 142, pp. 419–421, 1965. [Cited on page 9.]

[44] R. H. Dicke, P. J. E. Peebles, P. G. Roll, and D. T. Wilkinson, "Cosmic Black-Body Radiation," *Astrophys. J.*, vol. 142, pp. 414–419, 1965. [Cited on page 9.]

[45] J. C. Mather *et al.*, "Measurement of the Cosmic Microwave Background spectrum by the COBE FIRAS instrument," *Astrophys. J.*, vol. 420, pp. 439–444, 1994. [Cited on page 10.]

[46] E. M. Lifshitz, "On the gravitational stability of the expanding universe," *J. Phys. USSR.*, vol. 10, pp. 116–129, 1946. [Cited on page 10.]

[47] W. Hu and M. J. White, "A CMB polarization primer," *New Astron.*, vol. 2, p. 323, 1997. [Cited on page 10.]

[48] A. Albrecht, R. A. Battye, and J. Robinson, "Detailed study of defect models for cosmic structure formation," *Phys. Rev. D*, vol. 59, p. 023508, 1999. [Cited on pages 10, 18, 21, 22, 39, and 42.]

[49] A. Albrecht, D. Coulson, P. Ferreira, and J. Magueijo, "Causality and the microwave background," *Phys. Rev. Lett.*, vol. 76, pp. 1413–1416, 1996. [Cited on page 10.]

[50] N. Turok, U.-L. Pen, and U. Seljak, "The Scalar, vector and tensor contributions to CMB anisotropies from cosmic defects," *Phys. Rev. D*, vol. 58, p. 023506, 1998. [Cited on page 11.]

[51] N. Bevis, M. Hindmarsh, M. Kunz, and J. Urrestilla, "CMB power spectrum contribution from cosmic strings using field-evolution simulations of the Abelian Higgs model," *Phys. Rev. D*, vol. 75, p. 065015, 2007.

[52] Bevis, Neil and Hindmarsh, Mark and Kunz, Martin and Urrestilla, Jon, "CMB polarization power spectra contributions from a network of cosmic strings," *Phys. Rev. D*, vol. 76, p. 043005, 2007.

[53] L. Pogosian and T. Vachaspati, "Cosmic microwave background anisotropy from wiggly strings," *Phys. Rev. D*, vol. 60, p. 083504, 1999. [Cited on pages 11, 18, 22, 23, 25, 41, 42, 65, 66, 67, and 71.]

[54] D. J. Fixsen, E. S. Cheng, J. M. Gales, J. C. Mather, R. A. Shafer, and E. L. Wright, "The Cosmic Microwave Background spectrum from the full COBE FIRAS data set," *Astrophys. J.*, vol. 473, p. 576, 1996. [Cited on page 11.]

[55] L. Pogosian and M. Wyman, "B-modes from cosmic strings," *Phys. Rev. D*, vol. 77, p. 083509, 2008. [Cited on pages 11 and 62.]

[56] A. Lazanu and P. Shellard, "Constraints on the Nambu-Goto cosmic string contribution to the CMB power spectrum in light of new temperature and polarisation data," *JCAP*, vol. 02, p. 024, 2015. [Cited on pages 11, 63, and 72.]

[57] A. Vilenkin and E. P. S. Shellard, *Cosmic Strings and Other Topological Defects*. Cambridge University Press, 7 2000. [Cited on page 15.]

[58] T. W. B. Kibble, "Evolution of a system of cosmic strings," *Nucl. Phys. B*, vol. 252, p. 227, 1985, [Erratum: Nucl.Phys.B 261, 750 (1985)]. [Cited on pages 17 and 19.]

[59] D. P. Bennett and F. R. Bouchet, "High resolution simulations of cosmic string evolution. 1. Network evolution," *Phys. Rev. D*, vol. 41, p. 2408, 1990. [Cited on pages 17 and 19.]

[60] B. Allen and E. P. S. Shellard, "Cosmic string evolution: a numerical simulation," *Phys. Rev. Lett.*, vol. 64, pp. 119–122, 1990. [Cited on pages 17, 19, and 20.]

[61] Martins, C. J. A. P. and Shellard, E. P. S., "Quantitative string evolution," *Phys. Rev. D*, vol. 54, pp. 2535–2556, 1996. [Cited on pages 17, 19, 20, and 22.]

[62] C. J. A. P. "Martins and E. P. S. Shellard, "Extending the velocity dependent one scale string evolution model," *Phys. Rev. D*, vol. 65, p. 043514, 2002. [Cited on pages 17, 18, 19, 20, and 22.]

[63] U. Seljak and M. Zaldarriaga, "A Line of sight integration approach to cosmic microwave background anisotropies," *Astrophys. J.*, vol. 469, pp. 437–444, 1996. [Cited on pages 18, 23, and 41.]

[64] C. J. A. P. Martins and E. P. S. Shellard, "String evolution with friction," *Phys. Rev. D*, vol. 53, pp. 575–579, 1996. [Cited on page 20.]

[65] E. J. Copeland and T. W. B. Kibble, "Cosmic Strings and Superstrings," *Proc. Roy. Soc. Lond. A*, vol. 466, pp. 623–657, 2010. [Cited on page 20.]

[66] D. P. Bennett and F. R. Bouchet, "Evidence for a Scaling Solution in Cosmic String Evolution," *Phys. Rev. Lett.*, vol. 60, p. 257, 1988. [Cited on page 20.]

[67] A. Avgoustidis and E. P. S. Shellard, "Effect of reconnection probability on cosmic (super)string network density," *Phys. Rev. D*, vol. 73, p. 041301, 2006. [Cited on page 20.]

[68] J. N. Moore, E. P. S. Shellard, and C. J. A. P. Martins, "On the evolution of Abelian-Higgs string networks," *Phys. Rev. D*, vol. 65, p. 023503, 2002. [Cited on page 22.]

[69] C. J. A. P. Martins and E. P. S. Shellard, "Fractal properties and small-scale structure of cosmic string networks," *Phys. Rev. D*, vol. 73, p. 043515, 2006.

[70] J. J. Blanco-Pillado, K. D. Olum, and B. Shlaer, "Large parallel cosmic string simulations: New results on loop production," *Phys. Rev. D*, vol. 83, p. 083514, 2011.

[71] J. R. C. C. C. Correia and C. J. A. P. Martins, "Abelian–Higgs cosmic string evolution with multiple GPUs," *Astron. Comput.*, vol. 34, p. 100438, 2021. [Cited on page 22.]

[72] I. Y. Rybak and L. Sousa, "CMB anisotropies generated by cosmic string loops," *Phys. Rev. D*, vol. 104, no. 2, p. 023507, 2021. [Cited on page 22.]

[73] L. Pogosian, I. Wasserman, and M. Wyman, "On vector mode contribution to CMB temperature and polarization from local strings," 4 2006. [Cited on pages 23 and 41.]

[74] C. J. A. P. Martins, E. P. S. Shellard, and J. P. P. Vieira, "Models for Small-Scale Structure on Cosmic Strings: Mathematical Formalism," *Phys. Rev. D*, vol. 90, no. 4, p. 043518, 2014. [Cited on pages 25, 27, and 73.]

[75] I. Y. Rybak, A. Avgoustidis, and C. J. A. P. Martins, "Semianalytic calculation of cosmic microwave background anisotropies from wiggly and superconducting cosmic strings," *Phys. Rev. D*, vol. 96, no. 10, p. 103535, 2017, [Erratum: Phys.Rev.D 100, 049901 (2019)]. [Cited on pages 25 and 73.]

[76] A. Vilenkin, "Effect of Small Scale Structure on the Dynamics of Cosmic Strings," *Phys. Rev. D*, vol. 41, p. 3038, 1990.

[77] B. Carter, "Transonic elastic model for wiggly Goto-Nambu string," *Phys. Rev. Lett.*, vol. 74, pp. 3098–3101, 1995.

[78] Brandon Carter, "Brane dynamics for treatment of cosmic strings and vortons," in *2nd Mexican School on Gravitation and Mathematical Physics*, 5 1997.

[79] D. Austin, E. J. Copeland, and T. W. B. Kibble, "Evolution of cosmic string configurations," *Phys. Rev. D*, vol. 48, pp. 5594–5627, Dec 1993. [Online]. Available: https://link.aps.org/doi/10.1103/PhysRevD.48.5594 [Cited on pages 27 and 73.]

[80] J. H. P. Wu, P. P. Avelino, E. P. S. Shellard, and B. Allen, "Cosmic strings, loops, and linear growth of matter perturbations," *Int. J. Mod. Phys. D*, vol. 11, pp. 61–102, 2002. [Cited on page 58.]

Appendix A

The Stress-Energy Tensor: Derivation

In this appendix, we go over the details of calculating the stress-energy tensor of a wiggly string segment.

A.1 String with 1 kink

In this section, we may find the complete derivation of Eq.(4.24).

$$
\begin{aligned}
\Theta^{00} &= \mu_0\gamma e^{i\left(\mathbf{k}\cdot\mathbf{y}_0+k\upsilon\tau\hat{\mathbf{X}}\right)}\left[\int_{-d}^{0} d\sigma e^{ik\sigma\hat{\mathbf{X}}'_{13}}+\int_{0}^{d} d\sigma e^{ik\sigma\hat{\mathbf{X}}'_{23}}\right] \\
&= \mu_0\gamma e^{i\left(\mathbf{k}\cdot\mathbf{y}_0+k\upsilon\tau\hat{\mathbf{X}}\right)}\left[\frac{1-e^{-ikd\hat{\mathbf{X}}'_{13}}}{ik\hat{\mathbf{X}}'_{13}}+\frac{e^{ikd\hat{\mathbf{X}}'_{23}}-1}{ik\hat{\mathbf{X}}'_{23}}\right] \\
&= \mu_0\gamma\left[\cos(A)+i\sin(A)\right]\left\{\frac{1-\cos(B_1)+i\sin(B_1)}{ik\hat{\mathbf{X}}'_{13}}+\frac{cos(B_2)+i\sin(B_2)-1}{ik\hat{\mathbf{X}}'_{23}}\right\} \\
&= \mu_0\gamma\Bigg\{\left[\frac{\cos(A)}{i}-\frac{\cos(A)\cos(B_1)}{i}+\cos(A)\sin(B_1)+\sin(A)\right. \\
&\quad \left.-\sin(A)\cos(B_1)+i\sin(A)\sin(B_1)\right]\frac{1}{k\hat{\mathbf{X}}'_{13}} \\
&\quad +\left[\frac{-\cos(A)}{i}+\frac{\cos(A)\cos(B_2)}{i}+\cos(A)\sin(B_2)\right. \\
&\quad \left.-\sin(A)+\sin(A)\cos(B_2)+i\sin(A)\sin(B_2)\right]\frac{1}{k\hat{\mathbf{X}}'_{23}}\Bigg\}.
\end{aligned}
\tag{A.1}
$$

$$\Re\left(\Theta^{00}\right) = \mu_0\gamma\left[\cos(A)\left(\frac{\sin(B_1)}{k\hat{\mathbf{X}}'_{13}} + \frac{\sin(B_2)}{k\hat{\mathbf{X}}'_{23}}\right) + \sin(A)\left(\frac{\hat{\mathbf{X}}'_{23} - \hat{\mathbf{X}}'_{13}}{k\hat{\mathbf{X}}'_{23}\hat{\mathbf{X}}'_{13}} + \frac{\cos(B_2)}{k\hat{\mathbf{X}}'_{23}} - \frac{\cos(B_1)}{k\hat{\mathbf{X}}'_{13}}\right)\right], \tag{A.2}$$

A.2 String with 3 kinks

Here, we may find the complete derivation of Eq.(4.36). To do, we start by decomposing $\hat{\mathbf{X}}'_{13}$ and $\hat{\mathbf{X}}'_{23}$ into their $\hat{\mathbf{e}}_x$ and $\hat{\mathbf{e}}_y$ using Eq.(4.18).

For simplicity, let us define the following quantities:

$$\begin{aligned} H &= \left(\frac{\sin(B_1)}{k\hat{\mathbf{X}}'_{13}} + \frac{\sin(B_2)}{k\hat{\mathbf{X}}'_{23}}\right) \\ W &= \left(\frac{\hat{\mathbf{X}}'_{23} - \hat{\mathbf{X}}'_{13}}{k\hat{\mathbf{X}}'_{23}\hat{\mathbf{X}}'_{13}} + \frac{\cos(B_2)}{k\hat{\mathbf{X}}'_{23}} - \frac{\cos(B_1)}{k\hat{\mathbf{X}}'_{13}}\right) \end{aligned} \tag{A.3}$$

and thus we can write:

$$\begin{aligned} \Re\left(\Theta^{00}\right) &= \mu_0\gamma\left[\cos\left(A_{mp} - d\mathbf{k}\cdot\left(\sin(\beta/2)\hat{\mathbf{e}}_x - \cos(\beta/2)\hat{\mathbf{e}}_y\right)\right)H \right. \\ &\quad \left. + \sin\left(A_{mp} - d\mathbf{k}\cdot\left(\sin(\beta/2)\hat{\mathbf{e}}_x - \cos(\beta/2)\hat{\mathbf{e}}_y\right)\right)W\right] \\ &\quad + \mu_0\gamma\left[\cos\left(A_{mp} + d\mathbf{k}\cdot\left(\sin(\beta/2)\hat{\mathbf{e}}_x + \cos(\beta/2)\hat{\mathbf{e}}_y\right)\right)H \right. \\ &\quad \left. + \sin\left(A_{mp} + d\mathbf{k}\cdot\left(\sin(\beta/2)\hat{\mathbf{e}}_x + \cos(\beta/2)\hat{\mathbf{e}}_y\right)\right)W\right] \\ &= \mu_0\gamma\left[\cos\left(A'_{mp} - (L/4)\,\mathbf{k}\cdot\hat{\mathbf{e}}_x\right)H + \sin\left(A'_{mp} - (L/4)\,\mathbf{k}\cdot\hat{\mathbf{e}}_x\right)W\right] \\ &\quad + \mu_0\gamma\left[\cos\left(A'_{mp} + (L/4)\,\mathbf{k}\cdot\hat{\mathbf{e}}_x\right)H + \sin\left(A'_{mp} + (L/4)\,\mathbf{k}\cdot\hat{\mathbf{e}}_x\right)W\right] \\ &= 2\mu_0\gamma\cos\left((L/4)\,\mathbf{k}\cdot\hat{\mathbf{e}}_x\right)\left[\cos\left(A'_{mp}\right)H + \sin\left(A'_{mp}\right)W\right], \end{aligned} \tag{A.4}$$

where we used the trigonometric identities:

$$\begin{aligned}\cos(A-B)+\cos(A+B)&=2\cos(A)\cos(B)\,,\\ \sin(A-B)+\sin(A+B)&=2\sin(A)\cos(B)\end{aligned}\tag{A.5}$$

and the following relations:

$$d\sin(\beta/2)=\frac{L}{4}\,,\tag{A.6}$$

$$A'_{mp}=A_{mp}+d\mathbf{k}\cdot\left(\cos(\beta/2)\hat{\mathbf{e}}_y\right)\,,\tag{A.7}$$

where

$$A_{mp}=\mathbf{k}\cdot\mathbf{y_{mp}}+v\tau\hat{\dot{\mathbf{X}}}_{\mathbf{3}}\,.\tag{A.8}$$

A.3 String with 5 kinks

Thereafter, we have the following derivation of Eq.(4.44).

$$\begin{aligned}\Re\left(\Theta^{00}\right)=\mu_0\gamma&\left[\cos\left(A_{mp}-\frac{2L}{6}\mathbf{k}\cdot\hat{\mathbf{e}}_{\mathbf{x}}\right)H+\sin\left(A_{mp}-\frac{2L}{6}\mathbf{k}\cdot\hat{\mathbf{e}}_{\mathbf{x}}\right)W\right]\\ &+\mu_0\gamma\left[\cos(A_{mp})H+\sin(A_{mp})W\right]\\ &+\mu_0\gamma\left[\cos\left(A_{mp}+\frac{2L}{6}\mathbf{k}\cdot\hat{\mathbf{e}}_{\mathbf{x}}\right)H+\sin\left(A_{mp}+\frac{2L}{6}\mathbf{k}\cdot\hat{\mathbf{e}}_{\mathbf{x}}\right)W\right]\\ &=\mu_0\gamma\left(1+2\cos\left(\frac{2L}{6}\mathbf{k}\cdot\hat{\mathbf{e}}_{\mathbf{x}}\right)\right)\left[\cos\left(A_{mp}\right)H+\sin\left(A_{mp}\right)W\right]\,,\end{aligned}\tag{A.9}$$

where to obtain the last expression we have used the trigonometric identities defined in Eqs.(A.5).

A.4 String with 7 kinks

Finally. we may see the derivation of Eq.(4.52).

$$\begin{aligned}
\Re\left(\Theta^{00}\right) &= \mu_0\gamma\left[\cos\left(A_{mp} - d\hat{\mathbf{X}}'_{23} - \frac{2L}{8}\mathbf{k}\cdot\hat{\mathbf{e}}_{\mathbf{x}}\right)H + \sin\left(A_{mp} - d\hat{\mathbf{X}}'_{23} - \frac{2L}{8}\mathbf{k}\cdot\hat{\mathbf{e}}_{\mathbf{x}}\right)W\right] \\
&+\mu_0\gamma\left[\cos\left(A_{mp} - d\hat{\mathbf{X}}'_{23}\right)H + \sin\left(A_{mp} - d\hat{\mathbf{X}}'_{23}\right)W\right] \\
&+\mu_0\gamma\left[\cos\left(A_{mp} + d\hat{\mathbf{X}}'_{13}\right)H + \sin\left(A_{mp} + d\hat{\mathbf{X}}'_{13}\right)W\right] \\
&+\mu_0\gamma\left[\cos\left(A_{mp} + d\hat{\mathbf{X}}'_{13} + \frac{2L}{8}\mathbf{k}\cdot\hat{\mathbf{e}}_{\mathbf{x}}\right)H + \sin\left(A_{mp} + d\hat{\mathbf{X}}'_{13} + \frac{2L}{8}\mathbf{k}\cdot\hat{\mathbf{e}}_{\mathbf{x}}\right)W\right] \\
&= 2\mu_0\gamma\left(\cos\left(\frac{L}{8}\mathbf{k}\cdot\hat{\mathbf{e}}_{\mathbf{x}}\right) + \cos\left(\frac{3L}{8}\mathbf{k}\cdot\hat{\mathbf{e}}_{\mathbf{x}}\right)\right)\left[\cos\left(A'_{mp}\right)H + \sin\left(A'_{mp}\right)W\right],
\end{aligned} \tag{A.10}$$

where we also used the trigonometric identities defined in Eq.(A.5), (A.7) and (A.8). Here, to arrive at the last equality, we also decomposed $\hat{\mathbf{X}}'_{13}$ and $\hat{\mathbf{X}}'_{23}$ into their $\hat{\mathbf{e}}_x$ and $\hat{\mathbf{e}}_y$ components, as we did in the case for 3 kinks.

Appendix B

Analytical Consolidation of Subsegments

In this appendix, we detail the analytical consolidation of subsegments using geometric series and induction.

B.1 Demonstration using the Geometric Series

For $(N-1)/2$ odd, the summation in (Eq.(4.55) can be written as follows:

$$2\sum_{q=0}^{(N-3)/4}\cos\left((2q+1)\frac{L}{N+1}\mathbf{k}\cdot\hat{\mathbf{e}}_x\right)=2\sum_{q=0}^{n}\cos\left((2q+1)\theta\right)\,. \tag{B.1}$$

Euler's formula,

$$e^{i\phi}=\cos(\phi)+i\sin(\phi)\,, \tag{B.2}$$

implies:

$$\begin{cases}\Re\left(e^{i\phi}\right)=\cos(\phi)\\ \Im\left(e^{i\phi}\right)=\sin(\phi)\end{cases}\,. \tag{B.3}$$

Therefore, we can write Eq.(B.1) as:

$$2\sum_{q=0}^{n}\cos\left((2q+1)\theta\right)=2\sum_{q=0}^{n}\Re\left(e^{i(2q+1)\theta}\right)=2\Re\left(e^{i\theta}\sum_{q=0}^{n}e^{i2q\theta}\right)\,, \tag{B.4}$$

where the term with the summation is a geometric series. Any geometric series has the following expression:

$$\sum_{j=0}^{s}r^j=\frac{r^{s+1}-1}{r-1}\,,\ r\neq 1\,. \tag{B.5}$$

Thus the summation term in Eq.(B.4) can be written as:

$$\sum_{q=0}^{n} e^{i2q\theta} = \frac{e^{i2(n+1)\theta} - 1}{e^{i2\theta} - 1}\,,\ \theta \neq 0\,, \tag{B.6}$$

substituting in Eq.(B.4) we obtain:

$$\begin{aligned} 2\sum_{q=0}^{n} \cos\left((2q+1)\theta\right) &= 2\Re\left(e^{i\theta}\frac{e^{i2(n+1)\theta} - 1}{e^{i2\theta} - 1}\right) \\ &= 2\Re\left(e^{i\theta}\frac{e^{i(n+1)\theta}}{e^{i\theta}}\frac{\sin\left((n+1)\theta\right)}{\sin\left(\theta\right)}\right) \\ =&2\cos\left((n+1)\theta\right)\frac{\sin\left((n+1)\theta\right)}{\sin\left(\theta\right)}. \end{aligned} \tag{B.7}$$

Finally, using the following trigonometric identity :

$$2\cos(A)\sin(B) = \sin(A+B) + \sin(A-B)\,, \tag{B.8}$$

we obtain the final expression:

$$\begin{aligned} &2\cos\left((n+1)\theta\right)\frac{\sin\left((n+1)\theta\right)}{\sin\left(\theta\right)} \\ =&\frac{\sin\left(2(n+1)\theta\right) + \sin\left(0\right)}{\sin\left(\theta\right)} = \frac{\sin\left(2(n+1)\theta\right)}{\sin\left(\theta\right)}\ ,\ \left(n = \frac{N-3}{4}\right). \\ =&\frac{\sin\left(2(\left(\frac{N-3}{4}\right)+1)\theta\right)}{\sin\left(\theta\right)} = \frac{\sin\left(\left(\frac{N+1}{2}\right)\theta\right)}{\sin\left(\theta\right)} \end{aligned} \tag{B.9}$$

If $(N-1)/2$ is even the procedure is similar. The even summation term is:

$$\begin{aligned} &1 + 2\left(\sum_{q=1}^{(N-1)/4} \cos\left((2q)\frac{L}{N+1}\mathbf{k}\cdot\hat{\mathbf{e}}_x\right)\right) = 1 + 2\sum_{q=1}^{n}\cos\left(2q\theta\right) \\ &= 1 + 2\sum_{q=1}^{n}\Re\left(e^{i2q\theta}\right) = 1 + 2\sum_{q=0}^{n}\Re\left(e^{i2q\theta} - 1\right) \\ &= 1 + 2\Re\left(\frac{e^{i2(n+1)\theta} - 1}{e^{i2\theta} - 1} - 1\right) = 1 + 2\Re\left(\frac{e^{i(n+1)\theta}}{e^{i\theta}}\frac{\sin\left[(n+1)\,\theta\right]}{\sin\left[\theta\right]} - 1\right) \\ &= 1 + 2\left(\cos\left[n\theta\right]\frac{\sin\left[(n+1)\,\theta\right]}{\sin\left[\theta\right]} - 1\right) = \frac{\sin\left[(2n+1)\,\theta\right]}{\sin\left[\theta\right]} = \frac{\sin\left[\left(\frac{N+1}{2}\right)\theta\right]}{\sin\left[\theta\right]}\ , \end{aligned} \tag{B.10}$$

where $n = \frac{N-1}{4}$ and we used the Euler identity and trigonometric identity established in Eq.(B.8).

At last, the final expression in Eqs.(B.9) and (B.10) are also valid for $\theta = 0$.

$$\lim_{\theta \to 0} \frac{\sin\left[\left(\frac{N+1}{2}\right)\theta\right]}{\sin\left[\theta\right]} \to \left(\frac{N+1}{2}\right), \tag{B.11}$$

which is the same result as that obtained using the even summation term with $\theta = 0$:

$$\begin{aligned} &1 + 2\sum_{q=1}^{n} \cos\left(2q0\right), \left(n = \frac{N-1}{4}\right) \\ =&1 + 2\sum_{q=1}^{\frac{N-1}{4}} 1 = \frac{N+1}{2}, \end{aligned} \tag{B.12}$$

and using the odd summation term with $\theta = 0$:

$$\begin{aligned} &2\sum_{q=0}^{n} \cos\left((2q+1)0\right), \left(n = \frac{N-3}{4}\right) \\ =&2\left(1 + \sum_{q=1}^{\frac{N-3}{4}} 1\right) = \frac{N+1}{2}. \end{aligned} \tag{B.13}$$

B.2 Proof by Induction

To do a proof by induction, we must first demonstrate that our expression is valid for $n = 1$, and that if it is valid for a given n, it should also be valid for $n+1$. In our case, we have two expressions, one for $n = (N+1)/2$ odd an one for $n = (N+1)/2$ even, thus we need to prove:

1. The expression is valid for $n = 1$.
2. The expression is valid for $n = 2$.
3. If this expression is valid for $n-2$, it should valid for n.

Point 1 and 2 are already verified in section 4.2.5. Now, let us assume that:

$$F(n-2) = \frac{\sin\left[(n-2)x\right]}{\sin(x)} \tag{B.14}$$

is valid. The last term for both summations will always be written as:

$$F(n) - F(n-2) = 2\cos\left[(n-1)x\right], \tag{B.15}$$

thus one can write:

$$F(n) = F(n-2) + 2\cos\left[(n-1)x\right], \tag{B.16}$$

Verifying Eq.(B.16) allows to have an expression valid, by induction, for all n:

$$\begin{aligned} F(n) =& \frac{\sin\left[(n-2)x\right]}{\sin(x)} + 2\cos\left[(n-1)x\right] = \frac{\sin\left[(n-2)x\right] + 2\cos\left[(n-1)x\right]\sin(x)}{\sin(x)} \\ \iff & \frac{\sin\left[(n-2)x\right] + \Big[\sin\left[(n-1)x+x\right] - \sin\left[(n-1)x-x\right]\Big]}{\sin(x)} = \frac{\sin\left[nx\right]}{\sin(x)} \ , \end{aligned} \tag{B.17}$$

where we used the trigonometric identity defined in Eq.(A.5). As a result, point 3 is proven to be true, which means that:

$$F(n) = \frac{\sin\left[nx\right]}{\sin(x)} \ , \tag{B.18}$$

is verified for all n.